

Computational Fluid Mixing

ELIZABETH MARDEN MARSHALL and ANDRÉ BAKKER

Fluent, Inc.

5-1 INTRODUCTION

Mixing processes can be based on a number of mechanisms, from agitation to sparging to static flow manipulation. Agitation in a stirred tank is one of the most common operations, yet presents one of the greatest challenges in the area of computer simulation. Stirred tanks typically contain an impeller mounted on a shaft, and optionally can contain baffles and other internals, such as spargers, coils, and draft tubes. Modeling a stirred tank using computational fluid dynamics (CFD) requires consideration of many aspects of the process. First, any computational model requires that the domain of interest, in this case the volume occupied by the fluid inside the vessel, be described by a computational grid, a collection of small subdomains or cells. It is in these cells that problem-specific variables are computed and stored. The computational grid must fit the contours of the vessel and its internals, even if the components are geometrically complex. Second, the motion of the impeller in the tank must be treated in a special way, especially if the tank contains baffles or other internals. The special treatment employed affects both the construction of the computational grid and the solution method used to obtain the flow field numerically. In this chapter the process of modeling the flow inside a stirred tank is examined, and these special considerations are discussed at length.

In Section 5-2, an introduction to the field of computational fluid dynamics is given, with an emphasis on the fundamental equations that are used to describe processes that are common in mixing applications. An overview of the numerical methods used to solve these equations is presented in Section 5-3. Numerical simulations of stirred tanks are normally done in either two or three dimensions. In two dimensional (2D) simulations, the geometry and flow field are assumed to

be axisymmetric or independent of the angular dimension. The solution domain extends from the axis of the vessel out to the vessel wall. Approximations are required for elements that do have angular dependence, such as the impellers and baffles. These approximate methods are discussed in Section 5-4. In three dimensional (3D) simulations, the impellers, baffles, and other internals can be modeled using their exact geometry. The challenge in these simulations is to incorporate the motion of the impeller in the presence of the stationary tank and internals. Methods for performing 3D simulations are discussed in Section 5-5. Section 5-6 illustrates how CFD results can be interpreted for mixing analysis. Several application examples are presented in Section 5-7, and closing remarks, including a review of some of the common pitfalls to success, are given in Section 5-8.

Figure 5-1*a* shows the outline of a simple baffled stirred tank containing a Rushton turbine on a centrally mounted shaft. The tank has diameter T . The impeller has diameter D and is located a distance C off the bottom of the tank. These symbols are used throughout the chapter.

In addition, references will be made to the computational grid that is necessary for computing a numerical solution for the flow field in a stirred tank when the impeller is operational. This grid can take on many forms, as discussed in Section 5-3. One example of a computational grid for the vessel of Figure 5-1*a* is shown in Figure 5-1*b*.

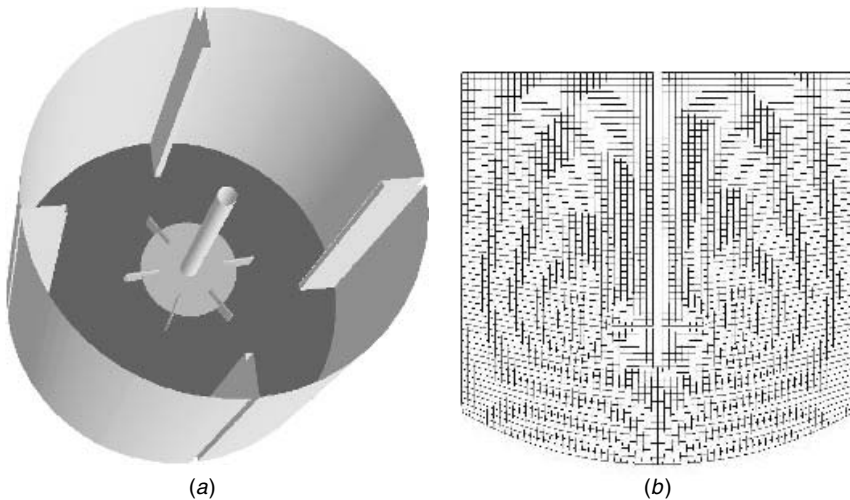


Figure 5-1 (a) Mixing vessel showing a Rushton turbine on a central shaft and baffles. (b) Example of a computational grid that can be used for solution of the flow field in this vessel.

5-2 COMPUTATIONAL FLUID DYNAMICS

Computational fluid dynamics (CFD) is the numerical simulation of fluid motion. While the motion of fluids in mixing is an obvious application of CFD, there are hundreds of others, ranging from blood flow through arteries, to supersonic flow over an airfoil, to the extrusion of rubber in the manufacture of automotive parts. Numerous models and solution techniques have been developed over the years to help describe a wide variety of fluid motion. In this section, the fundamental equations for fluid flow are presented.

Although the primary focus is on specific models that are relevant to the analysis of mixing processes, a number of advanced models for more complex flows are also discussed.

5-2.1 Conservation Equations

If a small volume, or element of fluid in motion is considered, two changes to the element will probably take place: (1) the fluid element will translate and possibly rotate in space, and (2) it will become distorted, either by a simple stretching along one or more axes or by an angular distortion that causes it to change shape. The process of translation is often referred to as *convection*, and the process of distortion is related to the presence of gradients in the velocity field and a process called *diffusion*. In the simplest case, these processes govern the evolution of the fluid from one state to another. In more complicated systems, sources can also be present that give rise to additional changes in the fluid. Many more phenomena can also contribute to the way a fluid element changes with time. Heat can cause a gas to expand, and chemical reactions can cause the viscosity to change, for example. Many of the processes such as those that are involved in the description of generalized fluid motion are described by a set of conservation or transport equations. These equations track, over time, changes in the fluid that result from convection, diffusion, and sources or sinks of the conserved or transported quantity. Furthermore, these equations are coupled, meaning that changes in one variable (say, the temperature) can give rise to changes in other variables (say, the pressure). The equations discussed below describe many of these coupled phenomena, with an emphasis on those processes that are typical in mixing applications.

5-2.1.1 Continuity. The continuity equation is a statement of conservation of mass. To understand its origin, consider the flow of a fluid of density ρ through the six faces of a rectangular block, as shown in Figure 5-2. The block has sides of length Δx_1 , Δx_2 , and Δx_3 and velocity components U_1 , U_2 , and U_3 in each of the three coordinate directions. To ensure conservation of mass, the sum of

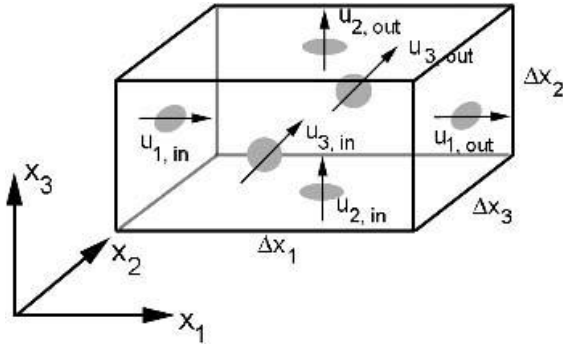


Figure 5-2 A rectangular volume with inflow and outflow can be used to illustrate a conservation equation.

the mass flowing through all six faces must be zero:

$$\rho(U_{1,out} - U_{1,in})(\Delta x_2 \Delta x_3) + \rho(U_{2,out} - U_{2,in})(\Delta x_1 \Delta x_3) + \rho(U_{3,out} - U_{3,in})(\Delta x_1 \Delta x_2) = 0 \tag{5-1}$$

Dividing through by $(\Delta x_1 \Delta x_2 \Delta x_3)$ the equation can be written as

$$\rho \frac{\Delta U_1}{\Delta x_1} + \rho \frac{\Delta U_2}{\Delta x_2} + \rho \frac{\Delta U_3}{\Delta x_3} = 0 \tag{5-2}$$

or, in differential form,

$$\rho \frac{\partial U_1}{\partial x_1} + \rho \frac{\partial U_2}{\partial x_2} + \rho \frac{\partial U_3}{\partial x_3} = 0 \tag{5-3}$$

A more compact way to write eq. (5-3) is through the use of Einstein notation:

$$\rho \frac{\partial U_i}{\partial x_i} = 0 \tag{5-4}$$

With this notation, whenever repeated indices occur in a term, the assumption is that there is a sum over all indices. Here, and elsewhere in this chapter, U_i is the i th component of the fluid velocity, and partial derivatives with respect to x_i are assumed to correspond to one of the three coordinate directions. For more general cases, the density can vary in time and in space, and the continuity equation takes on the more familiar form

$$\frac{\partial \rho}{\partial t} + \frac{\partial}{\partial x_i}(\rho U_i) = 0 \tag{5-5}$$

5-2.1.2 Momentum. The momentum equation is a statement of conservation of momentum in each of the three component directions. The three momentum equations are collectively called the *Navier–Stokes equations*. In addition to momentum transport by convection and diffusion, several momentum sources are also involved:

$$\frac{\partial(\rho U_i)}{\partial t} + \frac{\partial}{\partial x_j}(\rho U_i U_j) = -\frac{\partial p}{\partial x_i} + \frac{\partial}{\partial x_j} \left[\mu \left(\frac{\partial U_i}{\partial x_j} + \frac{\partial U_j}{\partial x_i} - \frac{2}{3} \frac{\partial U_k}{\partial x_k} \delta_{ij} \right) \right] + \rho g_i + F_i \quad (5-6)$$

In eq. (5-6) the convection terms are on the left. The terms on the right-hand side are the pressure gradient, a source term; the divergence of the stress tensor, which is responsible for the diffusion of momentum; the gravitational force, another source term; and other generalized forces (source terms), respectively.

5-2.1.3 Turbulence. A number of dimensionless parameters have been developed for the study of fluid dynamics that are used to categorize different flow regimes. These parameters, or numbers, are used to classify fluids as well as flow characteristics. One of the most common of these is the *Reynolds number*, defined as the ratio of inertial forces, or those that give rise to motion of the fluid, to frictional forces, or those that tend to slow the fluid down. In geometrically similar domains, two fluids with the same Reynolds number should behave in the same manner. For simple pipe flow, the Reynolds number is defined as

$$\text{Re} = \frac{\rho U d}{\mu} \quad (5-7)$$

where ρ is the fluid density, U the axial velocity in the pipe, d the pipe diameter, and μ the molecular or dynamic viscosity of the fluid. For mixing tanks, a modified definition is used:

$$\text{Re} = \frac{N D^2 \rho}{\mu} \quad (5-8)$$

where N is the impeller speed, in rev/s, and D is the impeller diameter. Based on the value of the Reynolds number, flows fall into either the laminar regime, with small Reynolds numbers, or the turbulent regime, with high Reynolds numbers. The transition between laminar and turbulent regimes occurs throughout a range of Reynolds numbers rather than at a single value. For pipe flow, transition occurs in the vicinity of $\text{Re} = 2000$ to 4000 , while in mixing tanks, it usually occurs somewhere between $\text{Re} = 50$ and 5000 , depending on the power number of the impeller. In the turbulent regime, fluctuations in the mean velocity and other variables occur, and for the model to be able to provide meaningful results, their effect needs to be incorporated into the CFD model. This is done through the use of a turbulence model.

Several methods are available for including turbulence in the Navier–Stokes equations. Most of these involve a process of time averaging the conservation equations. When turbulence is included, the transported quantity, say velocity,

is assumed to be the sum of an equilibrium and a fluctuating component, $U_i + u'_i$. After time averaging over many cycles of the fluctuation, terms containing factors of the fluctuating component average to zero. The only term that remains positive definite is one containing the product of two fluctuating terms. The remaining terms are identical to those in eq. (5-6). Thus, the *Reynolds-averaged Navier–Stokes (RANS) equation* for momentum is

$$\frac{\partial(\rho U_i)}{\partial t} + \frac{\partial}{\partial x_j}(\rho U_i U_j) = -\frac{\partial p}{\partial x_i} + \frac{\partial}{\partial x_j} \left[\mu \left(\frac{\partial U_i}{\partial x_j} + \frac{\partial U_j}{\partial x_i} - \frac{2}{3} \frac{\partial U_k}{\partial x_k} \delta_{ij} \right) \right] + \frac{\partial}{\partial x_j}(-\rho \overline{u'_i u'_j}) + \rho g_i + F_i \quad (5-9)$$

The new terms involving $\overline{u'_i u'_j}$ are called the *Reynolds stresses*. The overbar indicates that these terms represent time-averaged values. Reynolds stresses contribute new unknowns to the RANS equations and need to be related to the other variables. This is done through various models, collectively known as *turbulence models*.

Boussinesq Hypothesis. The Boussinesq hypothesis makes the assumption that the Reynolds stresses can be expressed in terms of mean velocity gradients. The following statement of the hypothesis shows the introduction of a new constant that is dimensionally equivalent to viscosity:

$$\overline{\rho u'_i u'_j} = \frac{2}{3} \rho k \delta_{ij} + \left[\mu_t \left(\frac{\partial U_i}{\partial x_j} + \frac{\partial U_j}{\partial x_i} \right) \right] \quad (5-10)$$

The new constant, μ_t , is the turbulent or eddy viscosity. It can be seen that when eq. (5-10) is substituted into eq. (5-9), the terms containing the partial derivatives can be combined and a new quantity, the effective viscosity, can be introduced:

$$\mu_{\text{eff}} = \mu + \mu_t \quad (5-11)$$

The hypothesis also introduces another term involving a new variable, k , the kinetic energy of turbulence. This quantity is defined in terms of the velocity fluctuations u' , v' , and w' in each of the three coordinate directions:

$$k = \frac{1}{2}(\overline{u'^2} + \overline{v'^2} + \overline{w'^2}) \quad (5-12)$$

It is the job of the turbulence model to compute the Reynolds stresses for substitution into eq. (5-9). In some cases, this is done by computing the parameters k and μ_t (or k and μ_{eff}) for substitution into eq. (5-10) and ultimately, eq. (5-9). All turbulence models use some level of approximation to accomplish this goal,

and it is the nature of the flow conditions in each specific application that determines which set of approximations is acceptable for use. A brief summary of some of the popular turbulence models in use today for industrial applications is given below.

k-ε Model. The $k-\varepsilon$ model is one of a family of two-equation models for which two additional transport equations must be solved to compute the Reynolds stresses. (Zero- and one-equation models also exist but are not commonly used in mixing applications.) It is a robust model, meaning that it is computationally stable, even in the presence of other, more complex physics. It is applicable to a wide variety of turbulent flows and has served the fluid modeling community for many years. It is semiempirical, based in large part on observations of high-Reynolds-number flows. The two transport equations that need to be solved for this model are for the kinetic energy of turbulence, k , and the rate of dissipation of turbulence, ε :

$$\frac{\partial(\rho k)}{\partial t} + \frac{\partial}{\partial x_i}(\rho U_i k) = \frac{\partial}{\partial x_i} \left(\mu + \frac{\mu_t}{\sigma_k} \right) \frac{\partial k}{\partial x_i} + G_k - \rho \varepsilon \quad (5-13)$$

$$\frac{\partial(\rho \varepsilon)}{\partial t} + \frac{\partial}{\partial x_i}(\rho U_i \varepsilon) = \frac{\partial}{\partial x_i} \left(\mu + \frac{\mu_t}{\sigma_\varepsilon} \right) \frac{\partial \varepsilon}{\partial x_i} + C_1 \frac{\varepsilon}{k} G_k + C_2 \rho \frac{\varepsilon^2}{k} \quad (5-14)$$

The quantities C_1 , C_2 , σ_k , and σ_ε are empirical constants. The quantity G_k appearing in both equations is a generation term for turbulence. It contains products of velocity gradients and also depends on the turbulent viscosity:

$$G_k = \mu_t \left(\frac{\partial U_i}{\partial x_j} + \frac{\partial U_j}{\partial x_i} \right) \frac{\partial U_j}{\partial x_i} \quad (5-15)$$

Other source terms can be added to eqs. (5-13) and (5-14) to include other physical effects, such as swirl, buoyancy, or compressibility, for example. The turbulent viscosity is derived from both k and ε and involves a constant taken from experimental data, C_μ , which has a value of 0.09:

$$\mu_t = \rho C_\mu \frac{k^2}{\varepsilon} \quad (5-16)$$

To summarize the solution process for the $k-\varepsilon$ model, transport equations are solved for the turbulent kinetic energy and dissipation rate. The solutions for k and ε are used to compute the turbulent viscosity, μ_t . Using the results for μ_t and k , the Reynolds stresses can be computed from the Boussinesq hypothesis for substitution into the momentum equations. Once the momentum equations have been solved, the new velocity components are used to update the turbulence generation term, G_k , and the process is repeated.

RNG $k-\epsilon$ Model. The renormalization group (RNG) model (Yakhot and Orszag, 1986) was developed in response to the empirical nature of the standard $k-\epsilon$ model. Rather than being based on observed fluid behavior, it is derived using statistical methods used in the field of RNG theory. It is similar in form to the standard $k-\epsilon$ model but contains modifications in the dissipation equation to better describe flows with regions of high strain, such as the flow around a bend or reattachment following a recirculation zone. In addition, a differential equation is solved for the turbulent viscosity. When the solution of this differential equation is evaluated in the high Reynolds number limit, eq. (5-16) is returned with a coefficient, C_{μ} , of 0.0845, within 7% of the empirical value of 0.09. While the RNG model works well for high Reynolds number flows, it also works well for transitional flows, where the Reynolds number is in the low turbulent range.

Realizable $k-\epsilon$ Model. The realizable $k-\epsilon$ model (Shih et al., 1995) is a fairly recent addition to the family of two-equation models. It differs from the standard $k-\epsilon$ model in two ways. First, the turbulent viscosity is computed in a different manner, making use of eq. (5-16) but using a variable for the quantity C_{μ} . This is motivated by the fact that in the limit of highly strained flow, some of the normal Reynolds stresses, $\overline{u_i^2}$, can become negative in the $k-\epsilon$ formulation, which is unphysical, or unrealizable. The variable form of the constant C_{μ} is a function of the local strain rate and rotation of the fluid and is designed to prevent unphysical values of the normal stresses from developing.

The second difference is that the realizable $k-\epsilon$ model uses different source and sink terms in the transport equation for eddy dissipation. The resulting equation is considerably different from the one used for both the standard and RNG $k-\epsilon$ models. The modified prediction of ϵ , along with the modified calculation for μ_t , makes this turbulence model superior to the other $k-\epsilon$ models for a number of applications. In particular, the model does better in predicting the spreading rate of round jets, such as those emitted from a rotating impeller blade.

RSM Model. The Reynolds stress model (RSM) does not use the Boussinesq hypothesis. Rather than assume that the turbulent viscosity is isotropic, having one value as in the $k-\epsilon$ model, the Reynolds stress model computes the stresses, $\overline{u_i u_j}$ individually. For 2D models, this amounts to four additional transport equations. For 3D models, six additional transport equations are required. Along with the transport equation for ϵ , which must also be solved in the RSM model, the full effect of turbulence can be represented in the momentum equations with greater accuracy than can be obtained from the $k-\epsilon$ models. Flows for which the assumption of isotropic turbulent viscosity breaks down include those with high swirl, rapid changes in strain rate, or substantial streamline curvature. As computer power and speed have increased during the past several years, the use of the Reynolds stress turbulence model has become more widespread, giving rise

to improved accuracy over other RANS-based turbulence models when compared to experimental results for a number of applications, such as the flow in unbaffled stirred vessels.

LES Model. A fairly recent entry to the group of commercially available turbulence models is the large eddy simulation (LES) model. This approach recognizes that turbulent eddies occur on many scales in a flow field. Large eddies are often sized according to the extents of the physical domain. Small eddies, however, are assumed to have similar properties and behavior for all problem domains, independent of their overall size or purpose. With the LES model, the continuity and momentum equations are filtered prior to being solved in a transient fashion. The filtering process isolates the medium and large scale eddies from those that are smaller than a typical cell size. The effects of the small eddies are included in the filtered equations through the use of a subgrid scale model. The transient simulation is then free to capture the random fluctuations that develop on medium and large scales. Despite the fact that a transient simulation is needed for this turbulence model, it has proven to be worth the effort. Simulations to date have predicted unstable behavior successfully in jets, flames, and both static mixers and stirred tanks. See, for example, Section 5-7.11, where LES is used to simulate the flow in an HEV static mixer. An overview of the turbulence models discussed in this section, including the primary advantages and disadvantages of each, is provided in Table 5-1.

5-2.1.4 Species. The species equation is a statement of conservation of a single species. Multiple-species equations can be used to represent fluids in a mixture with different physical properties. Solution of the species equations can predict how different fluids mix, but not how they will separate. Separation is the result of different body forces acting on the fluids, such as gravity acting on fluids of different density. To model separation, separate momentum equations are required for each of the fluids so that the body forces can act on the fluids independently (see Section 5-2.2.2). Species transport is nevertheless a very useful tool for predicting blending times or chemical reaction. For the species i' , the conservation equation is for the mass fraction of that species, $m_{i'}$, and has the following form:

$$\frac{\partial(\rho m_{i'})}{\partial t} + \frac{\partial}{\partial x_i}(\rho U_i m_{i'}) = -\frac{\partial}{\partial x_i} J_{i',i} + R_{i'} + S_{i'} \quad (5-17)$$

In eq. (5-17), $J_{i',i}$ is the i component of the diffusion flux of species i' in the mixture. For laminar flows, $J_{i',i}$ is related to the diffusion coefficient for the species and local concentration gradients (Fick's law of diffusion). For turbulent flows, $J_{i',i}$ includes a turbulent diffusion term, which is a function of the turbulent Schmidt number. $R_{i'}$ is the rate at which the species is either consumed or produced in one or more reactions, and $S_{i'}$ is a general source term for species. The general source term

Table 5-1 Summary of Turbulence Models

Turbulence Model	Description, Advantages, and Disadvantages
Standard $k-\epsilon$	The most widely used model, it is robust, economical, and has served the engineering community well for many years. Its main advantages are a rapid, stable calculation, and reasonable results for many flows, especially those with high Reynolds number. It is not recommended for highly swirling flows, round jets or for flows with strong flow separation.
RNG $k-\epsilon$	A modified version of the $k-\epsilon$ model, this model yields improved results for swirling flows and flow separation. It is not well suited for round jets and is not as stable as the standard $k-\epsilon$ model.
Realizable $k-\epsilon$	Another modified version of the $k-\epsilon$ model, the realizable $k-\epsilon$ model correctly predicts the flow in round jets and is also well suited for swirling flows and flows involving separation.
RSM	The full Reynolds stress model provides good predictions for all types of flows, including swirl, separation, and round and planar jets. Because it solves transport equations for the Reynolds stresses directly, longer calculation times are required than for the $k-\epsilon$ models.
LES	Large eddy simulation is a transient formulation that provides excellent results for all flow systems. It solves the Navier–Stokes equations for large scale turbulent fluctuations and models only the small scale fluctuations (smaller than a computational cell). Because it is a transient formulation, the required computational resources are considerably larger than those required for the RSM and $k-\epsilon$ style models. In addition, a finer grid is needed to gain the maximum benefit from the model and to accurately capture the turbulence in the smallest, subgrid scale eddies. Analysis of LES data usually requires some degree of advance planning.

can be used for nonreacting sources, such as the evaporated vapor from a heated droplet, for example. When two or more species are present, the sum of the mass fractions in each cell must add to 1.0. For this reason, if there are n species involved in a simulation, only $n - 1$ species equations need to be solved. The mass fraction of the n th species can be computed from the required condition:

$$\sum_{i'}^n m_{i'} = 1.0 \quad (5-18)$$

More details about reacting flow are presented in Section 5-2.2.1.

5-2.1.5 Heat Transfer. Heat transfer is often expressed as an equation for the conservation of energy, typically in the form of static or total enthalpy. Heat can be generated (or extracted) through many mechanisms, such as wall heating (in a jacketed reactor), cooling through the use of coils, and chemical reaction. In addition, fluids of different temperatures may mix in a vessel, and the time for the mixture to come to equilibrium may be of interest. The equation for conservation of energy (total enthalpy) is

$$\frac{\partial(\rho E)}{\partial t} + \frac{\partial}{\partial x_i} [U_i(\rho E + p)] = \frac{\partial}{\partial x_i} \left[k_{\text{eff}} \frac{\partial T}{\partial x_i} - \sum_{j'} h_j J_{j',i} + U_j (\tau_{ij})_{\text{eff}} \right] + S_h \quad (5-19)$$

In this equation, the energy, E , is related to the static enthalpy, h , through the following relationship involving the pressure, p , and velocity magnitude, U :

$$E = h - \frac{p}{\rho} + \frac{U^2}{2} \quad (5-20)$$

For incompressible flows with species mixing, the static enthalpy is defined in terms of the mass fractions, m_j , and enthalpies, h_j , of the individual species:

$$h = \sum_{j'} m_j h_j + \frac{p}{\rho} \quad (5-21)$$

The enthalpy for the individual species j' is a temperature-dependent function of the specific heat of that species:

$$h_{j'} = \int_{T_{\text{ref}}}^T c_{p,j'} dT \quad (5-22)$$

Once the enthalpy has been determined from the relationships shown above, the temperature can be extracted using eq. (5-22). This process is not straightforward because the temperature is the integrating variable. One technique for extracting the temperature involves the construction of a look-up table at the start of the calculation, using the known or anticipated limits for the temperature range. This table can subsequently be used to obtain temperature values for corresponding enthalpies obtained at any time during the solution.

The first term on the right-hand side of eq. (5-19) represents heat transfer due to conduction, or the diffusion of heat, where the effective conductivity, k_{eff} , contains a correction for turbulent simulations. The second term represents heat transfer due to the diffusion of species, where $J_{j',i}$ is the diffusion flux defined in Section 5-2.1.4. The third term involves the stress tensor, $(\tau_{ij})_{\text{eff}}$, a collection of velocity gradients, and represents heat loss through viscous dissipation. The

fourth term is a general source term that can include heat sources due to reactions, radiation, or other processes.

5-2.2 Auxiliary Models

While a wide range of applications can be modeled using the basic transport equations described above, others involve more complex physics and require additional modeling capabilities. Some of these models are discussed below.

5-2.2.1 Chemical Reaction. Chemically reacting flows are those in which the chemical composition, properties, and temperature change as the result of a simple or complex chain of reactions in the fluid. Depending on the implementation, reacting flows can require the solution of multiple conservation equations for species, some of which describe reactants, and others of which describe products. To balance the mass transfer from one species to another, reaction rates are used in each species conservation equation, and have as factors the molecular weights, concentrations, and stoichiometries for that species in all reactions.

Consider, for example, the single-step first-order reaction $A + B \rightarrow R$, for which the reaction rate is given by

$$R_i \propto C_A C_B + \overline{c_A c_B} \quad (5-23)$$

Here C_A and C_B denote the mean molar concentrations of reactants A and B, while c_A and c_B denote the local concentration fluctuations that result from turbulence. When the species are perfectly mixed, the second term on the right-hand side, containing the correlation of the concentration fluctuations, will approach zero. If the species are not perfectly mixed, this term will be negative and will reduce the reaction rate. The estimation of this correlation term is not straightforward, and numerous models are available (Hannon, 1992) for this purpose. Its presence suggests, however, that the reaction rate should incorporate not only the mean concentrations of the reactant species but the turbulent fluctuations of the reactant species as well, since the latter gives an indication of the degree to which these species are mixed.

One popular method for computing the reaction rates as a function of both mean concentrations and turbulence levels is through the Magnussen model (Magnussen and Hjertager, 1976). Originally developed for combustion, it can also be used for liquid reactions by tuning some of the model parameters. The model consists of rates calculated by two primary means. An Arrhenius, or kinetic rate, $R_{K,i',k}$, for species i' in reaction k , is governed by the local mean species concentrations and temperature in the following manner:

$$R_{K,i',k} = -\nu_{i',k} M_{i'} A_k T^{\beta_k} \exp\left(-\frac{E_k}{RT}\right) \prod_{j=1}^N [C_j]^{\eta_{j',k}} = K_{i',k} M_{i'} \prod_{j=1}^N [C_j]^{\eta_{j',k}} \quad (5-24)$$

This expression describes the rate at which species i' is consumed in reaction k . The constants A_k and E_k , the Arrhenius preexponential factor and activation energy, respectively, are adjusted for specific reactions, often as the result of experimental measurements. The stoichiometry for species i' in reaction k is represented by the factor $\nu_{i',k}$, and is positive or negative, depending upon whether the species serves as a product or reactant. The molecular weight of the species i' appears as the factor $M_{i'}$. The temperature, T , appears in the exponential term and also as a factor in the rate expression, with an optional exponent, β_k . Concentrations of other species, j' , involved in the reaction, $[C_{j'}]$, appear as factors with optional exponents associated with each. Other factors and terms, not appearing in eq. (5-24), can be added to include effects such as the presence of nonreacting species in the rate equation. Such third-body reactions are typical of the effect of a catalyst on a reaction, for example. Many of the factors appearing in eq. (5-24) are often collected into a single rate constant, $K_{i',k}$.

In addition to the Arrhenius rate, two mixing rates are computed that depend on the local turbulent kinetic energy and dissipation rate. One rate, $R_{M1,i',k}$, involves the mass fraction of the reactant in reaction k , m_R , with returns the smallest rate:

$$R_{M1,i',k} = \nu_{i',k} M_{i'} A \rho \frac{\varepsilon}{k} \frac{m_R}{\nu_{R,k} M_R} \quad (5-25)$$

where the subscript R refers only to the reactant species, $i' = R$. The other mixing rate, $R_{M2,i',k}$, involves the sum-over-product species mass fractions, m_p , and product stoichiometries, $\nu'_{j',k}$:

$$R_{M2,i',k} = \nu_{i',k} M_{i'} A B \rho \frac{\varepsilon}{k} \frac{\sum_P m_P}{\sum_{j'}^N \nu'_{j',k} M_{j'}} \quad (5-26)$$

In the mixing rate expressions, the values 4.0 and 0.5 are often used for the constants A and B , respectively, when the model is used for gaseous combustion. These values can be adjusted, however, for different types of reactions, such as those involving liquids.

After the rates in eqs. (5-24), (5-25), and (5-26) are computed, the smallest, or slowest, is used as a source term in the species transport equations for all species involved in any given reaction. The basic idea behind the Magnussen model is that in regions with high turbulence levels, the eddy lifetime, k/ε , is short, mixing is fast, and as a result the reaction rate is not limited by small scale mixing. In this limit, the kinetic rate usually has the smallest value. On the other hand, in regions with low turbulence levels, small scale mixing may be slow and limit the reaction rate. In this limit, the mixing rates are more important.

The Magnussen model was initially developed for simple, one- or two-step reaction sets, in which all reaction rates are fast relative to the small scale mixing, even though it has found use for more complex systems. Recently, for more complex reaction sets, a new model has been developed (Gran and Magnussen, 1996) called the *eddy dissipation concept* (EDC) *model*. This model assumes that reaction occurs in small turbulent structures, called the *fine scales*. A volume fraction

of the small scales is calculated, which depends on the kinematic viscosity of the fluid, the eddy dissipation rate, and the turbulent kinetic energy. Reactions are assumed to occur in the fine turbulent structures, over a time scale that depends on the kinematic viscosity and the energy dissipation rate. A source term for each chemical species is then calculated that depends on the volume fraction of the fine scales, the time scale, and the difference in species concentrations between the fine scale structures and the surrounding fluid. This extension of the Magnussen model provides improved accuracy for complex, multistep reaction sets in which not all reactions are fast relative to the rate at which small scale mixing occurs.

Numerous other reaction models exist that can be coupled to a CFD calculation. The probability density function (PDF) modeling approach (also known as the mixture fraction approach) is one that is based on the assumptions of infinitely fast reactions and chemical equilibrium at all times. In this model a collection of reacting species is described by a mixture fraction, which, under certain circumstances, is a conserved quantity. For the turbulent combustion of fuel and oxygen, for example, the mixture fraction is the elemental mass fraction in the incoming fuel stream. In turbulent conditions, fluctuations in the mixture fraction exist, along with fluctuations in the velocities and other variables. A PDF is used to describe these fluctuations. Choices are available for the assumed shape of the PDF, with the beta PDF being the most popular for engineering applications, since it offers the best agreement with experiment. This two-parameter function depends on the mean and variance of the mixture fraction. These variables are tracked by transport equations that are solved alongside the fluid equations. Based on the values of the mixture fraction (mean and variance) and enthalpy, the mass fractions of all reactant and product species can be obtained. Thus, whereas the kinetic rate expression uses time-averaged values for species mass fractions, the PDF model allows for fluctuations in these quantities. Although this model has many benefits for gaseous combustion systems, it is not the best choice for liquid reactions that are typical of mixing applications. This is because reacting liquid mixtures are not always characterized by chemical equilibrium at all times, and reaction rates can range from being very fast to being very slow compared to typical mixing rates.

Another reaction modeling approach incorporates the methodology used to describe micromixing, or mixing on the smallest scales (Bourne et al., 1981; Hannon, 1992; Fox, 1998). In the context of a CFD calculation, micromixing is on a scale that is smaller than a typical computational cell. Macromixing, on the other hand, is responsible for large scale blending, and mesomixing is in between these limits. The identification of these mixing regimes is drawn from assumptions at the core of turbulence modeling theory: namely, that turbulence energy is generated in large eddies within a domain and cascades to successively smaller eddies before being dissipated at the smallest scales. This cascade of turbulence is associated with a cascade of mixing, from macromixing on the large scales, to mesomixing throughout the midscales, to micromixing on the subgrid scales. One motivation for the interest in micromixing in liquid reactions is that

micromixing must occur before reactions can take place. It therefore plays an important role when the reaction times are on the same order as the mixing times. Micromixing models typically use a mixture fraction approach and use a PDF formulation for the turbulence–chemistry interaction. The micromixing models are incorporated through the calculation of the variance of the mixture fraction.

5-2.2.2 Multiphase Flows. When multiple fluids are involved in a flow, representing them by multiple species equations works only if the fluids are mixing and not separating. Any separation caused by the action of body forces, such as gravity or centrifugal force, can only be captured by treating the fluids with a multiphase model. When such a model is used, each of the fluids is assigned a separate set of properties, including density. Because different densities are used, forces of different magnitude can act on the fluids, enabling the prediction of separation. Five of the most popular multiphase models that are in wide use in commercial software today are described below.

Dispersed Or Discrete Phase Model. The dispersed phase model uses the Navier–Stokes equations to describe a continuous fluid phase and a Lagrangian particle tracking method to describe a dispersed phase consisting of particles, droplets, or bubbles. Heat, mass, and momentum exchange are permitted between the dispersed and fluid phases. Thus, gas bubbles can rise in a liquid, sand particles can settle, and water droplets can evaporate or boil, releasing steam to a background of warm gas, for example. The model is widely used for coal and liquid fuel combustion, bubble columns, and gas spargers in stirred tanks. It is best when the dispersed phase does not exceed 10% of the volume of the mixture in any region.

VOF Model. The volume of fluid (VOF) model is designed for two or more immiscible fluids. Because the fluids do not mix, each computational cell is filled with purely one fluid, purely another fluid, or the interface between two (or more) fluids. Because of this unique set of conditions, only a single set of Navier–Stokes equations is required. Each fluid is allowed to have a separate set of properties. The properties used are those of the fluid filling the control volume. If the interface lies inside the control volume, special treatment is used to track its position and slope in both the control volume and neighboring cells as the calculation progresses. This model is used to track free surface flows or the rise of large bubbles in a liquid, for example.

Eulerian Multiphase Model. The Eulerian multiphase model is designed for systems containing two or more interpenetrating fluids. The fluids can be in the form of liquids, gases, or solids. Whereas the dispersed phase model works best for low-volume fraction mixtures (<10%), the Eulerian multiphase model is general enough that any volume fraction of any phase is allowed. Separate sets of momentum and continuity equations are used to describe each fluid. Momentum transfer between the phases is incorporated through the use of exchange terms in

the momentum equation. When heat and mass transfer between phases occurs, exchange terms are used in the energy and continuity equations as well. The volume fractions of the phases are tracked, with the condition that the sum of the volume fractions for all phases is identically 1.0 at all times in all control volumes. Separate equations can also be used for turbulence and species transport for each phase. Although momentum, mass, heat, and species transfer between phases may be well understood, the same cannot be said for the coupling of the turbulence equations. This is an area that is currently undergoing active research at a number of institutions worldwide.

Eulerian Granular Multiphase Model. When the primary phase is a liquid or a gas and the secondary phase consists of solid particles, a modified form of the Eulerian multiphase model can be used. The Eulerian granular multiphase (EGM) model uses kinetic theory to describe the behavior of the granular or particulate phase, which is different in many ways from that of a fluid phase (see, e.g., Ogawa et al., 1980; Ding and Gidaspow, 1990; Syamlal et al., 1993). In particular, the viscosity of the granular phase undergoes a discontinuous change as the granular material transforms from a packed bed at rest to a fluid in motion, and this can only be captured by the special treatment at the heart of the EGM model. Also unique to the model is a solids pressure, which arises in part from inelastic collisions between particles. As is typical of a gas described by kinetic theory, a Maxwellian velocity distribution can be assumed for the granular phase. The width of this distribution, or spread in velocity fluctuations about the mean value, is related to the granular temperature, a parameter that can contribute to several other phenomena in granular multiphase flows. The maximum volume fraction that the granular phase can occupy is always less than 1.0 (typically, 0.6), owing to the void that is always present between the particles. These and other issues are addressed by the EGM model, allowing it to simulate a wide array of granular flow applications, from solids suspension in stirred tanks to fluidized bed flow patterns to flow in a riser.

Algebraic Slip Mixture Model. As with the Eulerian multiphase model, the algebraic slip mixture, or ASM model, is designed for use with two interpenetrating fluids. A full set of Navier–Stokes equations is solved for the primary fluid. Rather than solve a complete set for the secondary fluid, however, an algebraic equation for the slip velocity between the fluids is solved instead. The slip velocity is derived from the fluid properties and local flow conditions and is used to compute the velocity of the secondary phase. The ASM model is best when used for liquid–liquid or gas–liquid mixtures. It can also be used for lightly loaded granular mixtures, where the physics associated with the granular phase as it approaches the packing limit are not as important.

5-2.2.3 Non-Newtonian Viscosity. For Newtonian fluids, the viscosity often varies weakly with the temperature, by an amount that depends on the temperature range in use. Many fluids do not fit this simple pattern, however, and have viscosities that also depend on the shear rate in the fluid. The viscosity of these

non-Newtonian fluids can be described by one of a number of laws that involve the local shear rate of the fluid in one way or another. The dependence can be in the form of a power law (the shear rate raised to some power) and can involve a discontinuous transition after a minimum yield stress has been exceeded. In some cases, a fluid will transition from non-Newtonian to Newtonian behavior after a threshold stress has been exceeded. In general, shear-thinning fluids exhibit a drop in viscosity in regions of high shear, while shear-thickening fluids exhibit an increase in viscosity in these regions. For computational fluid dynamics, the consequence of non-Newtonian flow modeling is that the viscosity, a fluid property, becomes coupled to the fluid motion, making the equation set more difficult to solve if the viscosity is strongly varying within the limits of the flow field conditions.

Some non-Newtonian fluids are also described by a property called *viscoelasticity*. As for Newtonian fluids, these fluids deform when a shearing force is applied, but they have a partial memory of their state prior to the application of the force. Thus, when the force is withdrawn, they return, to a greater or lesser degree, to their previous state. Specialty CFD codes exist that have comprehensive models for both non-Newtonian and viscoelastic fluids. These codes are used for certain laminar mixing processes in stirred tanks and extruders.

5-3 NUMERICAL METHODS

The differential equations presented in Section 5-2 describe the continuous movement of a fluid in space and time. To be able to solve those equations numerically, all aspects of the process need to be discretized, or changed from a continuous to a discontinuous formulation. For example, the region where the fluid flows needs to be described by a series of connected control volumes, or computational cells. The equations themselves need to be written in an algebraic form. Advancement in time and space needs to be described by small, finite steps rather than the infinitesimal steps that are so familiar to students of calculus. All of these processes are collectively referred to as *discretization*. In this section, discretization of the domain, or grid generation, and discretization of the equations are described. A section on solution methods and one on parallel processing are also included.

5-3.1 Discretization of the Domain: Grid Generation

To break the domain into a set of discrete subdomains, or computational cells, or control volumes, a *grid* is used. Also called a *mesh*, the grid can contain elements of many shapes and sizes. In 2D domains, for example, the elements are usually either quadrilaterals or triangles. In 3D domains (Figure 5-3), they can be tetrahedra (with four sides), prisms (five sides), pyramids (five sides), or hexahedra (six sides). A series of line segments (2D) or planar faces (3D) connecting the boundaries of the domain are used to generate the elements.

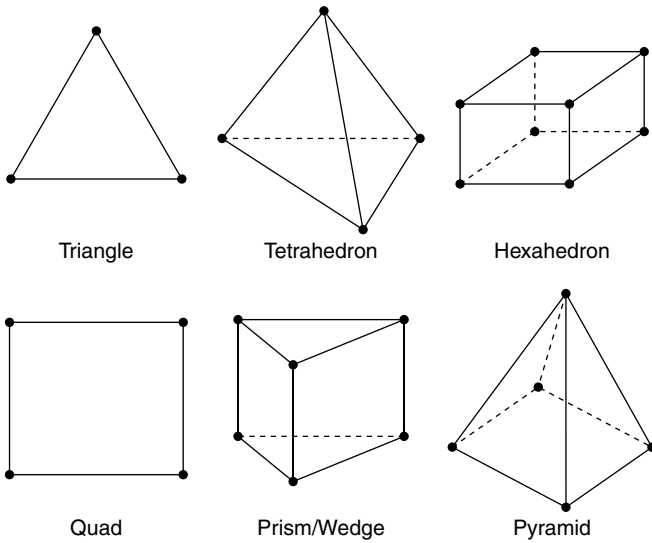
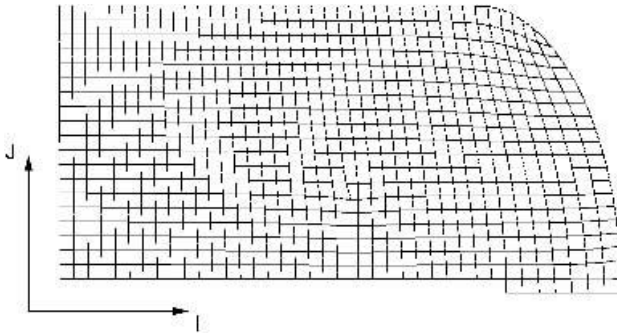


Figure 5-3 Element types that can be used in computational grids.

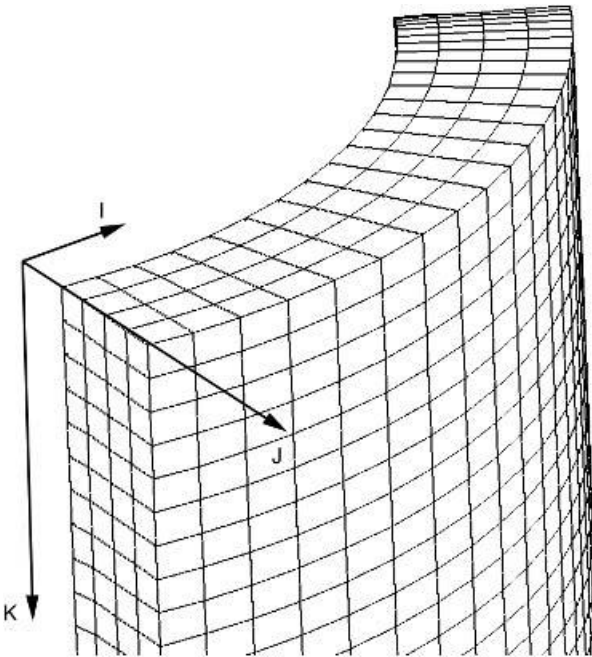
Structured grids are always quadrilateral (2D) or hexahedral (3D) and are such that every element has a unique address in I, J, K space, where I, J, and K are indices used to number the elements in each of the three computational directions (Figure 5-4). The I, J, and K directions can, but need not be, aligned with the coordinate directions x , y , and z . Unstructured grids do not follow this addressing rule (Figure 5-5). Hybrid meshes are unstructured meshes that make use of different types of elements (e.g., triangles and quadrilaterals, as in Figure 5-5*b*). Block structured meshes use quadrilateral (2D) or hexahedral (3D) elements and have I, J, K structures in multicell blocks rather than across the entire domain. The top section of Figure 5-5*b* is an example of a block structured grid, although the grid as a whole (including the bottom section) is unstructured.

In general, the density of cells in a computational grid needs to be fine enough to capture the flow details, but not so fine that the overall number of cells in the domain is excessively large, since problems described by large numbers of cells require more time to solve. Nonuniform grids of any topology can be used to focus the grid density in regions where it is needed and to allow for expansion in other regions.

In laminar flows, the grid near boundaries should be refined to allow the solution to capture the boundary layer flow detail. A boundary layer grid should contain quadrilateral elements in 2D and hexahedral or prism elements in 3D, and should have at least five layers of cells. For turbulent flows, it is customary to use a wall function in the near-wall regions. This is due to the fact that the transport equation for the eddy dissipation has a singularity at the wall, where k [in the denominator in the source terms in eq. (5-14)] is zero. Thus, the equation for ε must be treated in an alternative manner. Wall functions rely on the fact



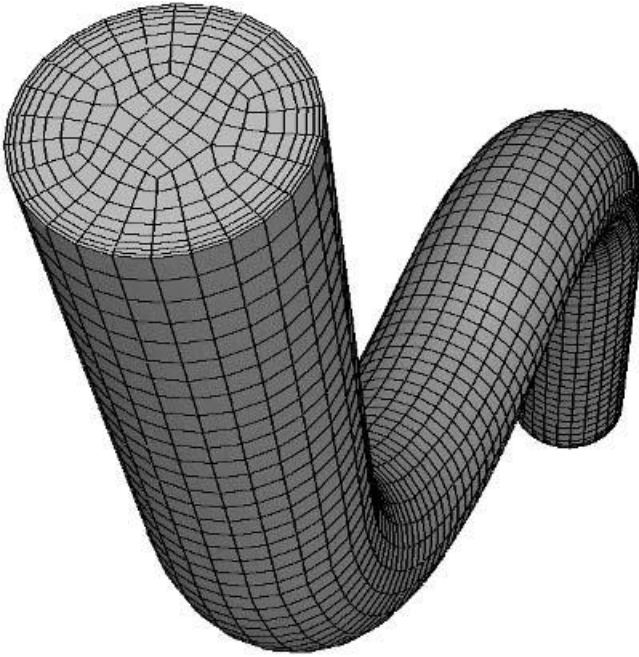
(a)



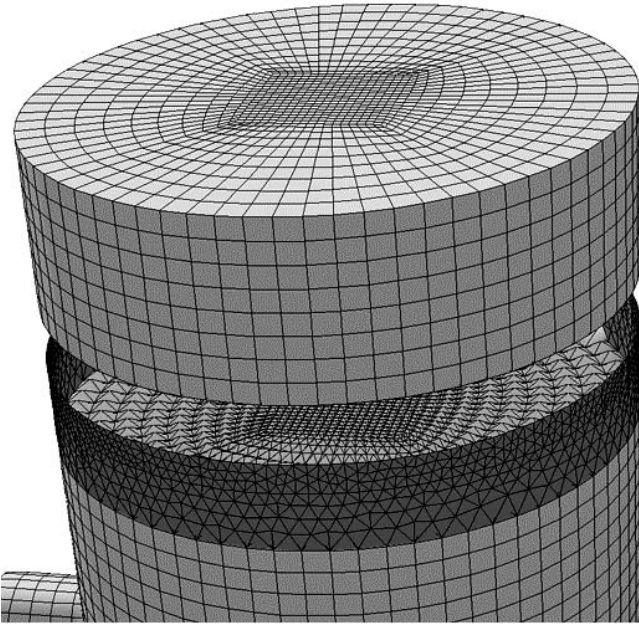
(b)

Figure 5-4 Structured grids in (a) 2D and (b) 3D showing the I, J, and K directions.

that the flow in a turbulent boundary layer consists of a narrow viscous sublayer and a broad, fully turbulent, or *log-law* layer in which the behavior is well documented. In particular, the shear stress due to the wall can be extracted from a linear relationship involving the log of the perpendicular distance to the wall. Guidelines exist so that the placement of the cell center in the cell nearest the wall lies outside the viscous sublayer and inside the log-law layer. If these guidelines are followed, the wall shear stress will be captured correctly, resulting in the best possible predictions for pressure drop and heat transfer in the simulation.



(a)



(b)

Figure 5-5 (a) Unstructured grid using hexahedral elements. (b) Unstructured grid using a mixture of elements.

5-3.2 Discretization of the Equations

Several methods have been employed over the years to solve the Navier–Stokes equations numerically, including the finite difference, finite element, spectral element, and finite volume methods. The focus of this chapter is on the finite volume method, which is described in detail below. Once the method and terminology have been presented, the other methods are discussed briefly in Section 5-3.2.3.

To illustrate the discretization of a typical transport equation using the finite-volume formulation (Patankar, 1980; Versteeg and Malalasekera, 1995), a generalized scalar equation can be used with the rectangular control volume shown in Figure 5-6*a*. The scalar equation has the form

$$\frac{\partial(\rho\phi)}{\partial t} + \frac{\partial}{\partial x_i}(\rho U_i\phi) = \frac{\partial}{\partial x_i} \left(\Gamma \frac{\partial\phi}{\partial x_i} \right) + S' \tag{5-27}$$

The parameter Γ is used to represent the diffusion coefficient for the scalar ϕ . If ϕ is one of the components of velocity, for example, Γ would represent the viscosity. All sources are collected in the term S' . Again, if ϕ is one of the components of velocity, S' would be the sum of the pressure gradient, the gravitational force, and any other additional forces that are present. The control volume has a node, P, at its center where all problem variables are stored. The transport equation describes the flow of the scalar ϕ into and out of the cell through the cell faces. To keep track of the inflow and outflow, the four faces are labeled with lowercase letters representing the east, west, north, and south borders. The neighboring cells also have nodes at their centers, and these are

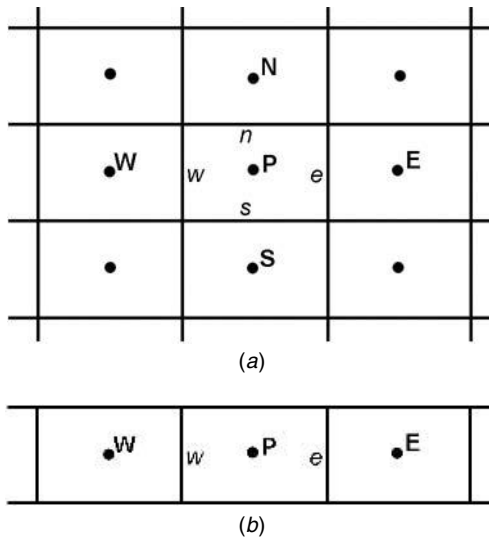


Figure 5-6 (a) Simple 2D domain showing the cell centers and faces. (b) 1D rectangular simplification of the 2D domain.

labeled with the capital letters E, W, N, and S. For the purpose of this example, flow in the one dimensional row of cells shown in Figure 5-6b is considered.

The first step in the discretization of the transport equation is an integration over the control volume. The volume integral can be converted to a surface integral by applying the divergence theorem. Using a velocity in the positive x-direction, neglecting time dependence, and assuming that the faces e and w have area A, the integrated transport equation takes the following form:

$$(\rho_e U_e \phi_e - \rho_w U_w \phi_w)A = \left(\Gamma_e \left[\frac{d\phi}{dx} \right]_e - \Gamma_w \left[\frac{d\phi}{dx} \right]_w \right) A + S \quad (5-28)$$

where S is the volume integral of the source terms contained in S' . This expression contains four terms that are evaluated at the cell faces. To obtain the face values of these terms as a function of values that are stored at the cell centers, a discretization scheme is required.

5-3.2.1 Discretization Schemes. Since all of the problem variables are stored at the cell center, the face values (e.g., the derivatives) need to be expressed in terms of cell center values. To do this, consider a steady-state conservation equation in one dimension without source terms:

$$\frac{d}{dx}(\rho U \phi) = \frac{d}{dx} \left(\Gamma \frac{\partial \phi}{\partial x} \right) \quad (5-29)$$

This equation can be solved exactly. On a linear domain that extends from $x = 0$ to $x = L$, corresponding to the locations of two adjacent cell nodes, with $\phi = \phi_0$ at $x = 0$ and $\phi = \phi_L$ at $x = L$, the solution for ϕ at any intermediate location (such as the face) has the form

$$\phi = \phi_0 + (\phi_L - \phi_0) \frac{\exp[\text{Pe}(x/L) - 1]}{\exp(\text{Pe} - 1)} \quad (5-30)$$

The Péclet number, Pe, appearing in this equation is the ratio of the influence of convection to that of diffusion on the flow field:

$$\text{Pe} = \frac{\rho U L}{\Gamma} \quad (5-31)$$

Depending on the value of the Péclet number, different limiting behavior exists for the variation of ϕ between $x = 0$ and $x = L$. These limiting cases are discussed below, along with some more rigorous discretization or differencing schemes that are in popular use today.

Central Differencing Scheme. For $\text{Pe} = 0$ (i.e., $U = 0$), there is no convection, and the solution is purely diffusive. This would correspond to heat transfer due to pure conduction, for example. In this case, the variable ϕ varies linearly from cell

center to cell center, so the value at the cell face can be found from linear interpolation. When linear interpolation is used in general, i.e., when both convection and diffusion are present, the discretization scheme is called *central differencing*. When used in this manner, as a general purpose discretization scheme, it can lead to errors and loss of accuracy in the solution. One way to reduce these errors is to use a refined grid, but the best way is to use another differencing scheme. There is one exception to this rule. Central differencing is the preferred discretization scheme when the LES turbulence model is used.

Upwind Differencing Schemes. For $Pe \gg 1$, convection dominates, and the value at the cell face can be assumed to be identical to the upstream or upwind value (i.e., $\phi_w = \phi_W$). When the value at the upwind node is used at the face, independent of the flow conditions, the process is called *first-order upwind differencing*. A modified version of first-order upwind differencing makes use of multidimensional gradients in the upstream variable, based on the upwind neighbor and its neighbors. This scheme, which makes use of a Taylor series expansion to describe the upwind gradients, is called *second-order upwind differencing*. It offers greater accuracy than the first-order upwind method, but requires additional computational effort.

Power Law Differencing Scheme. For intermediate values of the Péclet number, $0 \leq Pe \leq 10$, the face value can be computed as a function of the local Péclet number, as shown in eq. (5-30). This expression can be approximated by one that does not use exponentials, involving the Péclet number raised to an integral power. It is from this approximate form that the power law differencing scheme draws its name. This first-order scheme is identical to the first-order upwind differencing scheme in the limit of strong convection, but offers slightly improved accuracy for the range of Péclet numbers mentioned above.

QUICK Differencing Scheme. The QUICK differencing scheme (Leonard and Mokhtari, 1990) is similar to the second-order upwind differencing scheme, with modifications that restrict its use to quadrilateral or hexahedral meshes. In addition to the value of the variable at the upwind cell center, the value from the next neighbor upwind is also used. Along with the value at the node P, a quadratic function is fitted to the variable at these three points and used to compute the face value. This scheme can offer improvements over the second-order upwind differencing scheme for some flows with high swirl.

Choosing a Differencing Scheme. If the flow is aligned with the grid, first-order differencing schemes such as upwind and power law differencing are acceptable. Flow in a straight pipe modeled with a hexahedral grid is one example where these schemes would be sufficient. However, since flow patterns in both static and stirred mixers do not, in general, satisfy this condition, especially if unstructured grids are used, second-order differencing is recommended to reduce the numerical errors in the final solution. In general, first-order schemes allow the error to be

Table 5-2 Summary of Discretization Schemes

Discretization Scheme	Description, Advantages, and Disadvantages
Central	Good when diffusion dominates. Assumes that there is no convection and that variables vary linearly from cell center to cell center. For convective flows, errors can be reduced by the use of a refined grid. This scheme is recommended for LES simulations.
First-order upwind	Good when convection dominates and the flow is aligned with the grid. Assumes that the face value for each variable is equal to the upstream cell center value. Stable, and a good way to start off a calculation. A switch to a higher-order scheme is usually recommended once the solution has partially converged.
Second-order upwind	Good for full range of Peclet numbers. Computes the face value for each variable from gradients involving the upwind neighbor and its neighbors.
Power law	Good for intermediate values of Peclet number. Computes the face value for each variable from gradients expressed in the form of a power law function. For high Péclet numbers, results are equivalent to first-order upwind.
QUICK	Good for full range of Péclet numbers. Similar to second-order upwind, but restricted to quadrilateral and hexahedral meshes.

reduced linearly with the grid spacing, while second-order schemes allow the error to be reduced as the square of the grid spacing. A common practice in CFD is to obtain a partially converged solution using one of the first-order schemes and then switch to a higher-order scheme to obtain the final converged result. The discretization schemes discussed above are summarized in Table 5-2.

5-3.2.2 Final Discretized Equation. Once the face values have been computed using one of the above differencing schemes, terms multiplying the unknown variable at each of the cell centers can be collected. Large coefficients multiply each of these terms. These coefficients contain information that includes the properties, local flow conditions, and results from previous iterations at each node. In terms of these coefficients, A_i , the discretized equation has the following form for the simple 2D grid shown in Figure 5-6:

$$A_P\phi_P = A_N\phi_N + A_S\phi_S + A_E\phi_E + A_W\phi_W = \sum_{i, \text{neighbors}} A_i\phi_i \quad (5-32)$$

For a complex, or even a simple flow simulation, there will be one equation of this form for each variable solved, in each cell in the domain. Furthermore, the equations are coupled, since for example, the solution of the momentum equations will affect the transport of every other scalar quantity. It is the job

of the solver to solve these equations collectively with the most accuracy in the least amount of time.

5-3.2.3 Alternative Numerical Techniques. As mentioned earlier, other methods for solving the Navier–Stokes equations exist. Two of these are described briefly below.

Finite Difference Method. The finite difference, or Taylor series formulation replaces the derivatives in eq. (5-27) with finite differences evaluated at the variable storage sites (cell centers) using a truncated Taylor series expansion. The differences for each variable are computed using the cell value and/or the adjacent neighbor values, depending on the order of the derivative. The variation of the variable between storage sites is ignored during the solution process. Although this is an acceptable method to solve for some simply varying functions, it is not the best choice for general purpose CFD analysis because the method is limited to simple grids and does not conserve mass on coarse grids.

Finite Element Method. The finite element method uses piecewise linear or quadratic functions to describe the variation of the variable ϕ within a cell. By substituting the selected function into the conservation equation for each cell and applying the boundary conditions, a linear system of coupled equations is obtained. These equations are then solved (iteratively) for the unknown variable at all storage sites.

This method is popular for use with structural analysis codes and some CFD codes. In the early days of CFD, when structured orthogonal grids were used for most applications of the finite volume method, the finite element method offered the luxury of unstructured meshes with nonorthogonal elements of various shapes. Now that the use of unstructured meshes is common among finite volume solvers, the finite element method has been used primarily for certain focused CFD application areas. In particular, it is popular for flows that are neither compressible nor highly turbulent, and for laminar flows involving Newtonian and non-Newtonian fluids, especially those with elastic properties.

5-3.3 Solution Methods

The result of the discretization process is a finite set of coupled algebraic equations that need to be solved simultaneously in every cell in the solution domain. Because of the nonlinearity of the equations that govern the fluid flow and related processes, an iterative solution procedure is required. Two methods are commonly used. A segregated solution approach is one where one variable at a time is solved throughout the entire domain. Thus, the x -component of the velocity is solved on the entire domain, then the y -component is solved, and so on. One iteration of the solution is complete only after each variable has been solved in this manner. A coupled solution approach, on the other hand, is one where all variables, or at a minimum, momentum and continuity, are solved simultaneously in a single

cell before the solver moves to the next cell, where the process is repeated. The segregated solution approach is popular for incompressible flows with complex physics, typical of those found in mixing applications.

Typically, the solution of a single equation in the segregated solver is carried out on a subset of cells, using a Gauss–Seidel linear equation solver. In some cases the solution time can be improved (i.e., reduced) through the use of an algebraic multigrid correction scheme. Independent of the method used, however, the equations must be solved over and over again until the collective error is reduced to a value that is below a preset minimum value. At this point, the solution is considered converged, and the results are most meaningful. Converged solutions should demonstrate overall balances in all computed variables, including mass, momentum, heat, and species, for example. Some of the terminology used to describe the important aspects of the solution process is defined below.

5-3.3.1 SIMPLE Algorithm. For 3D simulations, the three equations of motion [eq. (5-6)] and the equation of continuity [eq. (5-5)] combine to form four equations for four unknowns: the pressure and the three velocity components. Because there is no explicit equation for the pressure, special techniques have been devised to extract it in an alternative manner. The best known of these techniques is the SIMPLE algorithm, semi-implicit method for pressure-linked equations (Patankar, 1980). Indeed, a family of algorithms has been derived from this basic one, each of which has a small modification that makes it well suited to one application or another.

The essence of the algorithm is as follows. A guessed pressure field is used in the solution of the momentum equations. (For all but the first iteration, the guessed pressure field is simply the last updated one.) The new velocities are computed, but these will not, in general, satisfy the continuity equation, so corrections to the velocities are determined. Based on the velocity corrections, a pressure correction is computed which when added to the original guessed pressure, results in an updated pressure. Following the solution of the remaining problem variables, the iteration is complete and the entire process is repeated.

5-3.3.2 Residuals. If the algebraic form of a conservation equation in any control volume [eq. (5-32)] could be solved exactly, it would be written as

$$A_P \Phi_P - \sum_{i, \text{neighbors}} A_i \Phi_i = 0 \quad (5-33)$$

Since the solution of each equation at any step in an iterative calculation is based on inexact information, originating from initial guessed values and refined through repeated iterations, the right-hand side of eq. (5-33) is always nonzero. This nonzero value represents the error or residual in the solution of the equation in the control volume:

$$A_P \Phi_P - \sum_{i, \text{neighbors}} A_i \Phi_i = R_P \quad (5-34)$$

The total residual is the sum over all cells in the computational domain of the residuals in each cell:

$$\sum_{P, \text{cells}} R_P = R \quad (5-35)$$

Since the total residual, R , defined in this manner, depends on the magnitude of the variable being solved, it is customary either to normalize or to scale the total residual to gauge its changing value during the solution process. Although normalization and scaling can be done in a number of ways, it is the change in the normalized or scaled residuals that is important in evaluating the rate and level of convergence of the solution.

5-3.3.3 Convergence Criteria. The convergence criteria are preset conditions for the (usually normalized or scaled) residuals that determine when an iterative solution is converged. One convergence criterion might be that the total normalized residual for the pressure equation drop below 1×10^{-3} . Another might be that the total scaled residual for a species equation drop below 1×10^{-6} . Alternatively, it could be that the sum of all normalized residuals drop below 1×10^{-4} . For any set of convergence criteria, the assumption is that the solution is no longer changing when the condition is reached and that there is an overall mass balance throughout the domain. When additional scalars are being solved (e.g., heat and species), there should be overall balances in these scalars as well. Whereas the convergence criteria indicate that overall balances probably exist, it is the wise engineer who will examine reports to verify that indeed they do.

5-3.3.4 Underrelaxation. The solution of a single differential equation, solved iteratively, makes use of information from the preceding iteration. If ϕ_n is the value of the variable from the preceding iteration and ϕ_{n+1} is the new value, some small difference or change in the variable brings the variable from the old value to the new one:

$$\phi_{n+1} = \phi_n + \Delta\phi \quad (5-36)$$

Rather than use the full computed change in the variable, $\Delta\phi$, it is often necessary to use a fraction of the computed change when several coupled equations are involved:

$$\phi_{n+1} = \phi_n + f\Delta\phi \quad (5-37)$$

This process is called *underrelaxation*, and underrelaxation factors, f , typically range from 0.1 to 1.0, depending on the complexity of the flow physics (e.g., laminar flow or turbulent reacting flow), the variable being solved (pressure or momentum), the solution method being used, and the state of the solution (during the first few iterations or near convergence). Underrelaxation makes the convergence process stable, but slower. Guidelines exist for the optimum choices for underrelaxation factors for a variety of conditions. As the solution converges, the underrelaxation factors should be gradually raised to ensure convergence that is both rapid and stable at all times.

5-3.3.5 Numerical Diffusion. Numerical diffusion is a source of error that is always present in finite volume CFD, owing to the fact that approximations are made during the process of discretization of the equations. It is so named because it presents itself as equivalent to an increase in the diffusion coefficient. Thus, in the solution of the momentum equation, the fluid will appear more viscous; in the solution of the energy equation, the solution will appear to have a higher conductivity; in the solution of the species equation, it will appear that the species diffusion coefficient is larger than in actual fact. These errors are most noticeable when diffusion is small in the actual problem definition.

To minimize numerical diffusion, two steps can be taken. First, a higher-order discretization scheme can be used, such as the QUICK or second-order upwinding schemes discussed earlier. Second, the grid can be built so as to minimize the effect. In general, numerical diffusion is more of a problem on coarse grids, so it is wise to plan ahead and avoid coarse meshes in regions where the most accuracy is sought. Numerical diffusion is usually less of a problem with quadrilateral or hexahedral meshes, provided that the flow is aligned with the mesh. Unfortunately, the flow is rarely aligned with the mesh throughout the entire flow field, so some degree of numerical diffusion is unavoidable.

5-3.3.6 Time-Dependent Solutions. To solve a time-dependent problem, the time derivative appearing in eq. (5-27) must be discretized. If $F(\phi)$ is the spatially discretized part of eq. (5-27), the time derivative can be approximated to first order as

$$\frac{\phi^{n+1} - \phi^n}{\Delta t} = F(\phi) \quad (5-38)$$

In this expression, ϕ^n is the solution at time t and ϕ^{n+1} is the solution at time $t + \Delta t$. While certain flow conditions, such as compressible flow, are best suited to an explicit method for the solution of eq. (5-38), an implicit method is usually the most robust and stable choice for a wide variety of applications, including mixing. The major difference between the explicit and implicit methods is whether the right-hand side of eq. (5-38) is evaluated at the current time [$F(\phi) = F(\phi)^n$] or at the new time [$F(\phi) = F(\phi^{n+1})$]. The implicit method uses the latter:

$$\phi^{n+1} = \phi^n + \Delta t F(\phi^{n+1}) \quad (5-39)$$

The assumption at the core of this quasi-steady approach is that the new value of the variable ϕ prevails throughout the entire time step, which takes the solution from time t to time $t + \Delta t$.

5-3.4 Parallel Processing

Parallel processing is a procedure in which a large calculation can be performed on two or more processors working in parallel. The processors can reside on the same (multiprocessor) computer or can be on a network of computers. For the calculation to run on the processors in a parallel fashion, the calculation domain

(the computational grid) must be divided into partitions, or subdomains. The equations in each partition are solved simultaneously on the multiple processors (using the segregated or coupled approach), and the results at the boundaries of the partitions are communicated to the neighbor partitions on a regular basis. As the number of nodes increases, the computation time for each node decreases, and the communication between partitions increases. In this limit, the efficiency of parallel computing decreases. Recent advances in parallel algorithms have pushed back this limiting behavior, however.

5-4 STIRRED TANK MODELING USING EXPERIMENTAL DATA

Stirred tanks typically contain one or more impellers mounted on a shaft, and optionally, baffles and other internals. Although it is a straightforward matter to build a 3D mesh to contour to the space between these elements, the mesh must be built so that the solution of the flow field incorporates the motion of the impeller. This can be done in two ways. First, the impeller geometry can be modeled directly, or explicitly, and the grid and solution method chosen so as to incorporate the motion of the impeller using either a steady-state or time-dependent technique. This approach is discussed in detail in Section 5-5. Second, the motion of the impeller can be modeled implicitly, using time-averaged experimental velocity data to represent the impeller motion. The second approach is the subject of this section.

5-4.1 Impeller Modeling with Velocity Data

When modeling the impeller using velocity data, the time-averaged velocities in the outflow of the impeller are prescribed, and the CFD solver calculates the flow in the remainder of the vessel. An illustration of this process is shown in Figure 5-7 for a radial flow impeller. The parabolic velocity profile in the impeller outflow region is prescribed as a boundary condition in the simulation, and the well-known radial flow pattern with circulation loops above and below the impeller results from the CFD calculation. It is important to note that the volume swept by the impeller is also part of the model but that other than for the fixed velocities in the outflow region, it is treated as part of the fluid domain by the CFD solver. Figure 5-7 also illustrates the fact that for this particular case it is indeed sufficient to prescribe the velocities in the impeller outflow only to obtain a good flow field prediction. Kresta and Wood (1991) and Bakker and Van den Akker (1994) presented quantitative validations for this particular case, and other authors have presented similar validations for other cases.

Over the years, practical experience has demonstrated that it is usually sufficient to prescribe the velocity data only along the edges of the impeller where the flow exits. One or two edges of the impeller are typically needed for this purpose. For an impeller that creates a purely radial flow pattern, such as the radial flow impeller of Figure 5-7, prescribing the velocities on the side of the impeller is sufficient, since flow is drawn into the impeller at the top and bottom edges.

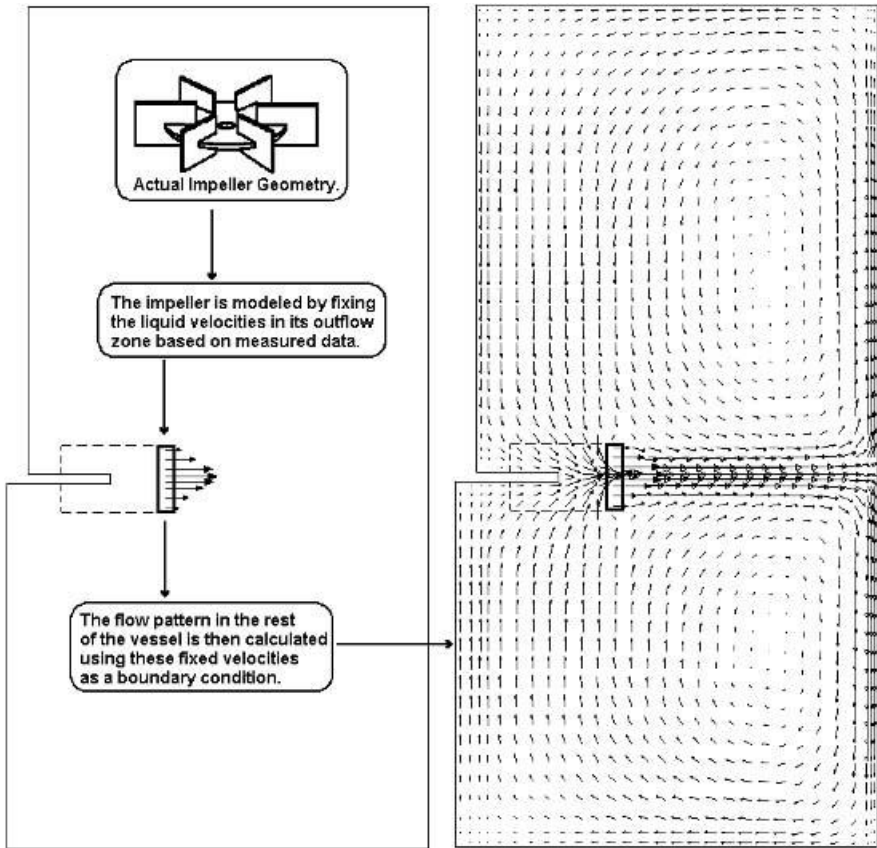


Figure 5-7 Velocity data measured radially outside a radial flow impeller are applied to a 2D CFD simulation, resulting in the well-known double-loop flow pattern.

In general for all impeller types, all three velocity components should be prescribed in the discharge region. For turbulent flow it is also recommended that values for the turbulent kinetic energy, k , and dissipation rate, ε , be prescribed. The turbulent kinetic energy can be computed from measured fluctuations in the velocity components using eq. (5-12). Using k , the eddy dissipation can be calculated using

$$\varepsilon = \frac{k^{3/2}}{L_t} \quad (5-40)$$

where L_t is a characteristic turbulent length scale in the outflow of the impeller. The authors often use $L_t = W_b/4$, where W_b is the width of the impeller blade. Note, however, that there is some debate in the literature about the exact value of the factor relating L_t and W_b .

Figure 5-8 shows where to prescribe the velocity data for various cases, including the previously discussed radial flow impeller (Figure 5-8a). For a

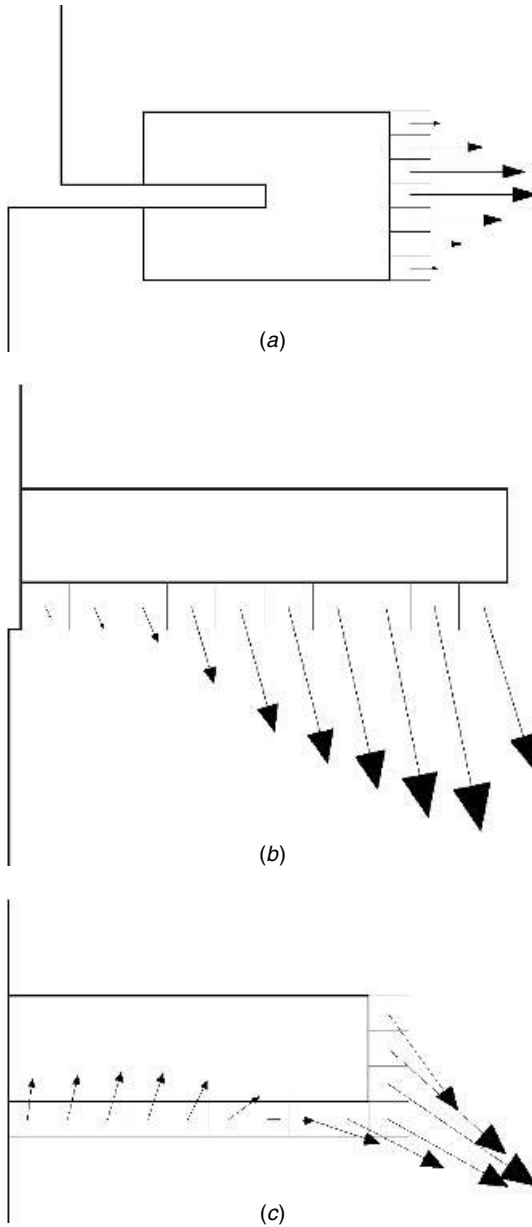


Figure 5-8 Suggested locations for prescribing impeller boundary conditions for (a) a radial flow impeller in the turbulent flow regime, (b) an axial flow impeller in the turbulent flow regime, (c) an axial flow impeller operating in the laminar flow regime. (Continued)

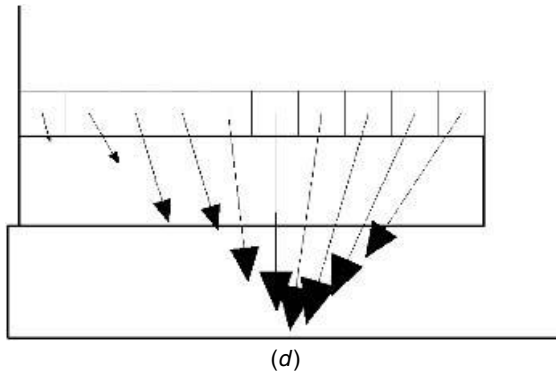


Figure 5-8 (d) An axial flow impeller close to the vessel bottom (e.g., $C/T < 0.1$).

down-pumping impeller that creates a purely axial flow pattern (Figure 5-8*b*), liquid will enter the impeller from the top and the side and exit the impeller on the bottom. In such a case it is sufficient to prescribe the liquid velocities along the bottom edge only. For an up-pumping impeller under the same conditions, the velocities would be prescribed along the top edge. When an axial flow impeller operates in the laminar flow regime, however, it will have a combined axial–radial flow (Figure 5-8*c*). On the bottom of the impeller, flow both enters and exits depending on the radial location. Furthermore, flow exits the impeller on the side. On the top of the impeller, flow enters but does not exit. Therefore, for this situation the proper modeling method is to prescribe complete velocity profiles on both the bottom and the side edges. Although it is not in general recommended to prescribe all velocity components on the top of the impeller as well, for laminar flow conditions the prediction of the swirling flow pattern in the top of the vessel can be improved by prescribing the tangential velocity component only along this edge, in addition to the prescriptions along the side and bottom. For an up-pumping impeller, the velocities should be prescribed along the top and the side edges, with the swirl (optionally) prescribed along the lower edge for laminar flows only.

In general, caution should be used when applying velocity data in circumstances where the impeller discharge has a strong interaction with the tank. This behavior has been examined experimentally and through the use of CFD by Fokema et al. (1994) for a pitched blade turbine. Indeed, when a down-pumping axial flow impeller is mounted very close to the vessel bottom (or an up-pumping impeller close to the liquid surface), velocities should not be prescribed in the impeller discharge region. Such cases present several difficulties. On the experimental side, measuring velocities in regions close to walls can be difficult and may result in inaccuracies. In the CFD simulation, there may be only a few computational cells between the vessel bottom and the impeller. In these circumstances, good results can often still be obtained if the velocities are prescribed at the top inflow of the impeller (Figure 5-8*d*).

5-4.2 Using Experimental Data

Several experimental methods are available for measuring the velocities imparted to the fluid by a working impeller. These include laser Doppler velocimetry (LDV) and particle image velocimetry (PIV). These methods are discussed in Chapter 4. Under ideal circumstances, the velocity data prescribed for a simulation would have been obtained from measurements made on an identical system. In practice, however, this is rarely the case. The experimental data that are available were probably obtained for conditions that are different from the system being modeled. Nonetheless, several scaling rules can be applied to the existing data so that appropriate velocity profiles for the case at hand can be generated.

The first step involves normalization of the available data. Typically, the measured liquid velocities are normalized by the impeller tip speed, U_{tip} , used during the experiment. The turbulent kinetic energy is usually normalized by U_{tip}^2 . The eddy dissipation can be normalized by U_{tip}^3/D , with a possible constant of proportionality. Radial measurement locations are typically normalized by the impeller radius, R , and axial locations by the impeller blade height, z , measured from the impeller centerline. To perform the simulation, profiles for the liquid velocities, k and ε , are obtained by multiplying the normalized profiles by the U_{tip} , U_{tip}^2 , and U_{tip}^3/D used in the simulation, respectively. The locations at which the velocity data are available are calculated by multiplying the normalized measurement locations by the actual impeller radius or blade height.

When prescribing the velocity data above or below the impellers, it is recommended that the computational grid be constructed such that the center of the cells where the velocities are prescribed fall within a quarter-cell height of the normalized axial measurement locations. Similarly, when prescribing data at the side of the impeller, it is recommended that the cell centers are within a quarter-cell width of the normalized radial measurement locations. For both cases, interpolation can then be used to determine the velocity values at the radial and axial grid locations of the individual cell centers, respectively.

The exact shape of the velocity profile in the outflow of an impeller does not depend solely on the impeller. It is also affected by such variables as the impeller Reynolds number, impeller off-bottom distance C/T , and impeller diameter D/T . If the flow is fully turbulent (i.e., $Re > 10^4$), the impeller outflow profiles are typically independent of Reynolds number. If the flow is transitional or laminar, however, care should be taken so that the velocity profiles used were either measured at a similar Reynolds number, or that the prescribed velocities are being interpolated from data sets measured over a range of Reynolds numbers. Similarly, for impeller off-bottom clearance and diameter, if data for various C/T and D/T values are available, interpolations can be used to obtain the prescribed velocities for the actual conditions.

5-4.3 Treatment of Baffles in 2D Simulations

As mentioned earlier, the time-averaging method used to record velocity data for an impeller makes the data useful for 2D simulations in the radial–axial

plane, where angular—and therefore time—dependence of the geometry and flow field is ignored. While ignoring the angular dependence of the impeller motion can be done in this manner, the angular dependence of the baffles needs to be addressed as well. Baffles are used to reduce the swirl introduced by the rotating impeller. One way of including this effect in a 2D simulation is to omit the swirling component of the velocity data in the numerical simulation, using the radial and axial components instead. Another way to model baffles is to set a boundary condition of zero swirl in the baffle region in the 2D simulation. By setting the boundary condition on the swirl only, the axial and radial velocities can be computed in the baffle region as they are in the remainder of the vessel.

5-4.4 Combining the Velocity Data Model with Other Physical Models

The steady-state implicit impeller model, which uses time-averaged experimental data, can be used to model other steady-state and time-dependent processes, as described below. Because of its simplicity, it has no effect on other scalar transport in the domain. The models that do require special consideration are those involving multiple phases, with separate sets of momentum boundary conditions, as described below. Species blending is also discussed, because it is a calculation that is commonly performed in conjunction with the implicit impeller model.

5-4.4.1 Volume of Fluid Model. In stirred tank applications, the volume of fluid (VOF) free surface model is useful for tracking the shape of the liquid surface during operation. This includes the transition to a parabolic shape during startup, which can lead to the (undesired) drawdown of air. The velocity data model can be used in 2D or 3D for simulations of this type. The VOF model can have a steady or time-dependent implementation, and both are fully compatible with this steady-state treatment of the impellers.

If air drawdown does occur, caution is needed. If air passes through cells where large momentum sources exist, resulting from the velocity data boundary conditions, the liquid–air interface will be broken, resulting in many small bubbles that will mix with the liquid. The VOF model is not equipped to handle this condition accurately, so the simulation should be terminated at this point. Thus, whereas the model can be used to predict if drawdown will occur, it should not be used to predict the flow conditions afterward.

5-4.4.2 Multiphase Model. Both solids suspension and gas sparging can be simulated using an experimental data model for the impeller. The manner in which the multiphase parameters are input depends on the multiphase model being used. For solids suspension, an Eulerian granular multiphase model is recommended, and separate sets of momentum equations are used for the liquid and solids phases. This model, run in a time-dependent fashion, is fully compatible with the time-averaged representation of the impellers. Experimental velocity data are set as a boundary condition independently for each of the phases. Note,

however, that there is usually some degree of slip between the fluid and granular phases, a value that increases with the density difference between the phases. Thus the velocities used to represent the impeller for a pure liquid need to be adjusted somewhat for the granular phase. This can be accomplished by estimating the slip velocity between the two phases. The measured data can be used to represent the impeller for the fluid phase, and a corrected set of data, obtained by subtracting the slip velocity from the experimental data, can be used to represent the impeller for the solids phase.

Gas sparging can be modeled using the Eulerian multiphase model or the algebraic slip mixture model. For the Eulerian multiphase model, two sets of momentum equations are used, and the same comments regarding the slip velocity between phases apply, although the issue is not as critical. That is, the velocity data used for the gas phase could be corrected slightly from the liquid-phase velocities but need not be because the gas phase has so little inertia compared to the liquid phase. When the algebraic slip mixture model is used, separate boundary conditions are not required for the individual phases, so a correction of the velocity data is not required.

Another consideration in the case of gas–liquid mixtures is the impact of the impeller on gas bubble size. In an actual stirred tank, the momentum of the rotating impeller often acts to break up gas bubbles as they pass through the region. This reduces the bubble size and can lead to an increase in the gas hold-up as well as a change in the momentum exchange term (drag) between the phases. When experimental data are used, this phenomenon is missing from the formulation but can often be incorporated into the calculation if subroutines, written by the user, are available to modify the model in the commercial software.

5-4.4.3 Turbulence. The use of a transient turbulence model, such as the large eddy simulation model, is inconsistent with the experimental data formulation because the latter is intrinsically steady-state. All of the RANS models, however, are fully compatible with the velocity data approach.

5-4.4.4 Species Blending. When a neutrally buoyant tracer, one with the same fluid properties, is added to the liquid in a vessel, a simplified approach to predicting the mixing time can be used. Rather than model the complete set of transport equations in a transient manner, the steady-state flow field can be computed first, including the inflow and outflow for the anticipated tracer and resulting mixture, respectively. Prior to beginning the transient species calculation for the tracer, the calculation of the flow field variables (pressure, momentum, and turbulence) can be disabled, since the overall properties of the mixture will not change. Thus, the dispersion of the tracer species can be tracked by solving only a single scalar transport equation. (The same technique can be used for heat transfer if the properties are the same and not temperature-dependent.) This method for computing species blending is fully compatible with the experimental data representation of the impellers.

5-5 STIRRED TANK MODELING USING THE ACTUAL IMPELLER GEOMETRY

To model the geometry of the impeller exactly, a 3D simulation must be performed. A number of solution approaches are available to incorporate the motion of the impeller, and the computational grid used must be able to adapt to the solver method employed. The models in popular use today are reviewed in the following sections. Particular attention is paid to the sliding mesh model, the most rigorous of them all. The solver methods described are all designed to capture the motion of a rotating impeller in a stationary tank, but they vary in accuracy. Three of the models are steady-state and one is time-dependent.

5-5.1 Rotating Frame Model

The rotating frame model solves the momentum equations for the entire domain in a rotating frame. The Coriolis force is included in the process. Problems solved in a rotating frame typically use the angular velocity of the primary rotating component, Ω , as the angular velocity of the frame. In stirred tanks, the impeller serves this purpose, so the frame is assumed to rotate with the impeller. Thus, the impeller is at rest in the rotating frame. The tank, however, rotates in the opposite direction, so must have a rotational boundary condition of $-\Omega$. If baffles exist, they would need to rotate into the fluid with the same angular velocity, $-\Omega$. Unfortunately, this simple steady-state model is not equipped to handle the motion of elements such as baffles into or through the fluid. The approach is therefore only useful for unbaffled tanks with smooth tank walls that are geometrically equivalent to a perfect surface of revolution. Thus an unbaffled cylindrical tank with an axisymmetric bottom shape and no angular-dependent internals could be simulated in this manner. Vessels with baffles, dip tubes, or inflow–outflow ports could not.

5-5.2 Multiple Reference Frames Model

A modification of the rotating frame model is the multiple reference frames (MRF) model (Luo et al., 1994). The modification is that more than one rotating (or nonrotating) reference frame can be used in a simulation. This steady-state approach allows for the modeling of baffled stirred tanks and tanks with other complex (rotating or stationary) internals. A rotating frame is used for the region containing the rotating components while a stationary frame is used for regions that are stationary (Figure 5-9). In the rotating frame containing an impeller, the impeller is at rest. In the stationary frame containing the tank walls and baffles, the walls and baffles are at rest. The fact that multiple reference frames can be used means that multiple impeller shafts in a rectangular tank can each be modeled with separate rotating frames (with separate rotation frequencies) while the remaining space can be modeled with a stationary frame.

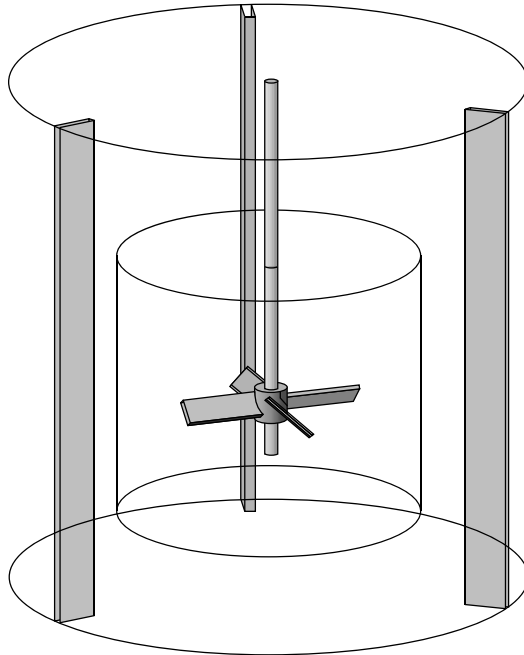


Figure 5-9 Cylindrical mixing tank with an MRF boundary surrounding the impeller.

The grid used for an MRF solution must have a perfect surface of revolution surrounding each rotating frame. The momentum equations inside the rotating frame are solved in the frame of the enclosed impeller while those outside the rotating frame are solved in the stationary frame. A steady transfer of information is made at the MRF interface as the solution progresses. While the solution of the flow field in the rotating frame in the region surrounding the impeller imparts the impeller rotation to the region outside this frame, the impeller itself does not move during this type of calculation. Its position is static. If the impeller is mounted on a central shaft in a baffled tank, this means that the orientation of the impeller blades relative to the baffles does not change during the solution. If the interaction between the impeller and baffles is weak, the relative orientation of the impeller and baffles does not matter. If the interaction is strong, however, the solution with the impeller in one position relative to the baffles will be different from that with the impeller in a different position. The model is therefore recommended for simulations in which the impeller–baffle interaction is weak. Note, however, that if the solution is to be used to obtain spatially averaged macroscopic properties of the flow field, such as power draw, the orientation of the impeller relative to the baffle may not matter. The careful engineer will perform two solutions with the impeller in two different locations and use both results (e.g., averaging them) rather than just one.

A modified version of the MRF model is the mixing plane model, in which the variables at the MRF boundary are spatially averaged in the circumferential direction prior to being passed from one side to the other. After the averaging process, all angular dependence on the boundary is eliminated, so the variables are functions of radial and axial position only. This approach is popular for turbomachinery, where many closely spaced rotors and stators are in relative motion. It has not had widespread use in the mixing community, however, owing in part to asymmetries in the flow field that are common in stirred tanks. For example, a tracer species introduced through a single dip tube on the side of the vessel would appear to be uniformly distributed on the interface shortly after reaching it, which is clearly unphysical. As another example, any stirred tank with inflow and outflow ports could have flow through the MRF interface that is not unidirectional. When the averaging process is done, this condition could also result in unphysical results. The mixing plane approach is therefore not recommended for most stirred tank applications.

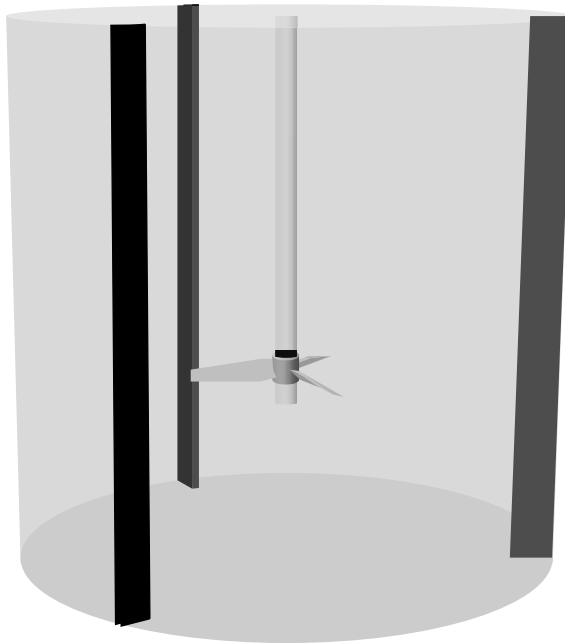
5-5.2.1 Validation of the MRF Model. To validate the MRF model, a Lightning A310, operating in a baffled vessel ($Re = 4.6 \times 10^5$), was simulated using a number of turbulence models (Marshall et al., 1999). Results for the velocity field, power number, and flow number were compared to measurements performed by Weetman (1997). The vessel used for the simulation had a diameter $T = 1.22$ m (Figure 5-10a) and three baffles. The A310 impeller (with surface grid shown in Figure 5-10b) had a diameter and off-bottom clearance of $D/T = C/T = 0.352$. A 120° sector of the domain was modeled using a grid of approximately 150 000 hexahedral cells.

Figure 5-11 shows a comparison of the velocity data from the LDV measurements with the velocities in a nonbaffle plane computed by the MRF model, using RSM for turbulence. The CFD calculation picks up the features of the flow field correctly. In Table 5-3, the results for flow number, N_Q (Section 5-6.4.2), and power number, N_P (Section 5-6.4.1), show good agreement for all turbulence models. The power drawn by the impeller was computed by integrating the pressure force over the impeller blades to obtain the torque. The flow rate was computed by integrating the flow through a circular discharge area below the impeller.

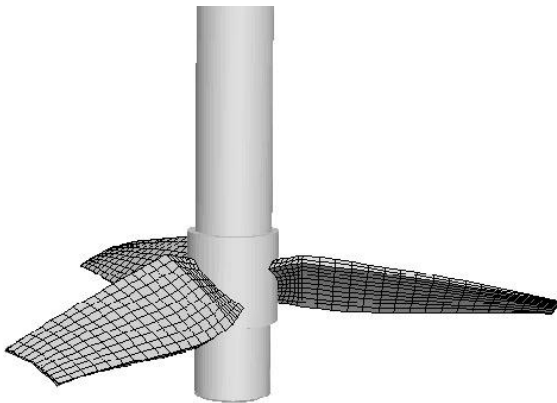
Table 5-3 Results of the MRF Impeller Model with Several Turbulence Models as Compared to Experiment

Turbulence Model	N_Q	N_P
Experiment ^a	0.56	0.30
Standard $k-\epsilon$	0.50	0.30
RNG $k-\epsilon$	0.53	0.28
Realizable $k-\epsilon$	0.52	0.29
RSM	0.51	0.29

^aExperimental data provided by the impeller manufacturer.



(a)



(b)

Figure 5-10 (a) Tank containing a Lightnin A310 impeller. (b) Grid detail for the impeller surface.

5-5.3 Sliding Mesh Model

The sliding mesh model is a time-dependent solution approach in which the grid surrounding the rotating component(s) physically moves during the solution (Figure 5-12). The velocity of the impeller and shaft relative to the moving mesh region is zero, as is the velocity of the tank, baffles, and other internals in

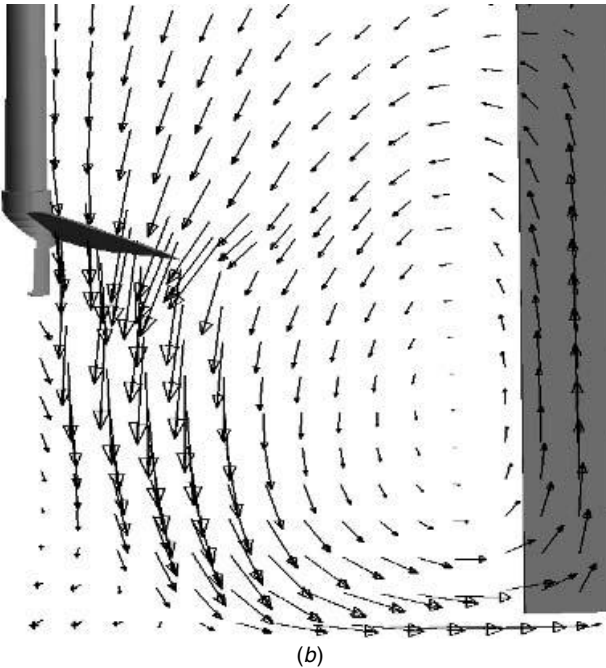
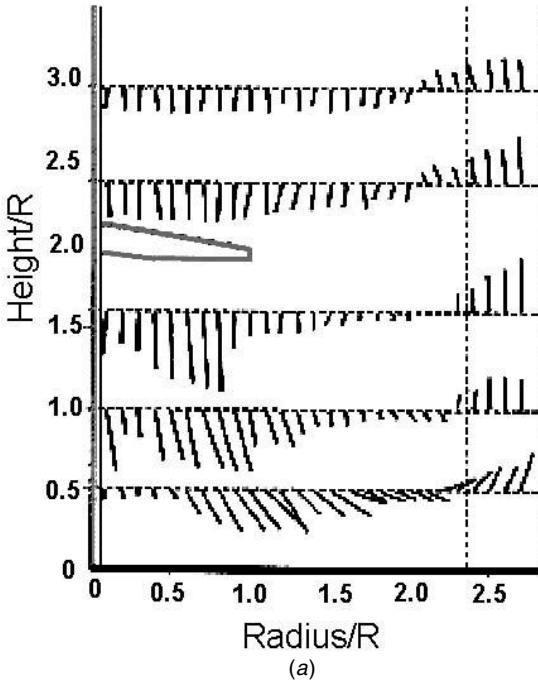


Figure 5-11 (a) Experimental data from Weetman (1997). (b) CFD solution using the MRF model for the impeller and RSM for turbulence.

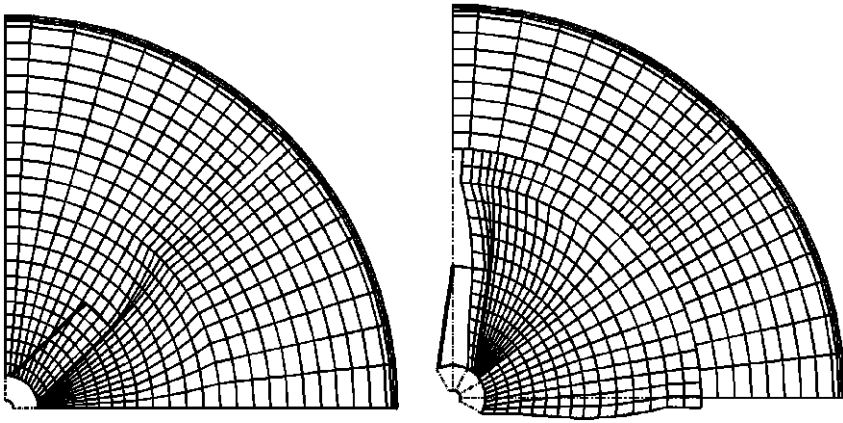


Figure 5-12 Sliding mesh in two orientations (shown in 2D).

the stationary mesh region. The motion of the impeller is realistically modeled because the grid surrounding it moves as well, giving rise to a time-accurate simulation of the impeller–baffle interaction. The motion of the grid is not continuous. Rather, it is in small, discrete steps. After each such motion, the set of conservation equations is solved in an iterative process until convergence is reached. The grid moves again, and convergence is once again obtained from an iterative calculation. During each of these quasi-steady calculations, information is passed through the interface from the rotating to the stationary regions and back again.

In order to rotate one mesh relative to another, the boundary between the meshes needs to be a surface of revolution. When in its initial (unrotated) position, the grid on this boundary must have two superimposed surfaces. During the solution, one will remain with the rotating mesh region, and the other will remain with the stationary mesh region. At any time during the rotation, the cells will not (necessarily) line up exactly, or conform to each other. When information is passed between the rotating and stationary grid regions, interpolation is required to match each cell with its many neighbors across the interface.

The sliding mesh model is the most rigorous and informative solution method for stirred tank simulations. Transient simulations using this model can capture low-frequency (well below the blade passing frequency) oscillations in the flow field (Bakker et al., 2000; Roussinova et al., 2000) in addition to those that result from the periodic impeller–baffle interaction.

5-5.3.1 Solution Procedures. Because this is a transient model involving the motion of the impeller, starting the simulation with the impeller at rest is analogous to modeling startup conditions. After a period of time the flow field reaches periodic steady state, but this period of time may correspond to dozens of revolutions. If the goal of the simulation is to study the periodic steady-state conditions, minimizing the time spent reaching this state is desirable.

One way to pass through the startup conditions rapidly is to move the impeller by large increments each time step in the early stage of the calculation. If the model is a 90° sector, for example, the first few revolutions of the impeller can be modeled using a coarse time step that corresponds to a 30° displacement. The time step can then be refined to correspond to a 10° displacement, and refined again (and again) until the desired temporal and spatial accuracy is achieved. The solutions during these initial coarse time steps do not need to be converged perfectly, provided that the simulation involves a single fluid phase and there are no inflow and outflow boundaries. In these instances, improved convergence can be obtained in the later stages of the calculation.

An alternative way to bypass calculation of the startup period is to solve for a steady-state solution first using the MRF model. The MRF model (Section 5-5.2) provides a solution for the moving impeller at a fixed orientation relative to the baffles. Tools are available in commercial codes to use the solution data from the MRF simulation and apply it to the sliding mesh simulation as an initial condition. A moderately coarse time step can be used initially (say, corresponding to a 10° rotation, as in the example above) and reduced at a quicker rate than would otherwise be advisable. This approach can also be used if inflow and outflow boundaries are present or if a multiphase calculation is to be performed. In the case of multiphase flows, however, care must be taken to wait until the periodic steady-state condition has been reached before introducing the secondary phase.

5-5.3.2 Validation of the Sliding Mesh Model. One validation of the sliding mesh model was presented in a paper by Bakker et al. (1997). A pitched blade turbine was operated in a baffled vessel with diameter $T = 0.3$ m under laminar conditions ($Re = 40$). The impeller diameter and off-bottom clearance were such that $D/T = C/T = 1/3$. A 90° sector of the stirred tank was modeled using approximately 50 000 cells.

Figure 5-13 shows a comparison between LDV data on the left and CFD results on a midbaffle plane on the right. Because the impeller was operating at a low rotational speed, its discharge was more radial than axial. This structure is captured by the CFD model, in agreement with the experimental data, where circulation loops above and below the impeller can be seen. Calculations for this system operating at higher Reynolds numbers through transition and into the turbulent regime were also performed. Results for the flow number (Section 5-6.4.2), computed throughout both laminar and turbulent regimes, are in excellent agreement with values based on LDV measurements, as shown in Figure 5-14.

5-5.3.3 Unstable Flows. In recent years, much attention has been paid to instabilities that are observed in stirred tanks. These instabilities typically have frequencies that are low compared to the impeller frequency and involve the slow asymmetric wobble of material or momentum from one side of the vessel to the other. Instabilities of this type can be predicted using the sliding mesh technique on a 360° model of a stirred tank, particularly if the LES turbulence model is

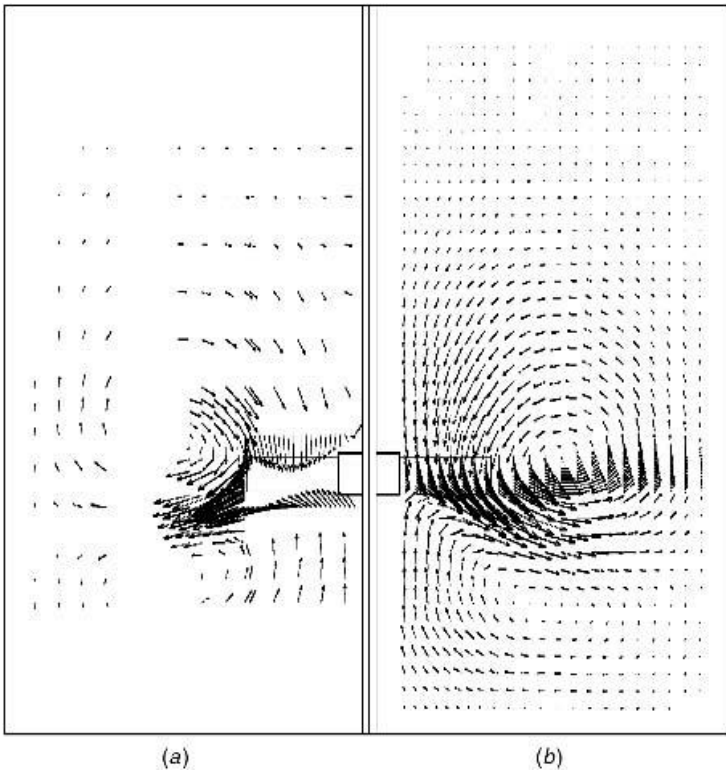


Figure 5-13 Comparison of (a) LDV data and (b) CFD sliding mesh results.

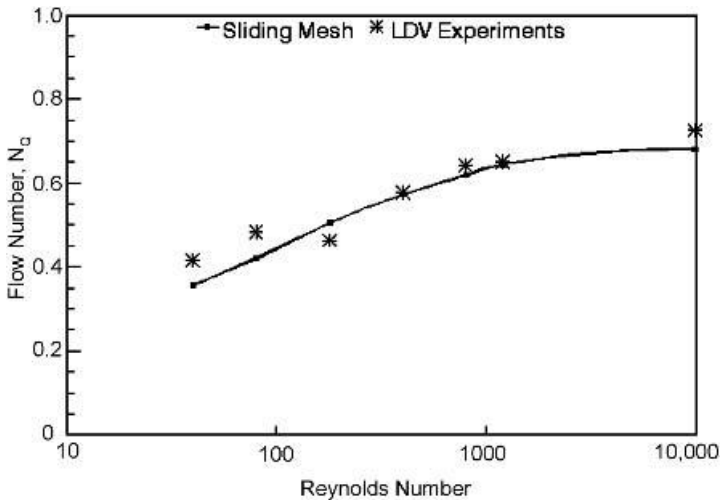


Figure 5-14 Flow number based on experimental measurements and computed by the sliding mesh model.

used (Bakker et al., 2000, 2001). Roussinova et al. (2001) showed exact agreement between the frequency predicted by LES simulations and low frequencies observed for a PBT impeller (see Chapter 2).

5-5.4 Snapshot Model

The snapshot model (Ranade and Dommeti, 1996) is a steady-state approach that captures the flow field at a single instant in time, when the impeller position relative to the baffles is fixed. When the impeller is rotating, the leading face of the blade exerts a force on the fluid in front of it and acts to push the fluid away. Behind the rotating blade, there is a void of low pressure, which acts to pull the surrounding fluid in. These two complementary functions can be represented as balanced mass sources in front of and in back of the impeller blade, and this premise is the basis of the snapshot model. A grid is built with the impeller in one position relative to the baffles, and a steady-state solution is performed. Mass sources in front of and behind the impeller blade are used to simulate the action of the impeller as if it were rotating. The flow field is therefore characteristic of a fully developed flow for a rotating impeller but is limited to a snapshot of the motion when the impeller is in the single position described by the model. Because the results are highly dependent on the accuracy of the source terms used, this approach, while offering 3D effects, has drawbacks similar to those of the velocity data model.

5-5.5 Combining the Geometric Impeller Models with Other Physical Models

The geometric impeller models described above can be used to model both steady-state and time-dependent processes, but attention must be paid to the timescales, where appropriate, and other special requirements of each. In this section, some of these considerations are reviewed for the two most popular of the geometric formulations: the MRF and sliding mesh models.

5-5.5.1 VOF Model. In stirred tank applications, the VOF model is useful for tracking the shape of the liquid surface during operation. Even though the steady-state shape of the surface is usually of interest, a transient VOF formulation is usually the best way to obtain it. With this in mind, either the steady-state MRF or transient sliding mesh model can be used for this purpose. If the MRF model is used, the gradual change in the free surface can be predicted using the VOF method. Note, however, that because the orientation of the impeller relative to the baffles is fixed, any irregularities in the free surface that result from the impeller rotation will not be captured. If these details are important, the sliding mesh model should be used.

When the VOF model is solved in conjunction with the sliding mesh model, the smallest required time step for the two models must be used. Since a smaller time step is often required for the VOF calculation than for the sliding mesh

calculation, this means that the motion of the impeller will advance in time at a slower rate than is necessary for a calculation involving the sliding mesh model alone. One way to circumvent this problem is to use the sliding mesh model to obtain periodic steady-state conditions using a single fluid first, and then introduce the second fluid with the VOF model and continue the transient calculation until a new periodic steady state is reached. For simple cases in which the free surface is axisymmetric, an implicit impeller model (using fixed velocity data) (Section 5-4) may be preferable for use with the VOF calculation.

5-5.5.2 Multiphase Model. Gas–liquid or liquid–solids mixtures can be solved using the Eulerian multiphase or ASM model in conjunction with either the sliding mesh or MRF model. Whereas the common goal of free surface modeling using VOF is to obtain the steady-state shape of the liquid interface, the goal of multiphase modeling can be to examine the unsteady behavior of the mixture as well as to predict the final settling of solids or final gas hold-up. The advantage of using the MRF model is that its steady-state basis can be combined with the time-stepping needed for complex multiphase flows. The disadvantage, however, is that the fixed orientation of the impeller blade with the baffles introduces error in the transient behavior by ignoring the impact of the impeller-baffle interaction on the flow.

For cases in which the transient behavior of the process is of interest, the sliding mesh model should be used instead. Here, the same issues apply that are important for VOF modeling. Generally speaking, a smaller time step is required for the Eulerian multiphase model than for the sliding mesh calculation. It is good practice to obtain a periodic steady-state solution of the single-phase liquid first using the sliding mesh model, prior to introducing the additional phases. The development of the solids suspension or gas hold-up can then be computed most accurately in the presence of the rotating impeller.

5-5.5.3 Turbulence. As discussed in Section 5-2, there are several steady-state turbulence models in widespread use today. These so-called RANS models address a time-averaged state of the fluid such that all turbulent fluctuations are represented by averaged values. The RANS models are often used with both the MRF and sliding mesh models, as well as with many other transient models used in CFD analysis. This practice is justified in part because the time scales of turbulence fluctuations are assumed small compared to those of the other processes being modeled, such as the blade passing time in a stirred tank. It has also been justified because until recently, other more rigorous treatments have not been available in commercial software or solvable in a realistic time on the computers of the day.

The large eddy simulation (LES) model (Section 5-2.1.3) is a fairly recent model to appear in commercial software. It offers considerably more rigor than the RANS models. It makes use of a steady-state model for the smallest turbulent eddies, but treats the large scale eddies in a transient manner. The use of LES is inconsistent with the use of the MRF modeling approach, because the approximation introduced with the MRF model is on a longer time scale than

the detail offered by the LES calculation. The use of LES with the sliding mesh model, on the other hand, is a powerful combination that has demonstrated great potential for capturing not just small scale fluctuations but large scale fluctuations as well, including instabilities with frequencies that are several times larger than the impeller rotation frequency (Bakker, 2001; Roussinova et al., 2001).

5-5.5.4 Species Transport. When the sliding mesh model is used, species blending can be tracked along with the transient motion of the impeller. The species is normally introduced after the system has reached periodic steady state, but need not be. If an inflow boundary is to be used for species calculations after periodic steady state has been reached, it should be assigned the velocity of the species jet (using the background fluid) during the startup period. One method that can be used to hasten the calculation during the startup period is to start with a solution based on the MRF model, as discussed in Section 5-5.3.1.

When the MRF model is used, transient species transport should be done with great care or avoided altogether. This is due to the fact that the velocities in the rotating frame, whether stored in the local or absolute frame, will give rise to erroneous behavior when they are used to convect a scalar in a transient manner. Graphical displays of the species distribution are suspect, even though the method can accurately capture the average species concentration as a function of time in the vessel as a whole.

5-5.5.5 Dispersed Phase Particle Tracking. The dispersed phase model, discussed in Section 5-2.2.2, allows for the coupled motion of a particle, bubble, or droplet stream with the fluid phase. When used with the sliding mesh model, the trajectories are computed in segments, with one segment per time step. The solver must ensure that the total time of each trajectory segment does not exceed the duration of the time step. If this condition is met, the particles can cross the sliding mesh interface without any incompatibility in the assumptions of either model. When combined with the MRF model, however, the implementation must be able to incorporate the particle motion in the rotating frame as well. Although there are techniques for doing so, it is not clear that the results are meaningful in all reference frames. This combination of models should therefore be avoided.

5-6 EVALUATING MIXING FROM FLOW FIELD RESULTS

Although there are numerous options for simulating the fluid flow inside a stirred tank, the goal of the simulation is to learn about the various aspects of the flow field. On a simple level, this might include velocity vectors in one or more regions, path lines followed by infinitesimal fluid elements as they wind their way through the vessel, or the distribution of a tracer species after some period of time has passed, for example. On another level, the analyst might want to

understand the power requirements for the motor, the time required to achieve adequate blending, or the fate of vortices trailing from the edges of the impeller blades. This type of information and more can generally be extracted from the CFD results or can be obtained from auxiliary CFD calculations based on those results. To illustrate how, we present summaries and examples in the following sections, designed to provide an overview of several of the methods used to make CFD analysis of mixing a meaningful endeavor.

5-6.1 Graphics of the Solution Domain

A stirred tank can be displayed in a number of ways to illustrate the relevant features of the vessel and its internals. These are described below.

5-6.1.1 Geometry Outline. Perhaps the simplest method for displaying the vessel is to draw an outline of the geometry. An outline consists of the features of the tank and internals, but little else. For 2D simulations, either a side view or dotted lines (or both) can be used to represent the impeller and the location where the experimental data are applied to represent it. For 3D simulations modeled using the explicit geometry, all edges are shown.

5-6.1.2 Surfaces. In addition to the features shown in an outline, the surfaces can also be drawn. If solid surfaces are used for the tank, the viewer cannot see inside unless the viewpoint is through an opening in the side or the top (Figure 5-15). Alternatively, solid surfaces can be used for the internals, and translucent surfaces can be used for the vessel walls (Figure 5-10*a*). When displayed with lighting, the image can accurately convey the 3D nature of the entire geometry.

5-6.1.3 Grids. For 2D simulations, a display of the grid (Figure 5-1*b*) is an excellent way to illustrate the potential level of accuracy in the solution. Despite having a deeply converged solution, a coarse grid cannot deliver accuracy on a scale any finer than the grid itself. A fine grid, however, has the potential to deliver a much better resolved flow field, assuming that the solution is converged adequately. Most grids are nonuniform, with fine and coarse grid regions that show the areas where the most (and least) accurate details can be expected. For 3D simulations, displays of the grid are more difficult to do in a meaningful way. When the grid is structured, a single grid plane can be displayed. In addition to showing the distortion in the grid (if the grid plane is distorted), this type of display can also show fine and coarse grid regions. For unstructured grids, single grid planes do not exist. A cut through the solution domain on, say, a surface of constant x -value, shows the cross-section through a number of cells and is not necessarily helpful. A more common approach is a display of the surface grid in 3D simulations (Figure 5-10*b*). If the surface grid is fine (or coarse) in a region,



Figure 5-15 Geometry using solid surfaces with a cut in the wall and top to look inside.

the chances are good that the volumetric mesh in that region is fine (or coarse) as well.

5-6.2 Graphics of the Flow Field Solution

There are many ways to examine the flow field results, some of which are described below.

5-6.2.1 Velocity Vectors. Velocity vectors can be used to illustrate the magnitude and direction of the flow field throughout the solution domain. For 2D simulations, a plot of all velocity vectors gives an overall picture of the fluid behavior. For 3D simulations, a plot of all vectors in the domain is too crowded to be useful. Vectors need to be plotted on one or more planes or surfaces instead, as shown in Figure 5-11*b* and again in Figure 5-13. Note that the planes can be

single grid planes (e.g., $J = 10$) or Cartesian grid planes ($x = 3.5$ m). Surfaces can be planar or nonplanar, such as a surface of constant temperature or a surface of constant radius. The important point is that for vector plots to be meaningful, the vectors (with length and orientation) need to be clearly visible, so the surfaces or planes used to plot them need be chosen accordingly.

5-6.2.2 Streamlines. In 2D simulations, a quantity called the *stream function*, ψ , is defined in terms of the density and gradients of the x- and y-components of the velocity, U and V . In terms of cylindrical coordinates, which are most appropriate for axisymmetric stirred tank models, the definition takes the form

$$\rho U = \frac{1}{r} \frac{\partial \psi}{\partial r} \quad \text{and} \quad \rho V = -\frac{1}{r} \frac{\partial \psi}{\partial x} \quad (5-41)$$

where U and V are the axial and radial components of velocity. The stream function is constant along a streamline, a line that is everywhere tangent to the velocity field. When defined in the manner above, ψ incorporates a statement of conservation of mass. The difference between the stream function defined on any two streamlines is equal to the mass flow rate between the streamlines. Thus when a pair of streamlines has close spacing, the implication is that the velocity is greater than when the same pair has wide spacing, since the same amount of mass must pass through the space between the lines. Streamlines therefore have the ability to convey not only the relative movement of the flow, but the relative speed as well. In Figure 5-16, streamlines in a 2D simulation of a stirred tank

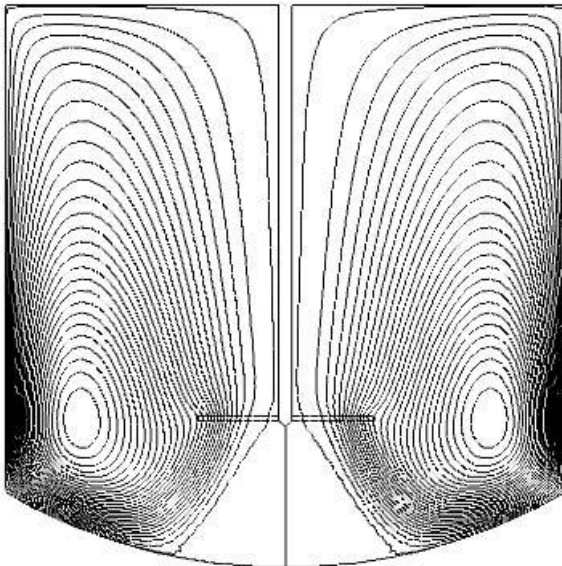


Figure 5-16 Streamlines for a 2D simulation of a pitched blade impeller with a single recirculation zone showing high- and low-speed regions.

are close as they pass through the impeller, where the boundary conditions are imposed and the flow speed is high. They are also close along the outer wall, but are more widely spaced elsewhere, where the flow recirculates in a larger area at a much slower speed.

5-6.2.3 Path Lines. Since the stream function is defined only for 2D flows, an alternative method is needed to visualize 3D flows in the same manner. Path lines can be used for this purpose. Path lines follow the trajectories that would be followed by massless particles seeded at any location within the domain. These particles move with the flow field and leave behind tracks in one form or another that allow the flow field to be visualized. In Figure 5-17, path lines are used to illustrate the flow through a static mixer. Path lines can be drawn as simple lines or as tubes, ribbons, or a series of dots. They can usually be colored by problem variables, such as temperature. When colored by time, they give information on residence time if inflow and outflow of fluid are involved.

5-6.2.4 Contours. Contours are lines where a chosen variable has a constant value. The streamlines illustrated in Figure 5-16 are actually contours of stream function, since ψ is constant on each of the lines shown. In addition to line contours, filled contours, plotted on an entire 2D domain or on a surface in a 3D domain, are also very useful for showing the maximum and minimum values as well as local gradients. In Figure 5-18, contours of a tracer species are shown on a cross-section through a 3D domain.

5-6.2.5 Isosurfaces. Isosurfaces in 3D flow fields are analogous to contour lines in a 2D flow field. These 3D surfaces are constructed in such a way that a particular variable has a constant value everywhere on it. If the isosurface has a constant value of the Cartesian coordinate x , for example, it is planar. If it

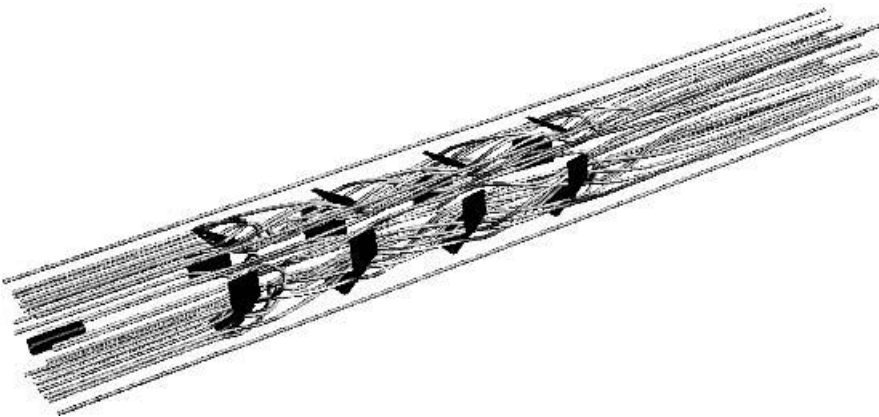


Figure 5-17 Path lines, colored by velocity magnitude, illustrating the flow through an HEV static mixer.

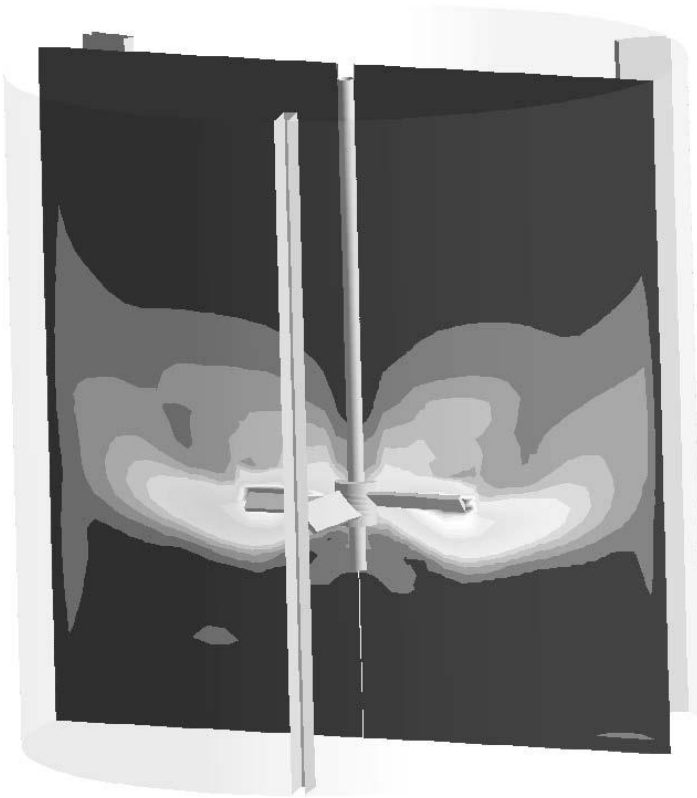


Figure 5-18 Filled contours of a tracer species shown on a planar surface in a 3D domain.

has a constant value of velocity in a stirred tank, it is complex in shape and can have several disconnected regions. Isosurfaces of this type can be plotted as solid surfaces with lighting (Figure 5-19), to convey the 3D nature of the variable distribution. They can also be used to plot contours, showing how one variable changes as another one is held fixed.

5-6.2.6 Particle Tracks. Whenever the discrete phase model is used (Section 5-2.2.2), particle tracks can be used to illustrate the trajectories of the particles, bubbles, or droplets. Trajectories can usually be displayed in a number of ways. For example, lines can be colored by the time of the trajectory or temperature of the particle itself. In addition to lines, ribbons and tubes can generally be used. The tracks can be computed and displayed using the mean fluid velocities, or in the case of turbulent flows, using random fluctuations in the mean fluid velocities as well. These *stochastic tracks* often give a more realistic picture of the extent to which the particles reach all corners of the solution domain than do tracks computed from the mean velocities alone.

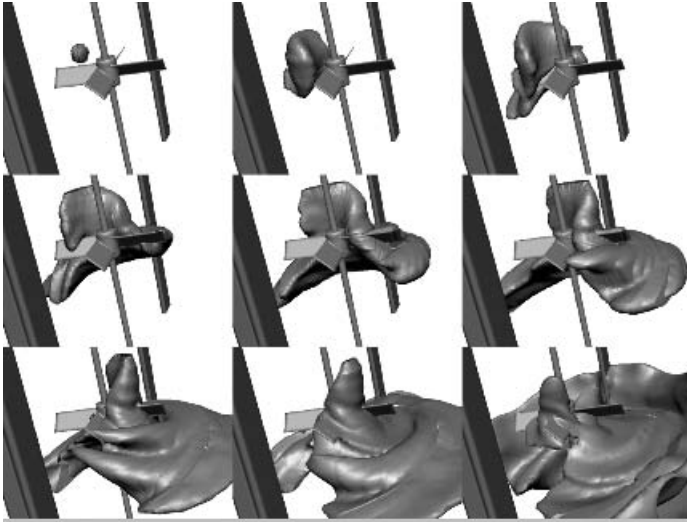


Figure 5-19 Dispersion of a tracer in a stirred tank. A blob of tracer is injected at time zero, and its dispersion is shown after $\frac{1}{4}$, $\frac{1}{2}$, $\frac{3}{4}$, 1, $1\frac{1}{4}$, $1\frac{1}{2}$, $1\frac{3}{4}$, and 2 impeller revolutions, respectively.

5-6.2.7 Animations. Animations can be created from groups of image files that follow a process from beginning to end, or during some period of operation. They can also be used to follow the motion of massless particles in a steady-state flow field. Numerous postprocessing packages are commercially available for the creation of animations, and many CFD packages have built-in functionality to do so as well.

Types of Animations. Some examples of how animations can be used for displaying flow field results are described below. In general, anywhere from 20 to hundreds of images or frames can be created and concatenated, or joined together to form the animation. The content of these images depends on whether the simulation is steady-state or time-dependent, and what the display goals are intended to be. In general when creating animations, care should be taken to avoid incorporating too much information into a single image, since some of this information will inevitably be lost on the viewer.

Time-Dependent Simulations. For time-dependent flow fields, images should be made at uniform time intervals for the purpose of creating a meaningful animation. Examples of time-dependent animations include

- Contours of tracer concentration on a single plane during blending
- Velocity vectors on a plane during a turbulent simulation modeled using large eddy simulation
- Gas from a sparger filling a stirred tank or a bubble column

- Lifting and suspension of solids off the vessel floor in a stirred tank
- Isosurfaces of vorticity trailing from a rotating impeller in a sliding mesh model

Path Lines. Path lines are normally created by a simultaneous calculation and display of trajectories, using the problem geometry and flow field data. To generate an animation of evolving path lines, frames of the trajectories at intermediate stages need to be created and stored. To do this, a total time for the animation needs to be determined along with a number of frames to be made. Tools are available in most visualization packages to generate the intermediate frames based on these inputs, using dots, lines, or other geometric entities. The intermediate frames can be written to files in one of a number of available formats. When played in succession, the concatenated frames will mimic the display that is generated by the original visualization software.

Moving Slice Planes. One method of illustrating the change in a variable throughout a 3D domain is through the use of animated slices. For example, in a stirred tank, the velocity field at different angular locations—from one impeller blade to the next or from one baffle to the next—might be of interest. Planar slices at equal angle intervals can be used for each frame, on which either contours or in-plane velocity vectors are displayed. A series of axial slices is another useful way to examine the change in a variable from one end of a mixer to another. This type of animation is particularly useful for static mixers.

Moving Isosurfaces. When injecting a tracer, one method of following its evolution is by animating isosurfaces of the tracer mass fraction. The animation is made most effective if the same numerical value is chosen for each frame. The value should be small in magnitude so that the expanding surface at later times can be captured. If the data for all times exist prior to the creation of the images, the data for the first and last times should be used to plan the best isosurface value to track for the duration of the process. When plotted as a solid surface with lighting, the 3D nature of the isosurface is easy to discern and the effect makes for an exciting and informative animation. The frames shown in Figure 5-19 are taken from an animation of this type.

Moving Impeller Blades. In stirred tank animations, it is always helpful if the motion of the impeller can be animated as well. This is possible in sliding mesh simulations, where the changing position of the impeller can be captured in successive frames. Some animation software can extract this motion from MRF simulation data, where the rotation speed of the impeller is known. Based on the time interval between frames, the impeller is advanced by a computed angle in each display created. When the frames are animated, a continuous motion of the impeller can be seen, along with other animated variables, such as path lines or changing contours on a stationary surface.

Moving Viewpoint. For steady-state external flows, animations based on a moving viewpoint are popular. These animations can also be used to illustrate the complex geometry of a system, such as a stirred tank and its internals. Beginning with a distant view, the camera can approach the object and peer inside to get close-up views of the components. For the Kenics static mixer described in Section 5-7.10, a sequence of frames representing equally spaced axial slices (Figure 5-29) can be used to illustrate the progression of mixing as the fluid moves through the helical elements.

Creating Animations from a Collection of Images. Numerous commercial software packages are available for creating an animation from a collection of images. Different image file formats are available for this purpose. Once the images have been concatenated to form the animation, tools are available in most animation packages to set the speed of the animation. A choice of about 0.05 s between frames usually results in a smoothly playing animation, but this also depends on the number of frames and the capabilities of the computer. It should be noted that the time interval mentioned here refers to the playing time, not the physical time between the data used for each frame display.

5-6.3 Other Useful Solution Variables

In Section 5-6.2, methods of plotting several common solution variables, such as velocity, stream function, and species concentration, were discussed. Plots of turbulent kinetic energy and dissipation are also of interest in turbulent flows, especially if other processes, such as chemical reactions, are to take place. In multiphase flows, the volume fraction of the phases is the most useful tool to assess the distribution of the phases in the vessel. In this section, three additional quantities are reviewed that are derived from the velocity field. These can provide a deeper understanding of the flow field than can plots of the velocity alone.

5-6.3.1 Vorticity. Vorticity, a vector quantity, is a measure of the rotation of the fluid. In terms of a fluid element, a nonzero vorticity implies that the element is rotating as it moves. The vorticity is defined as the curl of the velocity vector, \mathbf{U} :

$$\xi = \nabla \times \mathbf{U} \quad (5-42)$$

Vorticity can be defined in both 2D and 3D flows. In 2D flows, the direction is normal to the plane of the simulation. This means that for a 2D axisymmetric simulation of flow in a stirred tank, the vorticity is always in the circumferential direction:

$$\xi_{\theta} = \frac{\partial U_x}{\partial r} - \frac{\partial U_r}{\partial x} \quad (5-43)$$

In 2D simulations, positive values indicate counterclockwise rotations, while negative values indicate clockwise rotation. In a 3D simulation, vorticity can take on any direction, and plots of vorticity magnitude, rather than the individual

components, are often the most helpful. The units of vorticity are s^{-1} , the same as those used for shear rate. In Figure 5-20a, contours of vorticity are shown for a 2D flow in a stirred tank with velocity vectors superimposed on the display. White regions (near the impeller) have a maximum positive value, and black regions (near the walls) have a maximum negative value. These regions are those where steep normal gradients occur in the velocity. The fact that the vorticity is positive near the impeller and negative near the wall indicates simply that the direction of the curl is opposite in these two regions. In Figure 5-20b, isosurfaces of constant vorticity magnitude in a 3D simulation show the trailing vortices behind a Rushton impeller. The simulation was performed using the LES turbulence model.

5-6.3.2 Helicity. The helicity is defined as the dot product of the velocity vector with the vorticity vector:

$$\mathbf{H} = \mathbf{U} \cdot \boldsymbol{\xi} = \mathbf{U} \cdot (\nabla \times \mathbf{U}) \quad (5-44)$$

Clearly, the helicity has a value of zero in 2D simulations. In 3D simulations, it gives an indication of how well the local rotation of a fluid element is aligned with the velocity of the element. It is useful for illustrating longitudinal vortices, or spiral motion, as is often found in vortex cores. In Figure 5-21, isosurfaces of helicity are used to depict the longitudinal vortices generated in the Kenics static mixer described in Section 5-7.10.

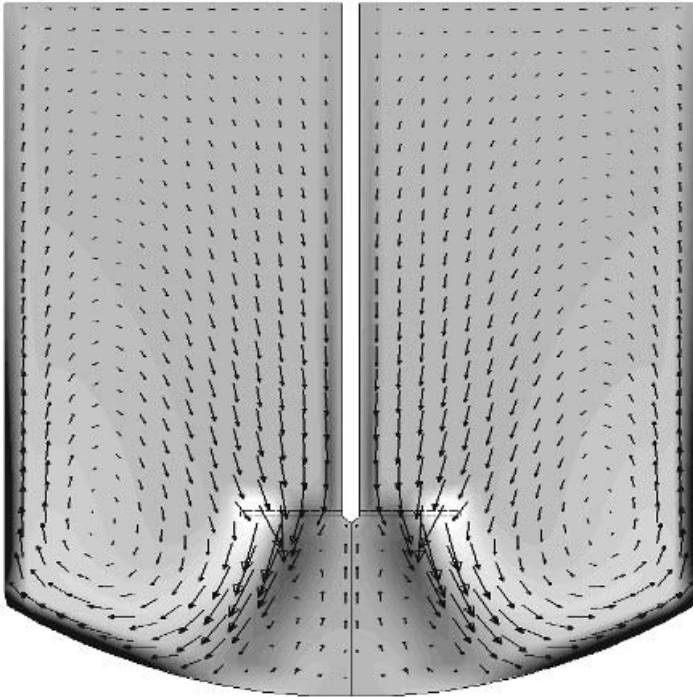
5-6.3.3 Rate of Deformation. The rate of deformation or strain rate tensor is a collection of terms that together describe the complete deformation of a fluid element in motion. The deformation can be the result of linear strain, which gives rise to a linear deformation or stretching of the element, and shear strain, which gives rise to an angular deformation or change in shape of the element. The symmetric tensor has components of the generalized form

$$S_{ij} = \frac{1}{2} \left(\frac{\partial U_i}{\partial x_j} + \frac{\partial U_j}{\partial x_i} \right) = S_{ji} \quad (5-45)$$

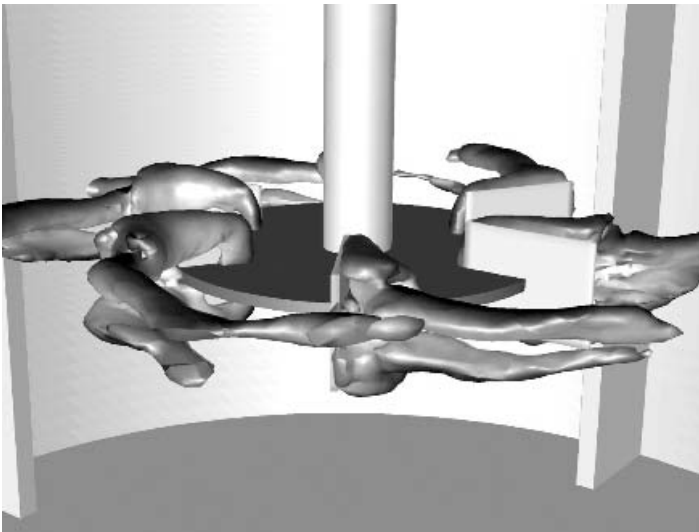
Although the tensor components themselves offer little insight into the behavior of the flow field, functions of the tensor components often do. In terms of the Cartesian coordinates x , y , and z , the diagonal terms are

$$S_{xx} = \frac{\partial U_x}{\partial x} \quad S_{yy} = \frac{\partial U_y}{\partial y} \quad S_{zz} = \frac{\partial U_z}{\partial z} \quad (5-46)$$

Each of these terms represents a linear strain rate or rate of elongation of the fluid element in each of the three coordinate directions. The sum of these diagonal terms is the *trace* or first invariant of the tensor. For incompressible fluids, this quantity is always zero, since the volume of the fluid element must be conserved.



(a)



(b)

Figure 5-20 (a) Contours of vorticity in a 2D simulation with superimposed velocity vectors. (b) Isosurfaces of vorticity magnitude behind a Rushton turbine.

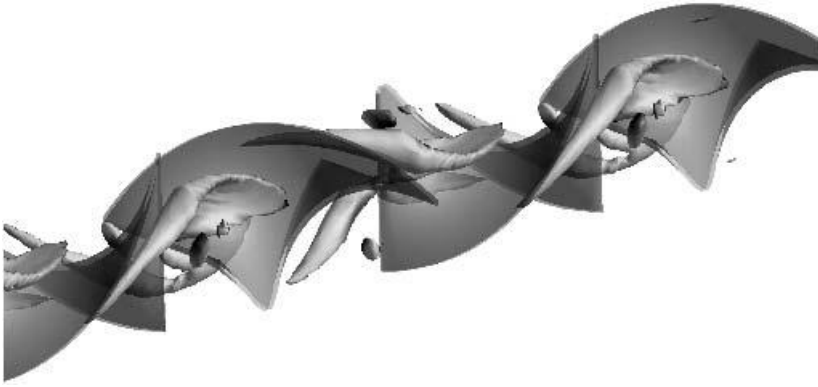


Figure 5-21 Isosurfaces of helicity are used to show the longitudinal vortices in a Kenics static mixer.

In addition to the trace, another quantity, often referred to simply as the *strain rate*, is of interest. The strain rate, taken from the modulus of the tensor, is a positive-definite representation of all possible components of the strain rate tensor. It is used to determine the viscosity in strain-dependent non-Newtonian fluids and is also helpful as a reporting tool for mixing applications. In particular, regions with a high strain rate play an important role in liquid dispersion.

5-6.4 Mixing Parameters

Parameters that are used to characterize stirred tank flows and mixing processes in general can be computed by correlations that can be found in the literature. In many cases, these parameters can also be computed from the CFD results. Examples of how to compute some of these parameters are given below.

5-6.4.1 Power Number. The *power number* is a dimensionless parameter that provides a measure of the power requirements for the operation of an impeller. It is defined as

$$N_p = \frac{P}{\rho N^3 D^5} \quad (5-47)$$

In eq. (5-47) P is the power applied to the impeller of diameter D , ρ the density, and N the impeller rotation speed in Hertz. Correlations are available that provide the dependence of N_p on the Reynolds number. Thus, if CFD is not available, the power requirements can generally be obtained from one of these correlations. The correlations can break down, however, if they do not address the D/T or C/T ratios of single impellers or the presence and spacing of multiple impellers. In such cases, CFD results can be used to compute N_p , or simply, the power requirements.

The power delivered to the fluid is the product of the impeller speed, $2\pi N$, in rad/s, and torque, τ , which is obtained by integration of the pressure on the impeller blade:

$$P = 2\pi N\tau \quad (5-48)$$

Reports are usually available for the torque delivered to the fluid by the impeller. In some cases, reports of power or even power number can be obtained from the software.

Integration of the Dissipation. In principle, the power delivered to the mixer is equivalent to that lost or dissipated in the fluid. An integration of both the viscous and turbulent dissipation throughout the volume should, therefore, be an acceptable way to compute the power draw. The dissipation rate predicted by the various turbulence models can vary significantly, however, and there is no guarantee that the turbulence model that gives the best flow pattern prediction also gives the best dissipation rate prediction. For laminar flows, even with a refined mesh near the impeller blades, CFD can have difficulty predicting viscous dissipation in a satisfactory manner. For this reason, the best method for extracting the power drawn by the impeller is by calculation of the torque on the blade surfaces.

5-6.4.2 Flow Number. The *flow number* is a measure of the pumping capacity of an impeller. Different measures for pumping capacity exist, but the flow number is used widely. It is defined as

$$N_Q = \frac{Q_\ell}{ND^3} \quad (5-49)$$

In this expression, Q_ℓ is the flow rate produced by the impeller. The subscript is used to ensure that the flow rate for the liquid phase alone is used in the calculation. To compute Q_ℓ for an impeller, a surface needs to be created for the discharge region. This surface would be circular for an axial flow impeller and a section of cylinder wall for a radial flow impeller. By integrating the total outflow through this surface, the flow rate, Q_ℓ , and subsequently the flow number, N_Q , can be obtained.

5-6.4.3 Evaluating Mixing Time. A transient blending calculation is the best method for determining the time required to achieve a certain level of blending. When a tracer is added to a fluid in a mixing tank, the transient calculation can be made exclusive of the flow field calculation if the properties of the tracer and background liquid are identical. When this is the case, a steady-state calculation can be performed for the background liquid using either experimental data or the MRF method, although care should be exercised when using the latter, as discussed in Section 5-5.5.4. If inflow and outflow ports are to be used, the simulation of the background liquid alone should include the inflow boundary conditions for velocity that will ultimately be used for the tracer. Once the

flow field for the background fluid is satisfactorily converged, the tracer can be introduced. Since the mixture fluid properties will not change with the addition of the tracer, the transport equations for momentum, continuity, and turbulence can be disabled while the transient species calculation takes place. The transient solution of this single scalar equation will be robust (since it is not coupled to other variables that are in a state of change) and economical, advancing rapidly with few iterations required each time step. Averages of the tracer concentration, along with standard deviations, can be computed throughout the vessel to determine when the tracer has become fully blended.

There are two exceptions to the use of the method described above, in which the flow field calculation can be disabled during the species calculation. First, if the sliding mesh model is used, the flow field data are required for each time step, so it is not possible to disable the flow field calculation to perform the species transport calculation. Second, if the tracer is to be added through an inlet or dip tube for a finite period of time, after which the inlet flow is disabled, calculation of the flow field should resume at that time, especially if the inlet delivers a jet of significant momentum to the vessel.

5-6.4.4 Information from LES Simulations. Large eddy simulations are transient simulations designed to capture the fluctuations that are the result of turbulent eddies. For this reason, LES images and animations have the potential to capture small and large scale activity that would otherwise be averaged to zero with a RANS turbulence model. Some of the small scale activity includes the birth and death of eddies or small vortices. Some of the large scale activity includes low-frequency instabilities in stirred tanks. A common way to visualize the turbulent structure present in LES simulations of mixers is by animating vectors or isosurfaces of vorticity magnitude.

5-7 APPLICATIONS

To illustrate the successful application of CFD to many types of process equipment, a number of examples are presented in this section. Unless otherwise noted, these simulations were performed with software from Fluent Inc.

5-7.1 Blending in a Stirred Tank Reactor

Mixing time correlations for stirred tank reactors are available, but these are often difficult to extend outside the experimentally studied parameter range. One advantage of CFD is that it can be used to evaluate industrial sized equipment or equipment for which no correlations are available. A comprehensive evaluation of the accuracy of mixing time predictions using CFD was presented by Oshinowo et al. (1999). The main conclusion drawn was that although unsteady tracer dispersion predictions based on a steady-state flow field are acceptable, the accuracy of the predicted mixing time is greatest when the mixing simulation is based on a

time-dependent calculation, using the sliding mesh model. For the latter method, either the LES model or a standard turbulence model such as RSM may be used.

Figure 5-19 shows an example of the dispersion of a chemical tracer in a stirred tank. A standard pitched blade turbine is used to mix two waterlike materials. The neutrally buoyant tracer is injected at time zero as a blob above the impeller, as shown on the top left in the figure. The flow field is calculated using the sliding mesh and LES models, and the dispersion of the tracer is derived from the flow field. The blob is stretched and the chemical is mixed with the rest of the fluid over time. It is interesting to see that despite the fact that there are four impeller blades and four baffles, the concentration field is not symmetric because of the off-axis injection. The consequence is that the full tank needs to be modeled instead of a 90° section. Bakker and Fasano (1993b) presented a successful comparison between blend time predicted by CFD and calculated from experimental correlations.

5-7.2 Chemical Reaction in a Stirred Tank

The blending of chemical reactants is a common operation in the chemical process industries. When a competitive side reaction is present, the final product distribution is often unknown until the reactor is built. This is partly because the effects of the position of the feed stream on the reaction by-products are difficult to predict. In this example from Bakker and Fasano (1993), the product distribution for a pair of competing chemical reactions is calculated with CFD and compared with experimental data from the literature. The model used here is a slightly modified version of the standard Magnussen model discussed in Section 5-2.2.1.

The following competitive-consecutive reaction system was studied:



This is the reaction system used by Bourne et al. (1981) and Middleton et al. (1986). The first reaction is much faster than the second reaction: $K_1 = 7300 \text{ m}^3/\text{mol} \cdot \text{s}$ versus $K_2 = 3.5 \text{ m}^3/\text{mol} \cdot \text{s}$. The experimental data published by Middleton et al. were used to determine the Magnussen model constants. Two reactors were studied, a 30 L reactor equipped with a $D/T = \frac{1}{2}$ Rushton turbine and a 600 L reactor with a $D/T = \frac{1}{3}$ Rushton turbine. In the CFD analysis, a converged flow field was computed first for each reactor, using experimental data for the impeller boundary conditions. The reactants A and B were then introduced to the tank on an equimolar basis. The reactant A was assigned a weak but uniform concentration throughout the vessel. The reactant B was added in a high concentration in a small region. The calculation of the flow field variables was disabled after the addition of the reactants, and the species calculations alone

were performed. Once the solution converged, the product distribution X_S was calculated using

$$X_S = \frac{2C_S}{C_R + 2C_S} \quad (5-51)$$

In the reaction model used here it was assumed that small scale mixing affected only the first reaction and that once this reaction had occurred, the species were locally well mixed. As a result, small scale turbulent mixing did not affect the second reaction. This was achieved by using different values of the Magnussen model constants for the two reactions.

Figure 5-22 shows a comparison between the experimental data from Middleton et al. and the CFD predictions for both reactors. The product distribution, X_S , is plotted as a function of impeller speed, in rpm. This graph shows that the model predicts the effects of scale and impeller rotational speed correctly and is usually within 10% of the experimental results. The effect of the inlet position of the feed stream on the formation of the by-product, S, was also studied. Figure 5-23 shows values of X_S for various feed locations. X_S varies only slightly when the inlet is located in the fluid bulk. However, when the feed is injected directly above the impeller, such that the feed stream passes immediately through the highly turbulent impeller zone, local mixing is much faster and does not limit the rate of the first reaction. As a result there is less reaction by-product, S, and the final X_S is only 50% of what it would be if the feed were located away from the impeller. This qualitatively agrees with the experimental results of Tipnis et al. (1993), who used a different set of reactions and tank geometries but also found that injection near the impeller resulted in a lower X_S value than

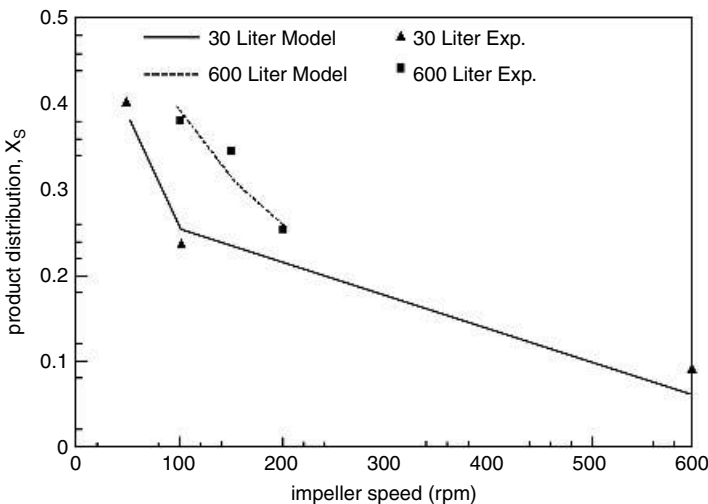


Figure 5-22 Product distribution, X_S as a function of impeller speed (rpm) for two vessels of different size, with the second reactant being added in the outflow of the impeller. Model predictions are compared with data from Middleton et al. (1986).

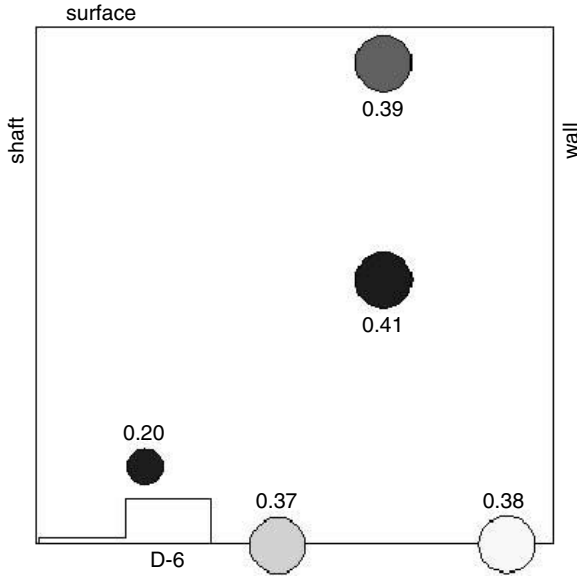


Figure 5-23 Product distribution X_S as a function of feed location for a 600 L vessel with a Rushton turbine operating at 100 rpm. The product distribution is reduced by about a factor of 2 when the feed is positioned directly above the impeller.

injection farther away from it. The relative differences found by Tipnis et al. are similar to those shown in this example. The effect of mixing on reaction is discussed further in Chapters 13, 17, and 2.

5-7.3 Solids Suspension Vessel

Stirred tanks for solids suspension applications have traditionally been designed using the just suspended impeller rotational speed, N_{JS} . Although much work about solids suspension has been published, most of it concentrates on providing correlations for the just suspended speed. Attempts to develop mathematical models for the solids suspension process are often based on the total power draw of the impeller, or the average liquid velocity in the tank, without taking local effects into account. The effect of the flow pattern on the spatial distribution of the solids has received relatively little attention. It is now known that the solids spatial distribution is strongly affected by the number of impellers, their location, and certain flow transitions. When either the D/T or C/T ratios are too large, a flow transition with reversed flow at the vessel base may occur. This results in an undesired increase in the power needed to suspend the solids, or more simply, N_{JS} .

Adding a second impeller typically has a very small effect on the just-suspended speed. In multiple-impeller systems, zoning occurs when the impeller separation is too large. The most efficient solids mixing occurs just before the

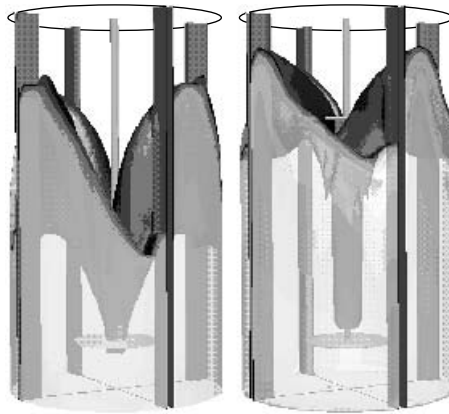


Figure 5-24 Solids suspension in a tall vessel. The solids distribution with a single impeller is shown on the left, and with a dual-impeller system is shown on the right.

flow between the impellers separates. Unfortunately, designing on the basis of the just suspended speed or on the basis of power consumption does not necessarily lead to an optimum multiple-impeller system. Figure 5-24 shows a comparison of the solids distribution for a single (left)- and a dual (right)-impeller system in a tall stirred tank, modeled using experimental data for the impellers and the Eulerian granular multiphase model for the solids suspension (Oshinowo et al., 2000). The results on the left show that in a tall tank equipped with a single impeller, the solids do not move up higher than about half the liquid level. When a second impeller is added, however, such that one long flow loop is formed, the solids reach the level of the second impeller, as shown on the right. When the second impeller is placed too far above the first impeller and zoning occurs, the solids do not reach the upper impeller (not shown; see Bakker et al., 1994b). From the differences between the solids suspension performance of these two configurations it can be concluded that consideration of the just suspended speed or power draw alone does not necessarily lead to the best design. The impeller system has to be designed so that it provides the optimum flow pattern for the suspension duty to be performed. To design such a system, the effects of the flow pattern on the solids distribution must be taken into account. Computer simulation provides an excellent tool for this purpose.

5-7.4 Fermenter

Large scale fermenters are used to make such products as yeast, vitamin C, xanthan gum, citric acid, and penicillin, for example. Fermentations are usually carried out in tall vessels with multiple-impeller systems. Air is sparged in at the bottom to provide the microorganisms in the vessel with a supply of oxygen. It is important that the mixer disperse the gas into fine bubbles, a condition that is required to ensure good mass transfer from the air to the broth. See Chapter 11

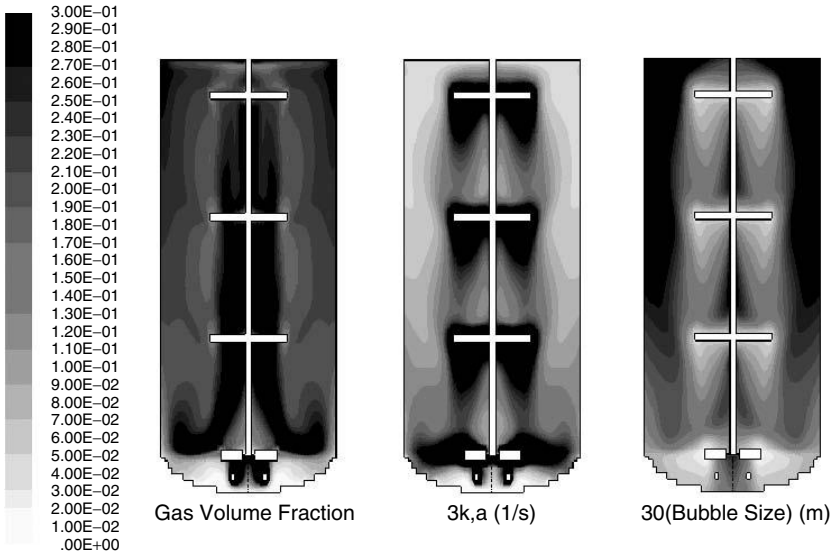


Figure 5-25 The local gas volume fraction (left), the local mass transfer coefficient k_1a (center), and the local bubble size (right). The bubble size is smallest near the impellers (white) and increases away from the impellers, due to coalescence. The mass transfer coefficient is highest near the impellers (black) because this is where the bubble size is small (leading to a large interfacial area) and where the turbulence intensity is high (leading to fast surface renewal around the bubbles).

for further discussion of gas dispersion and mass transfer, and Chapter 18 for a discussion of mixing in biological applications.

Figure 5-25 shows the results of a gas dispersion simulation of a fermenter. The fermenter is equipped with a radial flow CD-6 impeller with concave blades at the bottom, and three down-pumping HE-3 impellers on top. The vessel has no baffles but is equipped with 12 sets of eight cooling coils, which also act as swirl suppressors. Flow field simulations can be performed to design the impeller system such that there is sufficient liquid movement around these coils.

The gas–liquid simulations shown here were performed with software developed by Bakker (1992), which contains models for gas dispersion, bubble coalescence and breakup, and interphase mass transfer. The local gas volume fraction is shown on the left. The local mass transfer coefficient k_1a (with values multiplied by 3) is shown in the middle, and the local bubble size (with values multiplied by 30) is shown on the right. All figures share the same scale from 0 to 0.3 (which is why the mass transfer coefficient and local bubble size distributions are multiplied by a factor). The bubble size is smallest near the impellers and increases away from them, due to coalescence. The mass transfer coefficient is highest near the impellers, where the bubble size is smallest (leading to a large interfacial area) and where the turbulence intensity is highest (leading to fast surface renewal around the bubbles). The stair-stepped representation of the

curved vessel bottom was necessary using the software available at the time of this simulation. Rectangular cells have become obsolete with the introduction of boundary-fitted cells and unstructured grids.

5-7.5 Industrial Paper Pulp Chests

One example of a difficult mixing problem is found in the paper industry. Paper pulp, which is a suspension of thin, flexible fibers, exhibits a very complex rheology. As a result, multiple flow regimes are found in paper pulp storage tanks, or chests, which can be rectangular or cylindrical in shape. Laminar flow is common in some parts of the chest, while turbulent flow is common in others. The bottom of the chest is usually filleted, and either sloped, curved, or both. Although paper pulp chests are sometimes equipped with top-entering agitators, the preference in the paper industry is to use side-entering agitators.

The rheological properties of fiber suspensions are discussed in a paper by Gullichsen (1985). The fiber suspension initially behaves as a non-Newtonian fluid with a yield stress τ_y . Above τ_y the paper pulp behavior is non-Newtonian. When the shear stress exceeds a second threshold value, τ_d , the fiber network structure is disrupted and the suspension behavior is similar to that of a turbulent Newtonian fluid. As a result of this rheological behavior, fiber suspensions are extremely difficult to agitate. To provide motion through the whole tank, the shear stress has to exceed the yield stress everywhere in the fluid. Since gradients in the shear stresses can be expected, there will be regions in the fluid where the fiber network structure is disrupted and the flow is turbulent. At the same time the flow may be laminar or even stagnant in other parts of the chest. This combination of turbulent flow and laminar flow of a non-Newtonian fluid makes paper pulp storage chests difficult to model with CFD.

In an effort to address this problem, Bakker and Fasano (1993a) developed a model for the flow of paper pulp. To model the complex fiber suspension, the following method was used. For every computational cell, the computations are first performed as if the flow were turbulent. A check is then done to see if the total shear stress is indeed larger than τ_d . If this condition is not met, the calculations for that particular cell are repeated as if the flow were laminar. The local apparent viscosity is then calculated from the experimental shear stress versus shear rate curves and the local shear rate. The model has since been used successfully to predict the flow patterns in large industrial chests where zones with turbulent mixing, laminar mixing, and stagnant regions can easily be located. See Chapter 20 for additional discussion of mixing effects in the pulp and paper industry.

Figure 5-26 shows the flow pattern in one example of a stock chest for mixing and storage of paper pulp. The agitator is modeled using experimental data. The flow pattern with a solution of 1% pulp is shown in Figure 5-26 part (a); part (b) shows how the flow pattern changes when the concentration is increased to 5% and the same impeller speed is used. The results show that more power must be applied to maintain adequate flow conditions when the pulp concentration is

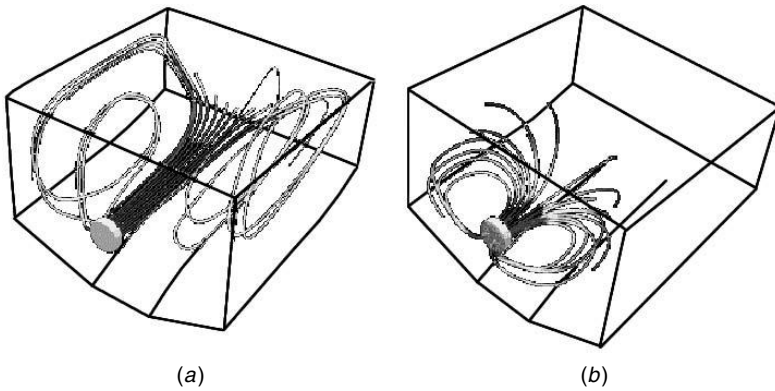


Figure 5-26 Flow pattern in a stock chest for the mixing and storage of paper pulp with (a) a solution of 1% pulp and (b) a solution of 5% pulp.

increased. The model is an excellent tool for the optimization of agitators for large industrial storage chests and has been used successfully over the years for many different paper pulp applications.

5-7.6 Twin-Screw Extruders

The twin-screw extruder is one of the most widely used tools, not only in the plastics and rubber industry but also in other areas, such as food processing. Single- and twin-screw extruders are used to melt, convey, compress, and mix the different compounds involved in any given process, and these steps can considerably affect the quality of the final product. This explains the large interest in screw analysis and, more specifically, the numerous attempts to model twin-screw extruders through numerical simulations. The challenges involved in such simulations (e.g., moving parts, thermal behavior, difficult meshing and remeshing tasks, and partial filling) often lead to many simplifications of the actual problem.

To ease the setup of a three dimensional unsteady twin-screw extruder, a technique referred to as *mesh superposition* (MST) has been developed (Avalosse and Rubin, 1999). This robust technique greatly simplifies the meshing of the geometric entities and does not present the complexities and limitations of other commonly used techniques. The transient algorithm was developed for 2D and 3D nonisothermal, generalized Newtonian fluids. It is designed to work with a finite element solver. A mesh is generated for each part of the flow simulation: one for the flow domain and one for each screw. The screws are assumed to be rigid and their motion is a combination of translation and rotation. At each time step the screw meshes are moved to a new position, overlapping the flow mesh. For each node of this new domain that lies within a given screw, a special formulation is used that imposes a velocity that matches the rotation speed of the screw. The movement of the screws imparts momentum to the surrounding

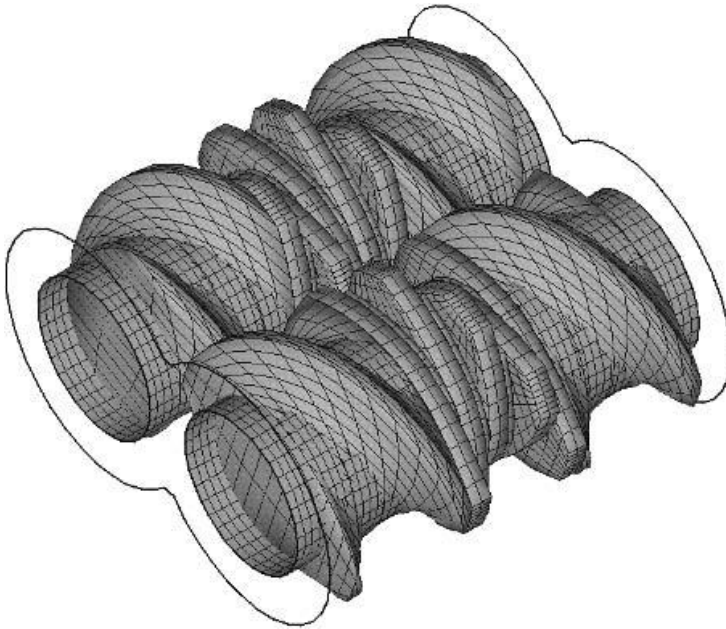
fluid. The flow is calculated in this manner for a set of successive screw positions at constant angular displacement. The history of the flow pattern is thus obtained and stored for further analysis. This application is discussed further in Chapter 16.

Figure 5-27*a* shows the grid for a typical twin-screw extruder. The grid in the screw regions is shown on the surfaces of the elements. The black lines show the outline of the region containing the fluid. Figure 5-27*b* shows the shear rate on a planar surface through the extruder. High shear rates are found near the tips of the extruder elements, as expected. This information is relevant when dealing with shear-sensitive materials. Other quantities of interest, such as residence time distributions, material thermal history, and stretching rates, for example, can also be obtained. This allows for a detailed comparison between alternative designs. For example, using this technique it was found that an extruder in which conveying elements were alternated with kneading elements provided 25% better mixing per unit length than a standard extruder that contained only conveying elements. The residence time distribution was narrower, however, with the standard design. Being able to obtain such detailed performance information without experimentation allows process engineers to design advanced and more efficient process equipment with confidence.

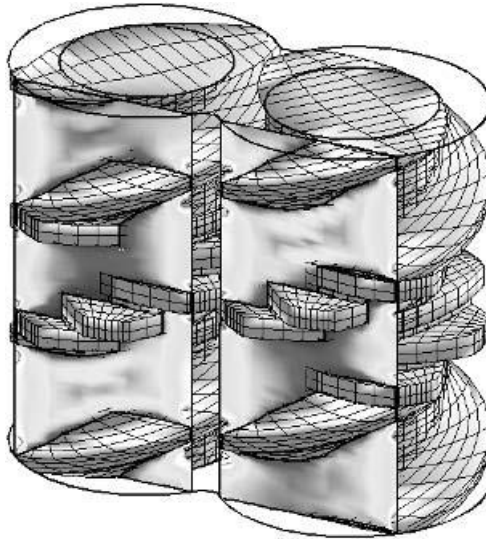
5-7.7 Intermeshing Impellers

The mesh superposition technique (MST) can also be used to model the flow in vessels equipped with multiple impellers whose swept volumes overlap. In this example, the mixing in such a system (a planetary mixer) operating at a very low Reynolds number (1×10^{-4}) is considered. Figure 5-28 shows two anchor impellers mounted on separate shafts. The impellers are set at a 90° angle relative to each other. Although the impellers do not touch each other, there is a volume that is swept by both impellers. Such a system cannot be modeled using the sliding mesh models implemented in most commercial CFD programs. The main benefits of using the mesh superposition technique for such a system are that each part can be meshed separately and that these intermeshing parts can rotate freely without having to be remeshed.

To create the mixer geometry, a cylindrical mesh is generated for the tank. Two other, completely independent meshes are defined for the blades. The three meshes are then combined into one. As the blades rotate, the transient flow pattern in the tank can be calculated and illustrated by the dispersion of tracer particles, as shown in the figure. As the total number of rotations increases, the tracer becomes more uniformly distributed. After six rotations, the dispersion of the tracer particles in the horizontal plane is satisfactory. Note, however, that the particles have moved little in the vertical direction. This is because the anchor impellers in use impart little or no axial momentum to the fluid. Twisted blades, which also impose an axial motion on the flow, might perform better to distribute the tracer throughout the vessel. The mesh superposition technique is well suited to study such systems. For other examples of flow in planetary mixers, see Tanguy et al. (1999) and Zhou et al. (2000).



(a)



(b)

Figure 5-27 (a) Surface grid for the screws in a twin-screw extruder. (b) Local shear rate on a planar slice through the twin-screw extruder, with white denoting regions of high shear rate and black denoting regions of low shear rate. Three meshes were used for this configuration, one for each screw and one for the flow domain.

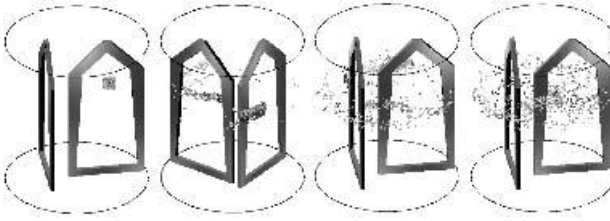


Figure 5-28 Dispersion of a particle tracer in a vessel equipped with two intermeshing anchor impellers, calculated using the mesh superposition technique. After six full rotations, the particles are well dispersed on the horizontal plane where they were released.

5-7.8 Kenics Static Mixer

Static mixers are used widely in the process industries. Static mixers consist of motionless elements mounted in a pipe, which create flow patterns that cause fluids to mix as they are pumped through the pipeline. Most of the experimental work on static mixers has concentrated on establishing design guidelines and pressure drop correlations. The number of investigations into the flow and mixing mechanisms is limited, probably due to difficulties encountered in obtaining meaningful experimental measurements.

The Kenics in-line mixer consists of a number of elements of alternating right- and left-hand 180° helices. The elements are positioned such that the leading edge of each element is perpendicular to the trailing edge of the preceding element. The length of the elements is typically one and a half tube diameters. This type of static mixer is used for mixing under laminar flow conditions, such as the mixing of polymers or food products like peanut butter and chocolate. To evaluate the mixing mechanism of the Kenics mixer, Bakker and Marshall (1992) and Bakker and LaRoche (1993) calculated the transport of two chemical species through a six-element device. The center of the inlet was 100% of one species, designated by white in Figure 5-29. The outside of the inlet was 100% of the other species, shown as black. The results are presented as a series of contour plots, showing the concentration fields of the chemical species at various axial positions along the tubes. The concentration fields after 18° , 54° , 90° , 126° , and 162° of rotation in each of the six Kenics mixing elements are shown. In the first element, the white core coming from the inlet is split into two white islands. These islands are stretched and move outward. The black, which was initially on the outside, is split into two semicircular filaments, which move toward the inside. Similar stretching and folding processes occur in the next several elements. At the inlet of the third element the black species is now on the inside, meaning that the concentration field has basically flipped inside out. This process of splitting, stretching, folding, and flipping inside out repeats itself every two elements, until the fluids are mixed. The number of elements can be adjusted to the requirements of the process, but typically varies between six and 18, depending on the Reynolds number. See, for example, Hobbs and Muzzio (1997), Hobbs et al. (1998), and Zalc et al. (2002).

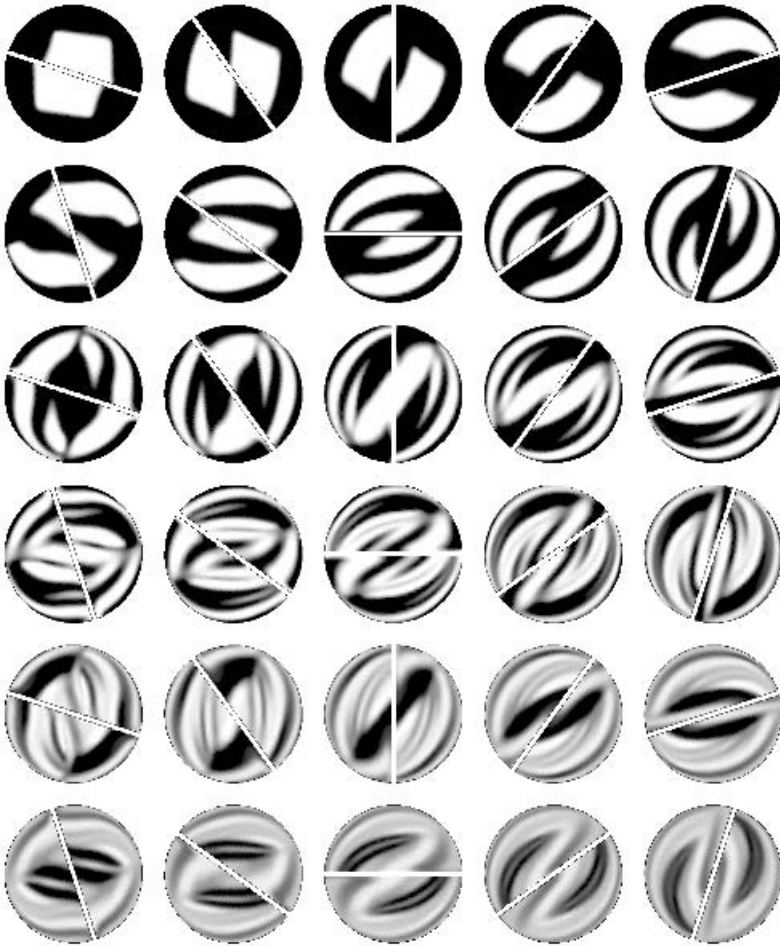


Figure 5-29 Concentration profiles in a Kenics static mixer. Rows 1 to 6 show the concentration in elements 1 to 6, respectively. Columns 1 to 5 show the concentration profiles at 18° , 54° , 90° , 126° , and 162° , respectively.

5-7.9 HEV Static Mixer

The traditional helical mixing element is used primarily for in-line blending under laminar and transitional flow conditions. The high efficiency vortex (HEV) mixer is used for turbulent blending of gases or miscible liquids. It consists of a series of tab arrays, which are placed along a length of pipe. The advantages of this design are that it is easily adapted to both cylindrical and square pipe cross-sections and that it has a relatively low pressure drop. HEV mixers have been in use in the process industries for several years now, for both liquid–liquid and gas–gas mixing. Applications include wastewater treatment, burners, exhaust stacks, beverage manufacturing, and many others. The wide range of applications and scales in

which the HEV mixer is used requires a technique to analyze custom applications on demand. Gretta (1990) investigated the flow pattern generated by the tabs using a combination of hot wire anemometry, hydrogen bubble visualization, and dye visualization and found that the tabs not only generate a pair of counterrotating longitudinal vortices but also shed *hairpin vortices*. The smaller hairpin vortices, generated in a transient manner, move downstream with the larger longitudinal vortices.

Bakker et al. (1994a) modeled the flow pattern generated by an HEV mixer using the Reynolds stress model for turbulence. This steady-state model correctly predicted the formation of the longitudinal vortices, but the hairpin vortices only showed up in the results as regions of high turbulence intensity at the edges of the tabs. Due to the steady-state nature of that model and the assumption of eightfold symmetry made for the purpose of the calculation, the mixing of fluids near the center of the pipe was underpredicted compared to what was known from operational experience and laboratory studies.

Because of the shortcomings of the RANS turbulence models in predicting the hairpin vortices, the HEV mixer was selected as a good candidate for the LES turbulence model. In the LES model, no symmetry assumptions were made, meaning that the full 360° pipe was modeled. The advantage of modeling the full pipe is that periodic interactions between the vortices that form behind the different tabs are not restrained. The simulation was started with a steady-state calculation based on the $k-\varepsilon$ turbulence model. After partial convergence, the LES model was enabled. As hoped, the transient results showed the periodic shedding of hairpin vortices off the back sides of the tabs. Figure 5-30 shows

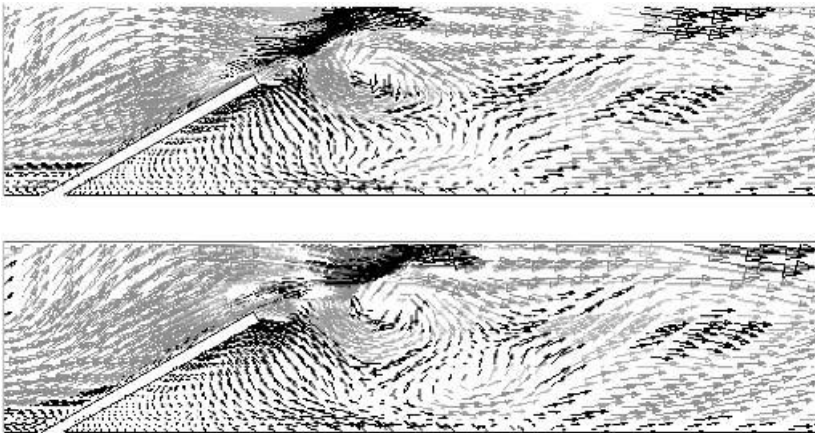


Figure 5-30 The hairpin vortex (in cross-section) that forms behind the tab in an HEV mixer at two different instances in time is shown. Vortices such as these are shed in a time-dependent fashion. The LES model was used for this simulation. A similar HEV mixer, solved using the steady-state Reynolds stress turbulence model, failed to capture this flow detail.

these vortices at two different instances in time. It is clear that the hairpin vortex forming around the tab in the top image has shifted downstream during the 0.06 s that separates the two flow pattern snapshots. This shows that the LES model is well suited to capture complex time-dependent vortex systems such as these.

5-7.10 LDPE Autoclave Reactor

Low density polyethylene (LDPE) reactors are used to manufacture polymer products. The reactors are typically of the tubular or autoclave variety. To make the (multimolecule chain) polymer, a minute amount of initiator is added to a (single-molecule) monomer. Several reaction steps take place in which the monomer is transformed to intermediate polymers, or radicals, and finally to a polymer product with a range of chain lengths (corresponding to a range of molecular weights). Heat is released in many of the reactions, and one goal of LDPE reactor design is to prevent hot spots that give rise to a condition called *thermal runaway*, which is characterized by an undesired product distribution. In this example, the nearly infinite set of reactions in the chain is approximated by six finite rate reactions using the method of moments (Kiparissides et al., 1997). These reactions are solved using the finite rate reaction model with the help of user-defined functions. As a consequence of the method of moments, quantities that describe the product distribution can also be computed. These include the molecular weight distribution, which, if narrow, indicates a high-quality (uniform) product.

A hybrid mesh of 166 000 cells, shown in Figure 5-31, is used for the simulation. The reactor contains both paddle and twisted blade impellers, whose

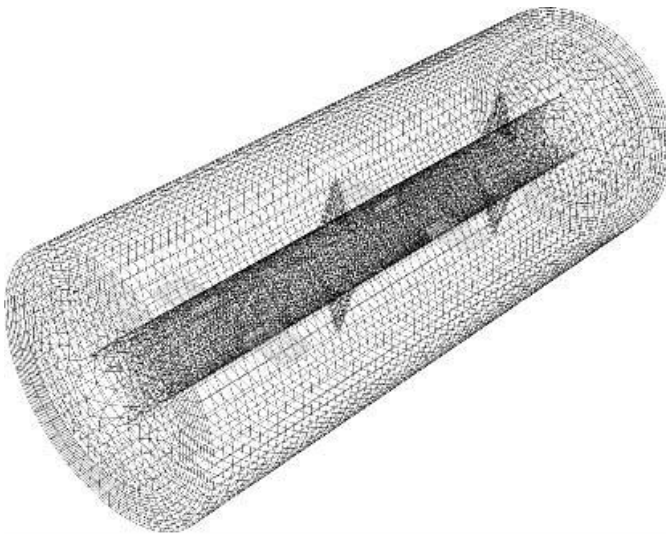


Figure 5-31 Surface mesh used for the LDPE reactor.

rotation is modeled using a sliding mesh. The monomer and initiator used are ethylene and DTBP, respectively. The initiator is premixed with the monomer and injected into the reactor through an annular ring at one end of the vessel. The mixture leaves the device through an annular exit at the opposite end. The flow field is characterized by high swirl, which is induced by the rapidly rotating impellers in the unbaffled vessel. The RNG $k-\epsilon$ model is used to account for turbulence in the highly swirling flow.

Four axial slices are used in the next two figures to show the progression of two problem variables as the mixture advances through the reactor. In these figures, the inlet annulus is at the top of the figure and the outflow annulus is at the bottom. In Figure 5-32 the conversion of the monomer (to both radicals and product polymers) is shown to increase gradually to about 7% as the flow passes through the vessel, in reasonably good agreement with published data (Read et al., 1997). (Higher values are shown in dark gray.) Contours of the molecular weight distribution (Figure 5-33) vary from 41 500 to 41 900, or by about 1%.

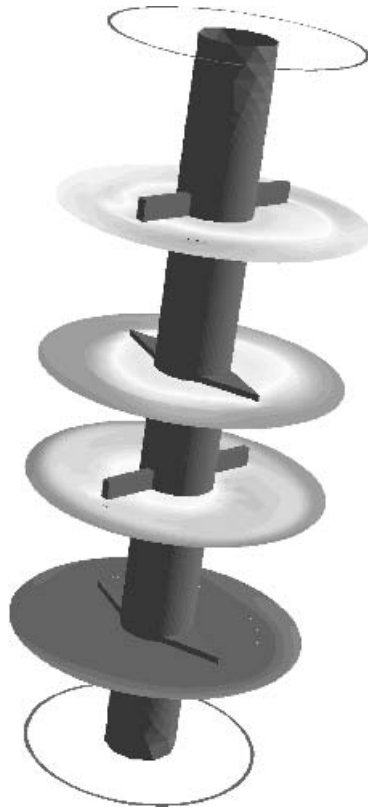


Figure 5-32 Conversion of monomer increases to about 7% as the material moves through the reactor from top to bottom. The conversion is highest at the bottom of the reactor, where the contours are darkest.



Figure 5-33 Contours of molecular weight distribution are used to assess the range of molecular weights in the product.

As the mixture moves through the reactor, the spread in the distribution narrows, indicating a product of high quality. The solution also indicates that the molecular viscosity increases as the chains of radicals grow, consistent with expectations.

5-7.11 Impeller Design Optimization

Ever since the 1950s the Rushton turbine has been the standard impeller for gas dispersion applications. It features six flat blades mounted on a disk. As shown in Figure 5-20*b*, the flow behind the impeller blades separates and trailing vortices form. On gassing, gas accumulates in the low-pressure regions behind the blades and cavities form. This leads to a significant drop in power draw and loss of gas dispersion ability. During the late 1980s and early 1990s, modified Rushton turbines with semicircular blades became standard. These models reduce flow separation and cavity formation behind the blades but do not eliminate them completely.

To date, the disk-style gas dispersion impellers studied in the literature have blades that are symmetric with respect to the plane of the disk. This is not necessarily optimal, since the gas usually enters from the bottom, causing a distinctly asymmetric flow pattern. In this example, the operation of the Chemineer BT6 gas dispersion impeller is reviewed (Bakker, 1998; Myers et al., 1999). The BT6 impeller, with vertically asymmetric blades, is designed to accommodate the various flow conditions above and below the impeller disk. The turbulent flow pattern created by the BT6 was modeled using a fully unstructured tetrahedral mesh with approximately 500 000 cells. The MRF approach and RNG $k-\varepsilon$ turbulence model were used. Second-order upwind differencing was used for the momentum and turbulence equations. The flow pattern was converged using the SIMPLEC pressure-velocity coupling method, which allows for the use of high underrelaxation factors, resulting in fast convergence.

The triangular mesh on the impeller blade is shown in Figure 5-34. The blades have a concave shape, which consists of three curves of different radii and length. The top part of the blade is longer than the bottom part. The back side of the blade is rounded. After the flow field was converged, the torque on the impeller was calculated by integrating the pressure on the impeller blade surfaces. From the torque, the impeller power number, based on the nominal diameter at the impeller disk level, was calculated to be 2.3, which is in excellent agreement with experiments.

Figure 5-35 shows the velocity field around the impeller blades. The velocity vectors are drawn in the frame of reference of the impeller. It is clear that no flow separation occurs behind the impeller blades. This means that cavity formation under gassed conditions will be reduced. Indeed, visualization studies have shown that gas is captured under the top overhang and dispersed from a deep vortex on the inside of the blade. No large gas-filled cavities have been observed behind the blade. As a result, the BT6 has a gassed power curve that is flatter than that of

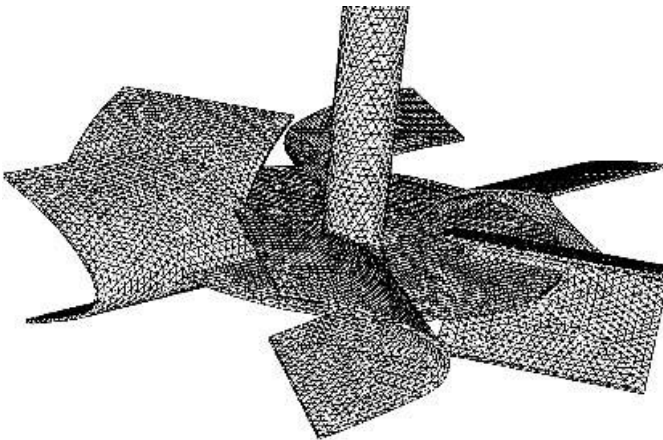


Figure 5-34 Triangular surface mesh on a Chemineer BT6 impeller.

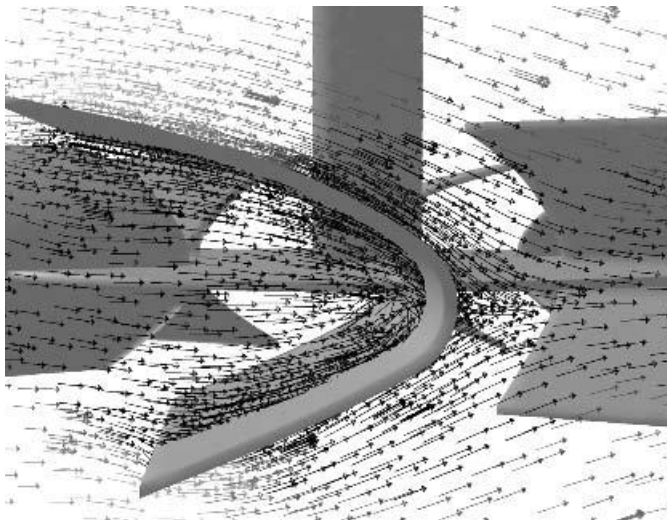


Figure 5-35 Velocity field around the blades of a BT6 impeller. No flow separation occurs behind the blades.

other impellers. It can disperse more gas before flooding than the impellers with symmetric semicircular blades and is less affected by changes in liquid viscosity.

5-7.12 Helical Ribbon Impeller

High viscosity mixing applications occur in most chemical process industry plants. For instance, the polymer industries must blend high viscosity reaction masses to thermal and chemical uniformity. This industry must also blend small amounts of low viscosity antioxidants and colorants into polymer streams. The personal-care products industry encounters many high viscosity mixing applications in the preparation of creams, lotions, pastes, and drugs. Other high viscosity applications occur in the production of food, paint, drilling mud, and greases, to name a few. Viscosities can be in a range from about $1 \text{ Pa} \cdot \text{s}$ all the way up to $25\,000 \text{ Pa} \cdot \text{s}$ in some extreme cases. The quality of the final mixed product in these applications can be very important economically.

Low viscosity mixing applications can usually be handled efficiently with impeller systems consisting of one or more turbines. To obtain adequate mixing under the laminar flow conditions encountered in high viscosity applications, on the other hand, close-clearance impellers such as anchors and helical ribbons are required. These impellers sweep the whole wall surface of the vessel and agitate most of the fluid batch through physical contact. Helical ribbon impellers are typically used for industrial applications where the viscosity is in the range $20\,000$ to $25\,000 \text{ Pa} \cdot \text{s}$. Wall scrapers can be mounted on the impeller blades to improve heat transfer.

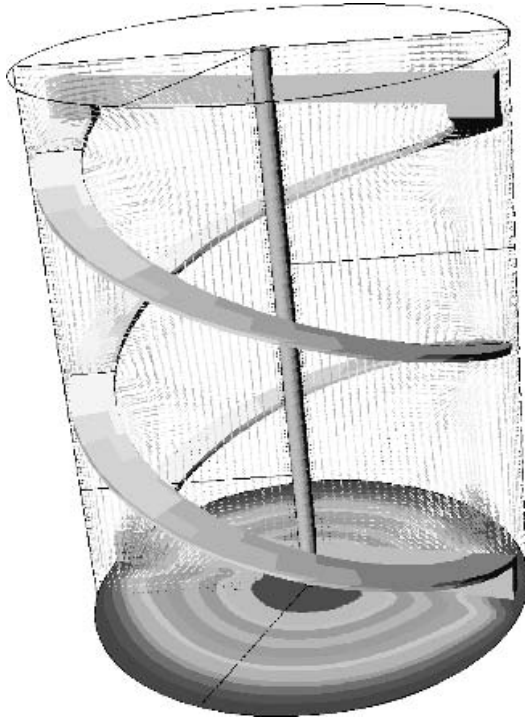


Figure 5-36 Flow field in a vessel equipped with a helical ribbon impeller. Velocity vectors in a vertical plane are shown. The bottom of the vessel is colored by velocity magnitude.

Figure 5-36 shows the flow pattern in the vertical plane of a vessel equipped with a helical ribbon. A fully structured hexahedral mesh with approximately 100 000 cells was used. The structured 3D mesh was created by extruding and twisting a 2D planar mesh. The fluid is viscous and the impeller Reynolds number is approximately 10. The velocity vectors show that the impeller pumps down at the wall and up in the center. Contours of velocity magnitude on the tank bottom show that there are low velocities in the center and higher velocities near the outside wall. Small circulation loops form between the impeller blades and the vessel wall, as discussed in the general literature. These indicate the need for an even larger D/T or the use of wall scrapers if optimum heat transfer is to be obtained.

5-7.13 Stirred Tank Modeling Using LES

In turbulent flows, large scale eddies with coherent structures are primarily responsible for the mixing of passive scalars. The large scale eddies embody themselves in the form of identifiable and organized distributions of vorticity. In addition, the mixing process involves all mechanisms typically found in vortex dynamics, such as stretching, breakup, concatenation, and self-induction of

vortices. Recent experimental work (Bakker and Van den Akker, 1994) suggests that large scale time-dependent structures with periods much longer than the time of an impeller revolution are involved in many of the fundamental hydrodynamic processes in stirred vessels. For example, local velocity data histograms may be bimodal or trimodal, even though they are being analyzed as having only one mode in most laser Doppler experiments. In solids suspension processes, solids can be swept from one side of the vessel to the other in an oscillating pattern, even in dilute suspensions. Digital particle image velocimetry experiments have shown that large scale asymmetries with periods of up to several minutes exist in stirred vessels equipped with axial flow impellers.

The advantage of large eddy simulation (LES) over other turbulence models is that it explicitly resolves the large eddies, which are responsible for much of the mass, energy, and momentum transport. Only the small eddies are represented by a time-averaged subgrid scale model. In mixing tank simulations, the LES turbulence model is typically combined with a sliding mesh model for the impeller so that the most rigorous time-accurate solution can be obtained. One parameter that is pivotal to the success of an LES simulation is the density of the grid throughout the domain. To determine an optimum grid size, the following, straightforward method is recommended. First a steady-state, three dimensional calculation is performed that uses the standard $k-\epsilon$ turbulence model and the MRF model for the impeller. From the converged flow field, volume averages for the following three turbulent length scales are calculated:

- Integral length scale: $L_t = k^{3/2}/\epsilon$
- Taylor length scale: $L_a = (15\nu u'^2/\epsilon)^{0.5}$
- Kolmogorov scale: $L_k = (\nu^3/\epsilon)^{1/4}$

The integral length scale is a measure of the large scale turbulence. The Kolmogorov length scale is a measure of the smallest scale eddies at which dissipation occurs. The Taylor length scale is an intermediate length scale that can be used as a guide to determine the grid size required for LES simulations. For a typical turbulent small scale vessel, $L_t/T \sim 10^{-1}$, $L_a/T \sim 10^{-2}$, and $L_k/T \sim 10^{-3}$. Based on the Taylor length scale, a suitable grid size for an LES simulation would be on the order of $10^{-2}T$, which would result in a grid on the order of 10^6 cells. The large number of cells, along with the transient solution method (one that requires a small time step), contribute to the increased calculation time required by the LES model as compared with RANS models. Figure 5-37 shows how the CPU time and required grid size for the LES model compare with other turbulence modeling options.

In this example, the use of LES and the sliding mesh model to predict large scale chaotic structures in stirred tanks is demonstrated for a single high efficiency impeller. A full hexahedral mesh was used for the simulation. The vessel diameter is 0.29 m, and the impeller rotates at 60 rpm, resulting in a Reynolds number of 13 000. The central differencing scheme for the momentum equations was used along with a time step of 0.01 s. The RNG modification of the Smagorinsky

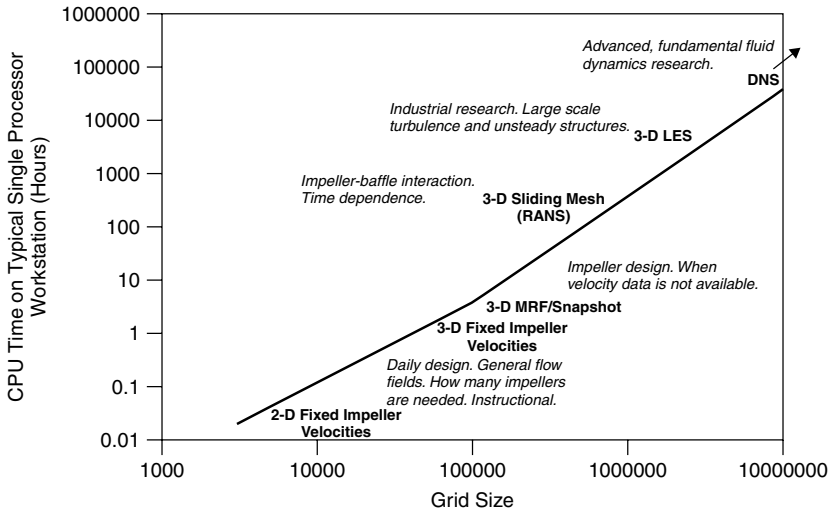


Figure 5-37 CPU time and grid size requirements for various impeller modeling options.

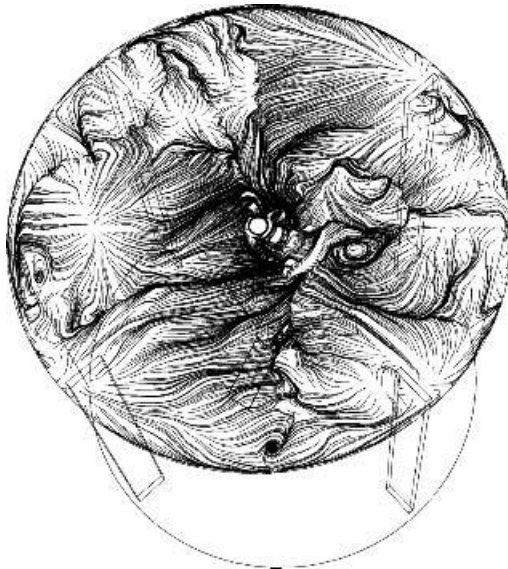


Figure 5-38 Flow pattern at the surface of a vessel equipped with a high efficiency impeller calculated using an LES turbulence model.

model was used for the subgrid scale turbulence. A period of approximately 40 s was simulated. The results show that the flow pattern indeed exhibits large scale unsteady motion, similar to what has been reported from experimental data in the literature. Figure 5-38 shows the flow field at the liquid surface at one instant

in time, using oil flow lines, which are path lines that are confined to the surface from which the flow followers are released. The turbulent structure of the flow is clearly visible.

When performing such LES calculations, it is advised to visualize the results by creating flow field images after every time step. These can then be used to create animations. Similarly, statistical data can be obtained by creating monitor points or lines in the domain and saving important variables in these locations. The time series that are obtained in this manner can be analyzed further using standard statistical and signal analysis techniques.

5-8 CLOSING REMARKS

It could be said that what comes out of a CFD simulation is only as good as what goes in. Although this is true in part, there are many other considerations that can lead to the success—or lack thereof—of CFD. One is based on the choice of software. Many commercial packages are available today, and resources to help find and evaluate them are given in Section 5-8.1. Comments on basic hardware requirements for CFD codes, which are computationally intensive, are given in Section 5-8.2. Issues regarding the learning curve, or the time required for an engineer to “come up to speed” and be successful with CFD, are discussed in Section 5-8.3. Once the proper software, proper hardware, and trained user are in place, there are still some common pitfalls to be avoided. These, along with some of the benefits of CFD, are discussed in Section 5-8.4.

5-8.1 Additional Resources

Many commercial and even some freeware or shareware CFD codes are available, each with different capabilities, special physical models, numerical methods, geometric flexibility, and user interfaces. Specialized pre- and postprocessing programs are also available for generation of the geometry and grid, input of model parameters, and viewing of results. Excellent overviews of these products can be found on the Web (see, e.g., CEWES, Christopher, Larsson, and Wyman).

5-8.2 Hardware Needs

In the past, CFD use was often associated with the realm of high-powered computer systems. But much of today’s modeling work can be accomplished on low-end Unix workstations or high-end personal computers (PCs). A typical PC configuration might be a one- or two-processor system, running Windows or Linux. Unix workstations with one, two, or more processors are also commonly used. These systems are more than adequate for moderately sized, steady-state or time-dependent analyses. For complicated models, or those using a large number of computational cells (>1 million), multiprocessor workstations are often used. Although supercomputers are still employed for high-end research and

development work, they are not commonly needed for typical engineering design applications. Another recent trend involves the clustering of multiple inexpensive PCs into a parallel- or cluster-computing network. Such systems provide supercomputing power at a fraction of the cost.

5-8.3 Learning Curve

The user friendliness of CFD software has also increased significantly during recent years. In the past, CFD software was characterized by text- or command-file-based interfaces and difficult-to-configure solvers that made fluid flow analysis the exclusive domain of highly trained experts. However, the latest generation of commercial CFD software has been developed with graphical user interfaces. They have much more stable and robust solvers and allow easy geometry exchange between CAD programs and the CFD solver. This has allowed engineers who are not experts in fluid dynamics to make efficient use of CFD and use this technology on a day-to-day basis in their design and optimization work. Most commercial CFD companies provide training and ongoing technical support with a software license. The average engineer typically requires one week of training to get started using one of these modern CFD packages.

5-8.4 Common Pitfalls and Benefits

Despite the increased user friendliness of modern CFD software, there are still a number of potential pitfalls that can beset the analyst. Some of the mistakes made most commonly when using CFD are listed below.

- *Use of a low-quality, coarse grid.* Details that are smaller than the cell size cannot be resolved. Often, small flow features in one region need to be resolved in great detail in order to predict large flow features accurately in other regions. For example, a jet penetrating a vessel will appear to diffuse more rapidly than in actual fact if a coarse grid is used in the jet region. Satisfying grid needs such as this may lead to a finer grid containing far more cells than estimated initially.
- *Use of unconverged results.* CFD solvers are iterative and it is often tempting to cut a calculation short when deadlines are approaching or the coffee break is over. However, the analyst should always ensure that proper convergence has been obtained before using the results from any CFD solver.
- *Use of the wrong physical property data.* This is not as trivial as it sounds. For example, viscosity curves may have been determined in one temperature and shear rate range, but if the actual shear rates or temperatures in the flow domain are outside this range, the curves may no longer be valid and incorrect results may be obtained. As another example, accurate average particle size and density are needed to best predict solids suspension behavior.

Fortunately, none of these problems is fundamental to the CFD technology itself. A coarse grid may be refined, unconverged calculations continued, and accurate physical constants may be measured. These easily avoided pitfalls are far outweighed by the following benefits:

- CFD can be used to augment design correlations and experimental data.
- CFD provides comprehensive data that are not easily obtainable from experimental tests.
- CFD reduces scale-up problems, because the models are based on fundamental physics and are scale independent. Models of the actual unit can be simulated just as easily as models of lab scale versions, so predictions, and indeed optimization of the actual unit, can be achieved.
- When evaluating plant problems, CFD can often be used to help understand the root cause of a problem, not just the effect.
- CFD can be used to complement physical modeling. Some design engineers actually use CFD to analyze new systems before deciding which and how many validation tests need to be performed.
- Many “what if” scenarios can often be analyzed in less time than experimental tests would take.

In summary, if the CFD analyst is careful when addressing the issues of problem setup and solution convergence, the potential benefits that can be extracted from the simulation are numerous. Furthermore, the computational resources available today, in terms of both speed and power, should encourage engineers to make use of high density grids and complex models so as to achieve results of the best possible quality.

ACKNOWLEDGMENTS

The authors gratefully acknowledge the contributions of the following people: Lanre M. Oshinowo for numerous discussions and his assistance with the blending and stirred vessel solids suspension simulations; Richard D. LaRoche for his conceptual contributions and his cooperation on the static mixer simulations; Ahmad H. Haidari for sharing his many ideas; Thierry Avalosse and Yves Rubin for the twin-screw extruder simulations; and Bernard Alsteens for the intermeshing impeller simulations. Furthermore, Liz Marshall wishes to thank Ronald J. Weetman for many helpful discussions over the years on mixing processes and analysis; and André Bakker wishes to thank Kevin J. Myers, Julian B. Fasano, Mark F. Reeder, Lewis E. Gates, John M. Smith, Robert F. Mudde, Jaap J. Frijlink, Marijn M. C. G. Warmoeskerken, Ivo Bouwmans, and Harrie E. A. van den Akker for many fruitful discussions and contributions.

NOMENCLATURE

A	magnussen mixing rate constant (—)
A_k	Arrhenius constant for reaction k (variable units)
B	Magnussen mixing rate constant (—)
c_A	fluctuation in the concentration of species A (mol/m^3)
C	off-bottom clearance (m)
C_1	turbulence model constant (—)
C_2	turbulence model constant (—)
C_A	concentration of species A (mol/m^3)
$C_{j'}$	concentration of species j' (mol/m^3)
D	impeller diameter (m)
E	total enthalpy (J)
E_k	activation energy for reaction k (J/mol)
f	underrelaxation factor (—)
$F(\phi)$	spatially discretized transport equation
F_i	net force in the i direction (N)
g	gravitational acceleration (m/s^2)
G_k	generation term for turbulence ($\text{kg/m} \cdot \text{s}^3$)
h	static enthalpy (J)
$h_{j'}$	enthalpy for the species j' (J)
$J_{i',i}$	diffusion flux of species i' in direction I ($\text{kg/m}^2 \cdot \text{s}^1$)
k	turbulent kinetic energy (m^2/s^{-2})
k_{eff}	effective conductivity ($\text{W/m} \cdot \text{K}$)
$K_{i',k}$	reaction rate of species i' in reaction k (variable units)
L	length of domain in definite integral over coordinate x (m)
L_a	Taylor length scale (m)
L_k	Kolmogorov scale (m)
L_t	integral length scale (m)
$m_{i'}$	mass fraction of species i' (—)
$M_{i'}$	molecular weight of species i' (kg/kg-mol)
N	impeller rotational speed (s^{-1})
N_p	power number (—)
N_Q	flow number (—)
p	pressure (Pa)
P	power drawn by an impeller (W)
Pe	Péclet number
Q_l	liquid flow rate (m^3/s)
r	spatial coordinate in the radial direction (m)
R	universal gas constant ($\text{J/mol} \cdot \text{K}$)
R	impeller radius (m)
Re	Reynolds number (—)

$R_{i'}$	generalized source term for reactions in the species i' transport equation ($\text{kg}/\text{m}^3 \cdot \text{s}$)
$R_{K_{-i'},k}$	kinetic reaction rate for species i' in reaction k ($\text{kg}/\text{m}^3 \cdot \text{s}^{-1}$)
$R_{M1-i',k}$	mixing limited reaction rate for the reactant species i' in reaction k ($\text{kg}/\text{m}^3 \cdot \text{s}$)
$R_{M2-i',k}$	mixing limited reaction rate for the product species i' in reaction k ($\text{kg}/\text{m}^3 \cdot \text{s}$)
S_h	generalized source term for the enthalpy equation (W/m^3)
$S_{i'}$	net species source term in the species i' transport equation ($\text{kg}/\text{m}^3 \cdot \text{s}$)
t	time (s)
T	tank diameter (m)
T	temperature (K)
T_{ref}	reference temperature for formation enthalpy (K)
\mathbf{U}	velocity vector (m/s)
u'_i	fluctuating velocity component (due to turbulence) in the direction i (m/s)
U_i	velocity in the direction i (m/s)
U_{tip}	impeller tip speed (m/s)
W_b	width of impeller blade (m)
x_i	spatial coordinate in direction i (m)
X_s	product distribution (—)
z	impeller blade height (m)

Greek Symbols

β_k	temperature exponent in Arrhenius rate expression (—)
Γ	generalized diffusion coefficient (variable units)
δ_{ij}	Kronecker delta (—)
ε	turbulent kinetic energy dissipation rate (m^2/s^3)
$\eta_{j',k}$	exponent for concentration of species j' in reaction k (—)
μ	molecular viscosity ($\text{kg}/\text{m} \cdot \text{s}$)
μ_{eff}	effective viscosity ($\text{kg}/\text{m} \cdot \text{s}$)
μ_t	turbulent viscosity ($\text{kg}/\text{m} \cdot \text{s}$)
ν	kinematic viscosity (m^2/s)
$\nu_{i'}$	stoichiometry of species i' (—)
ξ	vorticity (s^{-1})
ρ	liquid density (kg/m^3)
σ_k	turbulence model constant (—)
σ_ε	turbulence model constant (—)
σ_μ	turbulence model constant (—)
τ	shear stress (Pa)
τ_d	disruptive shear stress (Pa)
τ_y	yield stress (Pa)
ϕ	generalized conserved quantity (variable units)
Ω	angular speed (rad/s)

REFERENCES

- Avalosse, T., and Y. Rubin (1999). Analysis of mixing in co-rotating twin screw extruders through numerical simulation, *Proc. 15th Polymer Society Conference*, Hertogenbosch, The Netherlands.
- Bakker, A. (1992). Hydrodynamics of stirred gas–liquid dispersions, Ph.D. dissertation, Delft University of Technology, The Netherlands.
- Bakker A. (1998). Impeller assembly with asymmetric concave blades, U.S. patent 5,791,780.
- Bakker A., and J. B. Fasano (1993a). A computational study of the flow pattern in an industrial paper pulp chest with a side entering impeller, presented at the annual AIChE meeting, Nov. 1992; *AIChE Symp. Ser. 293*, **89**, 118–124.
- Bakker A., and J. B. Fasano (1993b). Time dependent, turbulent mixing and chemical reaction in stirred tanks, presented at the annual AIChE meeting, St. Louis, MO, Nov. *AIChE Symp. Ser. 299*, **90**, 71–78.
- Bakker A. and R. LaRoche (1993). *Flow and mixing with Kenics static mixers*, *Cray Channels*, Volume **15**(3), p. 25–28.
- Bakker, A., and E. M. Marshall (1992). Laminar mixing with Kenics in-line mixers, *Fluent User's Group Meeting Proc.*, Burlington, VT, Oct. 13–15, pp. 126–146.
- Bakker, A., and H. E. A. Van den Akker (1994). Single-phase flow in stirred reactors, *Chem. Eng. Res. and Des., Trans. Inst. Chem. Eng.*, **72**, 583–593.
- Bakker A., N. Cathie, and R. LaRoche (1994a). Modeling of the flow and mixing in HEV static mixers, presented at the 8th European Conference on Mixing, Cambridge, Sept. 21–23; *Inst. Chem. Eng. Symp. Ser.*, **136**, 533–540.
- Bakker A., J. B. Fasano, and K. J. Myers (1994b). Effects of flow pattern on the solids distribution in a stirred tank, *Proc. 8th European Conference on Mixing*, Cambridge, Sept. 21–23; *Inst. Chem. Eng. Symp. Ser.*, **136**, 1–8.
- Bakker, A., R. D. LaRoche, M. H. Wang, and R. V. Calabrese (1997). Sliding mesh simulation of laminar flow in stirred reactors, *Trans. Inst. Chem. Eng.*, **75A**, Jan.
- Bakker, A., L. Oshinowo, and E. Marshall (2000). The use of large eddy simulation to study stirred vessel hydrodynamics, *Proc. 10th European Conference on Mixing*, Delft, The Netherlands, pp. 247–254.
- Bakker A., A. Haidari, and E. M. Marshall (2001). Modeling stirred vessels using large eddy simulation, presented at the 18th Biennial North American Mixing Conference, Pocono Manor, PA.
- Bourne, J. R., F. Kozicki, and P. Rys (1981). Mixing and fast chemical reaction: I. Test reactions to determine segregation, *Chem. Eng. Sci.*, **36**, 1643.
- CEWES MSRC (n.d.). Computational fluid dynamics software data log, http://phase.go.jp/nhse/rib/repositories/cewes_cfd/catalog/index.html.
- Christopher, W. (n.d.). CFD codes list, http://www.icemcfd.com/cfd/CFD_codes.html.
- Ding, J., and D. Gidaspow (1990). A bubbling fluidization model using kinetic theory of granular flow, *AIChE J.*, **36**, 523–538.
- Fluent (1998). *Fluent 5 User's Guide*, Fluent, Inc., Lebanon, NH.
- Fokema, M. D., S. M. Kresta, and P. E. Wood (1994). Importance of using the correct impeller boundary conditions for CFD simulations of stirred tanks, *Can. J. Chem. Eng.*, **72**, 177–183.

- Fox, R. O. (1998). On the relationship between Lagrangian micromixing models and computational fluid dynamics, *Chem. Eng. Process.* **37**, 521–535.
- Gidaspow, D., M. Syamlal, and Y. C. Seo (1986). Hydrodynamics of fluidization: super-computer generated vs. experimental bubbles, *J. Powder Bulk Solids Technol.*, **10**, 19–23.
- Gran, I. R., and B. F. Magnussen (1996). A numerical study of a bluff-body stabilized diffusion flame: 2. Influence of combustion modeling and finite-rate chemistry, *Combust. Sci. Technol.*, **119**, 119–191.
- Gretta W. J., and C. R. Smith (1993). The flow structure and statistics of a passive mixing tab, *J. Fluids Eng.* **115**, 255–263.
- Gullichsen J. (1985). Medium consistency processing: Fundamentals, *Bleach Plant Operations/TAPPI Seminar Notes*, pp. 135–142.
- Hannon, J. (1992). Mixing and chemical reaction in tubular reactors and stirred tanks, Ph.D. dissertation, Cranfield Institute of Technology, Cranfield, Bedfordshire, England.
- Hobbs, D. M., and F. J. Muzzio (1997). The Kenics static mixer: a three-dimensional chaotic flow, *Chem. Eng. J.*, **67**(3), 153–166.
- Hobbs, D. M., P. D. Swanson, and F. J. Muzzio (1998). Numerical characterization of low Reynolds number flow in the Kenics static mixer, *Chem. Eng. Sci.* **53**(8), 1565.
- Kiparissides, C., D. S. Achilias, and E. Sidiropoulou (1997). Dynamical simulation of industrial poly(vinyl chloride) batch suspension polymerization reactors, *Ind. Eng. Chem. Res.*, **36**, 1253.
- Kresta, S. M., and P. E. Wood (1991). Prediction of the three dimensional turbulent flow in stirred tanks, *AIChE J.*, **37**, 448–460.
- Larsson, J. (n.d.). CFD online, <http://www.cfd-online.com>.
- Leonard, B. P., and S. Mokhtari (1990). ULTRA-SHARP nonoscillatory convection schemes for high-speed steady multidimensional flow, NASA TM 1-2568 (ICOMP-90-12), NASA Lewis Research Center.
- Luo, J. Y., R. I. Issa, and A. D. Gosman (1994). *Prediction of impeller induced flows in mixing vessels using multiple frames of reference*, *Inst. Chem. Eng. Symp. Ser.* **136**, 549–556.
- Magnussen, B. F., and B. H. Hjertager (1976). On mathematical models of turbulent combustion with special emphasis on soot formation and combustion, *Proc. 16th International Symposium on Combustion*, Combustion Institute, Pittsburgh, PA.
- Marshall, E. M., Y. Tayalia, L. Oshinowo, and R. Weetman (1999). *Comparison of turbulence models in CFD predictions of flow number and power draw in stirred tanks*, presented at Mixing XVII, Banff, Alberta, Canada.
- Middleton, J. C., F. Pierce, and P. M. Lynch (1986). Computations of flow fields and complex reaction yield in turbulent stirred reactors and comparison with experimental data, *Chem. Eng. Res. Des.*, **64**, 18–21.
- Myers, K. J., A. J. Thomas, A. Bakker, and M. F. Reeder (1999). Performance of a gas dispersion impeller with vertically asymmetric blades, *Trans. Inst. Chem. Eng.*, **77**, 728–730.
- Ogawa, S., A. Umemura, and N. Oshima (1980). On the equation of fully fluidized granular materials, *J. Appl. Math. Phys.*, **31**, 483.
- Oldshue, J. Y., and N. R. Herbst (1992). *A Guide to Fluid Mixing*, Lightnin, Rochester, NY.

- Oshinowo L., A. Bakker, and E. M. Marshall (1999). *Mixing time: a CFD approach*, presented at Mixing XVII, Banff, Alberta, Canada.
- Oshinowo L. M., E. M. Marshall, A. Bakker, and A. Haidari (2000). Benefits of CFD in modeling solids suspension in stirred vessels, presented at the AIChE Annual Meeting, Los Angeles.
- Patankar, S. V. (1980). *Numerical Heat Transfer and Fluid Flow*, Hemisphere, Washington, DC.
- Ranade, V. V., and S. M. S. Dommeti (1996). Computational snapshot of flow generated by axial impellers in baffled stirred vessels, *Trans. Inst. Chem. Eng.*, **74**.
- Read, N. K., S. X. Zhang, and W. H. Ray (1997). Simulations of a LDPE reactor using computational fluid dynamics, *AIChE J.*, **43**, 104–117.
- Roussinova, V. T., B. Grgic, and S. M. Kresta (2000). Study of macro-instabilities in stirred tanks using a velocity decomposition technique, *Chem. Eng. Res. Des.*, **78**, 1040–1052.
- Roussinova, V., S. M. Kresta, and R. J. Weetman 2001. Low frequency macroinstabilities in a stirred tank: scale-up and prediction based on large eddy simulations, presented at the 18th Biennial North American Mixing Conference, Pocono Manor, PA, June.
- Shih, T.-H., W. W. Liou, A. Shabbir, and J. Zhu (1995). A new $k-\epsilon$ eddy-viscosity model for high Reynolds number turbulent flows: model development and validation, *Comput. Fluids*, **24**, 227–238.
- Syammlal, M., W. Rogers, and T. J. O'Brien (1993). *MIFX Documentation*, Vol. 1, *Theory Guide*, DOE/METC-9411004, NTIS/DE9400087, National Technical Information Service, Springfield, VA.
- Tanguy, P. A., F. Thibault, C. Dubois, and A. Ait-Kadi (1999). Mixing hydrodynamics in a double planetary mixer, *Chem. Eng. Res. Des.*, **77**(4), 318–324.
- Tipnis, S. K., W. R. Penney, and J. B. Fasano (1993). An experimental investigation to determine a scale-up method for fast competitive parallel reactions in agitated vessels, presented at the AIChE Annual Meeting, St. Louis, MO.
- Versteeg, H. K., and W. Malalasekera (1995). *An Introduction to Computational Fluid Dynamics: The Finite Volume Method*, Longman Scientific & Technical, Harlow, Essex, England.
- Weetman, R. J. (1997). Automated sliding Mesh CFD computations for fluidfoil impellers, *Proc. 9th European Conference on Mixing*, Paris.
- Wyman, N. (n.d.). CFD review, <http://www.cfdreview.com>.
- Yakhot, V., and S. A. Orszag (1986). Renormalization group analysis of turbulence: I. Basic theory, *J. Sci. Comput.*, **1**, 1–51.
- Zalc, J. M., E. S. Szalai, F. J. Muzzio, and S. Jaffer (2002). Characterization of flow and mixing in an SMX static mixer, *AIChE J.* **48**(3), 427–436.
- Zhou, G., P. A. Tanguy, and C. Dubois (2000) Power consumption in a double planetary mixer with non-newtonian and viscoelastic materials, *Chem. Eng. Res.* **78**(3), 445–453.

Mechanically Stirred Vessels

RAMESH R. HEMRAJANI

ExxonMobil Research and Engineering Company

GARY B. TATTERSON

North Carolina A&T State University

6-1 INTRODUCTION

There are a number of ways to perform mixing in vessels. Mechanical agitation, gas sparging, and jets are often used. Due to the variety of processing needs and process objectives, a number of different mixer geometries have been developed. This chapter is intended to introduce some of the more prominent geometries used for mechanical agitation in vessels. Blending in-line in pipes and in stirred vessels are topics of Chapters 7 and 9, respectively.

Mixing and contacting in agitated tanks can be accomplished in continuous, batch, or fed-batch mode. A good mixing result is important for minimizing investment and operating costs, providing high yields when mass transfer is limiting, and thus enhancing profitability.

Processing with mechanical mixers occurs under either laminar or turbulent flow conditions, depending on the impeller Reynolds number, defined as $Re = \rho ND^2/\mu$. For Reynolds numbers below about 10, the process is laminar, also called *creeping flow*. Fully turbulent conditions are achieved at Reynolds numbers higher than about 10^4 , and the flow is considered transitional between these two regimes.

Fluid mixing is carried out in mechanically stirred vessels for a variety of objectives, including for homogenizing single or multiple phases in terms of concentration of components, physical properties, and temperature. The fundamental mechanism involves physical movement of material between various parts of the entire mass using rotating impeller blades. Over 50% of the world's

chemical production involve these stirred vessels for manufacturing high-added-value products. These vessels are commonly used for:

- Blending of homogeneous liquids such as lube oils, gasoline additives, dilution, and a variety of chemicals
- Suspending solids in crystallizers, polymerization reactors, solvent extraction, etc.
- Blending and emulsification of liquids for hydrolysis/neutralization reactions, extraction, suspension polymerization, cosmetics, food products, etc.
- Dispersing gas in liquid for absorption, stripping, oxidation, hydrogenation, ozonation, chlorination, fermentation, etc.
- Homogenizing viscous complex liquids for polymer blending, paints, solution polymerization, food products, etc.
- Transferring heat through a jacket and/or internal coils for heating or cooling

An optimum approach to designing these mixing systems consists of the following steps:

- Define the process mixing requirements, such as blending quality, drop sizes, degree of solids suspension, mass transfer rates, etc.
- A suitable impeller type must then be chosen based on the type of fluid system and mixing requirements.
- The overall mixing system can then be designed, which involves determining the appropriate number of impellers, sizing the impeller, determining mixer speed, and estimating energy requirements.
- Other components, such as baffles, must also be specified based on desired flow patterns.
- One must design the mechanical components, such as shaft diameter, impeller blade thickness, baffles and supports, bearings, seals, etc. (see Chapter 21).

6-2 KEY DESIGN PARAMETERS

To design an effective stirred tank, an efficient impeller should be chosen for the process duty. More than one impeller may be needed for tanks with high aspect ratio ($Z/T > 1.5$). Sizing of the impeller is done in conjunction with mixer speed to achieve the desired process result. The appropriate size and type of wall baffles must be selected to create an effective flow pattern. The mixer power is then estimated from available data on impeller characteristics, and the drive size is determined. The mixer design is finalized with mechanical design of the shaft, impeller blade thickness, baffle thickness and supports, inlet/outlet nozzles, bearings, seals, gearbox, and support structures.

6-2.1 Geometry

A conventional stirred tank consists of a vessel equipped with a rotating mixer. The vessel is generally a vertical cylindrical tank. Nonstandard vessels such as those with square or rectangular cross-section, or horizontal cylinder vessels are sometimes used. The rotating mixer has several components: an impeller, shaft, shaft seal, gearbox, and a motor drive. Wall baffles are generally installed for transitional and turbulent mixing to prevent *solid body rotation* (sometimes called *fluid swirl*) and cause axial mixing between the top and bottom of the tank. This is illustrated in a video clip recorded on the Visual Mixing CD affixed to the back cover of the book. A conventional vertical cylindrical stirred tank with a top-entering mixer is shown in Figure 6-1. Occasionally, a small impeller, called a *tickler* or *kicker*, is installed close to the tank bottom to maintain agitation when the liquid level drops below the main impeller.

In tall tanks, the mixer may be installed from the bottom (Figure 6-2) to reduce the shaft length and provide mechanical stability. The mixers can be side entering (Figure 6-3) for large product storage and blending tanks or inserted from the top at an angle (Figure 6-4) for nonbaffled small tanks. The flows generated with side entering and angled mixers are asymmetric, and therefore wall baffles are no longer needed. In horizontal cylindrical tanks, the mixer can be installed on the side or from top, as shown in Figures 6-5 and 6-6, respectively.

6-2.1.1 Impeller Types. The typical impellers used in transitional and turbulent mixing are listed in Table 6-1. These have been divided into different general classes, based on flow patterns, applications, and special geometries. The classifications also define application types for which these impellers are used. For example, axial flow impellers are efficient for liquid blending and solids suspension, while radial flow impellers are best used for gas dispersion. Up/down impellers can be disks and plates, are considered low-shear impellers, and are commonly used in extraction columns. The pitched blade turbine, although classified as an axial flow impeller, is sometimes referred to as a mixed flow impeller, due to the flow generated in both axial and radial directions. Above a D/T ratio of 0.55, pitched blade turbines become radial flow impellers (see the Visual Mixing CD for an illustrative video). Further details of these applications and impeller selection criteria are given later in the chapter.

Table 6-1 Impeller Classes and Specific Types

Axial flow	Propeller, pitched blade turbine, hydrofoils
Radial flow	Flat-blade impeller, disk turbine (Rushton), hollow-blade turbine (Smith)
High shear	Cowles, disk, bar, pointed blade impeller
Specialty	Retreat curve impeller, sweptback impeller, spring impeller, glass-lined turbines
Up/down	Disks, plate, circles

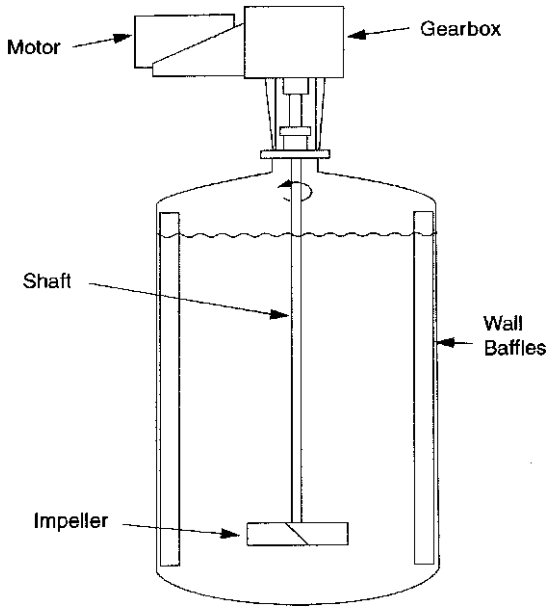


Figure 6-1 Conventional stirred tank with top-entering agitator.

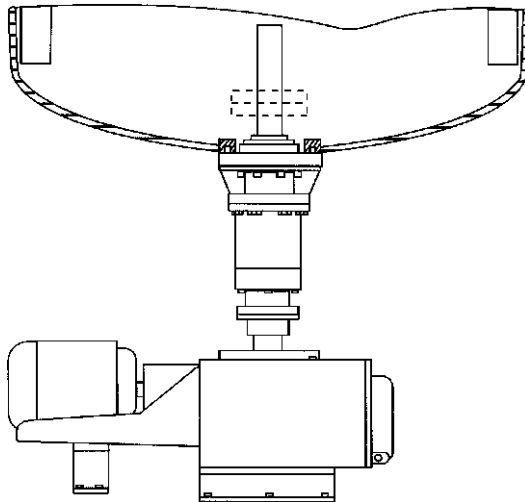


Figure 6-2 Bottom-entering agitator.

6-2.1.2 Wall Baffles. Baffles are generally used in transitional and turbulent mixing, except in severe fouling systems, which require frequent cleaning of tank internals. For laminar mixing of viscous fluids, baffles are not needed. In square and rectangular tanks, the corners break up the tangential flow pattern and thus

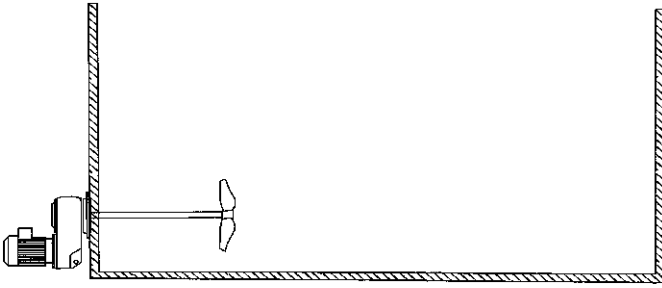


Figure 6-3 Side-entering mixer for large product storage and blending tanks.

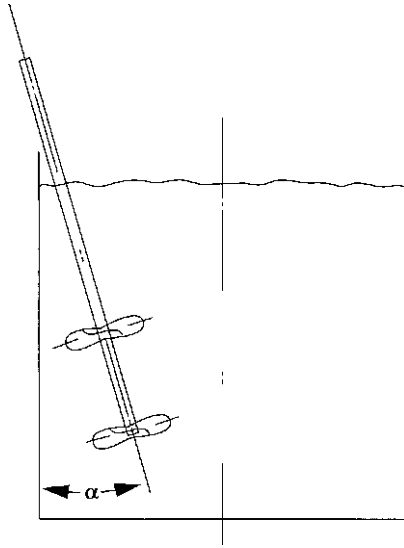


Figure 6-4 Angular top-entering mixer for small tanks with portable mixers.

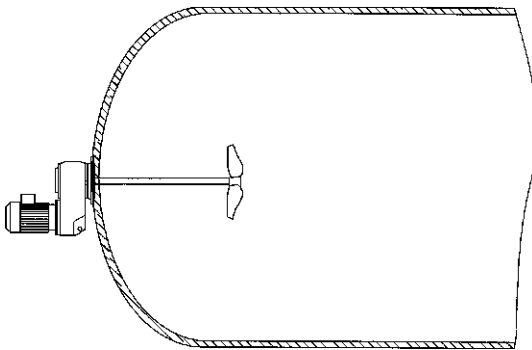


Figure 6-5 Side-entering mixer for horizontal cylindrical vessel.

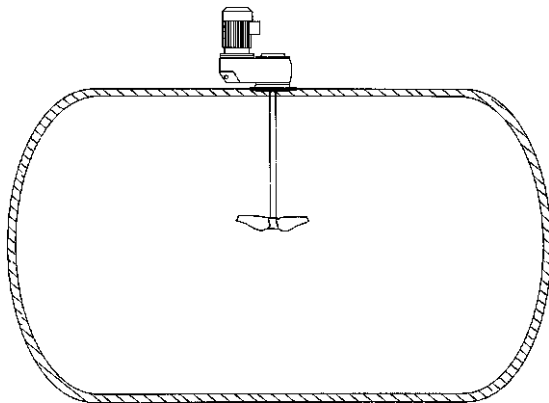


Figure 6-6 Top-entering mixer for horizontal cylindrical vessel.

provide a baffling effect, and wall baffles may not be needed. Baffles are also not used for side-entering mixers in large product tanks and angled mixers in small agitated tanks.

Wall baffles typically consist of solid surfaces positioned in the path of tangential flows generated by a rotating impeller. Wall baffling has a significant influence on the flow behavior and resulting mixing quality. In the absence of baffles, the flow created by impeller rotation is two dimensional and causes swirling action, i.e., solid body rotation. Wall baffles transform tangential flows to vertical flows, provide top-to-bottom mixing without swirl, and minimize air entrainment. Baffles increase the drag and power draw of the impeller.

A standard baffle configuration consists of four vertical plates having width equal to 8 to 10% ($T/12$ to $T/10$) of the tank diameter. Narrower baffles are sometimes used for high viscosity systems, buoyant particle entrainment (width = 2% of T), or when a small vortex is desired. A small spacing between baffles and the tank wall (1.5% of T) is allowed to minimize dead zones particularly in solid-liquid systems. Wall baffles increase the power consumption of the mixer and generally enhance the process result.

For glass-lined vessels and retreat curve blade impellers and glass-lined turbines, five different types of baffles (shown in Figure 6-7) are commonly used: finger, flattened pipe, h style, concave baffle, and fin. These baffles can be conveniently supported in the vessel heads of glass-lined reactors. Of these, the fin baffle has become a more standard choice.

Other types of baffling (e.g., surface baffles, retractable baffles, twisted baffles, and partition baffles) are also used for satisfying specific process needs. Surface baffles can prevent gas entrainment from the vapor head. Retractable baffles are used in systems where rheology changes during the process, and baffles must be removed at low Reynolds numbers. Partition baffles are used for staging of tall vessels. The selection, sizing, and location of baffles depend on the process requirements and mixing regime.

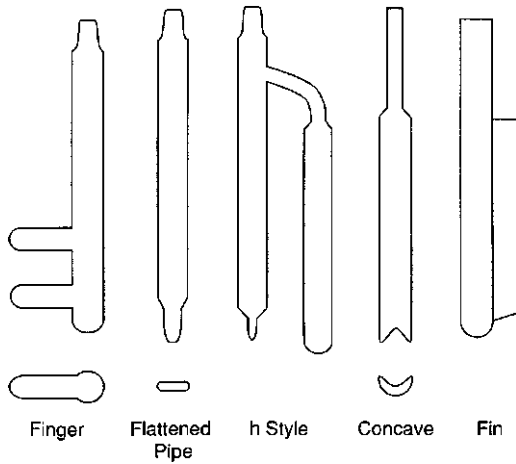


Figure 6-7 Common glass-lined baffle types.

6-2.1.3 Tank Bottoms. The conventional stirred vessel uses a cylindrical tank with a flat or dished bottom. Dished bottom heads can be 1 : 2 ellipsoidal, ASME dish, or hemispherical. Information on the geometry of pressure vessel heads can be found in Dimoplon (1974). The flow patterns below the impeller can be different with different heads and result in different mixing efficiencies. For solids suspension in flat-bottomed tanks, solids tend to accumulate in the corners. Dished bottoms are preferred to maximize suspension quality. Large tanks are constructed with flat bottoms or with a shallow cone or inverted cone, as in crude oil storage tanks. Deep cone bottoms are used in tanks when inventories and heels must be minimized. Such a geometry may require a special impeller shaped to conform to the cone geometry and placed near the bottom of the cone to provide agitation at low liquid levels.

6-2.1.4 Draft Tubes. A draft tube is a tube installed centrally within the vessel. Axial flow impellers located inside a draft tube are used to provide an efficient top-to-bottom circulation pattern, which is important for flow-controlled processes. Draft tubes reduce the standard deviations in process variables such as concentration, density, and viscosity. They are also useful in tanks with a high ratio of height to diameter.

6-2.1.5 Motor/Gearbox. The motor and gearbox constitute the drive system of the mixer. The motor can be electric (induction or DC), or driven by air pressure, hydraulic fluid, steam turbine, or diesel and gas engine. Typical power ratings of commercially available electric motors are given in Table 6-2. A gearbox is used to obtain the desired mixer shaft speed from the motor speed; the speed is fixed based on the frequency of the power supply, typically 1750 rpm at 60 Hz electric power. Depending on the desired mixer shaft speed, a gearbox can

Table 6-2 Standard Motor Power and Mixer Speeds

Motor Power (hp)						Mixer Speed (rpm)					
$\frac{1}{4}$	$\frac{1}{2}$	1	$1\frac{1}{2}$	2	3	4	5	6	$7\frac{1}{2}$	9	11
5	$7\frac{1}{2}$	10	15	20	25	$13\frac{1}{2}$	$16\frac{1}{2}$	20	25	30	37
30	40	50	60	75	100	45	56	68	84	100	125
125	150	200	250	300	350	155	190	230	280	350	
400	500	600									

have a two- or three-step gear reduction. Although the gearbox can be fabricated to provide any gear ratio, there are standard gear ratios to provide mixer shaft speeds given in Table 6-2 and represented by Rautzen et al. (1976) as a chart of the available motor horsepowers and the corresponding available shaft speeds for each given horsepower.

6-2.1.6 Inlets/Outlets. The location and design of inlets and outlets are based on the process, type of feed, and sensitivity of the process result to the rate of feed dispersion. For slow batch processes, the feed inlet can be from the top. It should be pointed at an active surface away from the tank wall and the impeller shaft. For processes requiring quick dispersion of the feed, the inlet nozzle should be located in a highly turbulent region such as the suction or discharge of the impeller, as discussed extensively in Chapter 13. The inlet nozzle should be sized to prevent backmixing of the tank contents into the inlet pipe, where lack of mixing may cause poor process results. Specific guidance is available from Jo et al. (1994). When feeding solids into a liquid, the feed rate must be controlled to closely match the rate of solid wetting, incorporation, and dispersion by the mixer.

The outlet is generally located on the side near the tank bottom or in the bottom head if the vessel needs to be drained completely. When solids are present, this bottom outlet can get plugged and can cause poor contacting of liquid and solids unless fitted with a flush-bottomed valve. A small impeller, installed very close to the tank bottom, also helps to eliminate this problem and provides mixing at low liquid levels. In continuously operated agitated tanks, the outlet must be located far from the inlet to minimize short-circuiting of the feed.

6-2.1.7 Heat Transfer Surfaces. When the process requires heat addition to or removal from the process fluid, the mixing tank must be equipped with appropriate heat transfer surfaces. Liquid motion supplied by the mixer enhances the heat transfer coefficient. Commonly used heat transfer surfaces, shown in Figure 6-8, include jackets, internal helical coils, and internal baffle coils. A jacket can be a tank outside the main tank, baffled, half-pipe, or dimpled. Each of these heat transfer surfaces can also be used in combination with a single coil or multiple heating coils installed within the space between the impeller and the tank wall. A suitable heat transfer fluid must be supplied on the service side of the heat transfer surfaces.

Positioning of internal coils should be such that they are not placed in the discharge flow of the impeller. Since the impeller discharge flow is typically

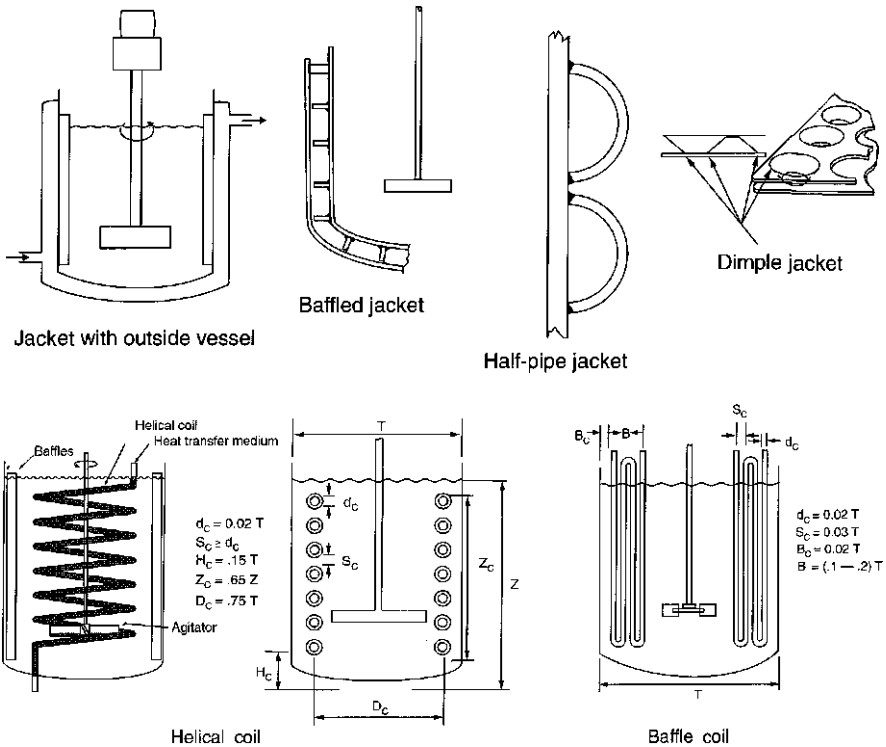


Figure 6-8 Heat transfer surfaces for stirred tanks.

pulsating, the coils and supports may suffer excessive fatigue and wear. Helical coils can be sized to act as a draft tube and enhance internal circulation and mixing. (See Chapter 14 for additional information on heat transfer and heat transfer correlations.)

6-2.1.8 Gas Sparger. A gas sparger is used when a gas is introduced into the liquid for efficient gas–liquid contacting for mass transfer and/or reaction. While the mixer design and operation control the gas–liquid interfacial area, a well-designed and well-located sparger can enhance the gas–liquid process result by maximizing contacting and eliminating maldistribution. A commonly used sparger configuration consists of a ring with equally spaced sparger holes positioned below the impeller. The sparger diameter should be less than the impeller diameter, typically 0.8 times the impeller diameter. Other shapes can also be effective as long as the sparger holes are well distributed across the tank cross-section and are active. A common problem with gas spargers in a gas–liquid–solids system is that the sparger can be sanded in quickly with solids. Under such conditions, maldistribution of gas can be significant. Each sparger

hole may have to be individually controlled. The reader is referred to Chapter 11 for additional information on gas–liquid mixing and to Chapter 18 for special considerations in sparger design for biological reactors.

6-2.2 Impeller Selection

There are literally hundreds of impeller types in commercial use. Determination of the most effective impeller should be based on the understanding of process requirements and knowledge of physical properties. Impellers can be grouped as turbines for low to medium viscosity fluids and close-clearance impellers for high viscosity fluids. Turbine impellers are further characterized, based on flow patterns, as axial flow and radial flow. Recent developments in the impeller technology have been focused on increasing axial flow at reduced shear. These impellers use a hydrofoil blade profile for efficient and more streamlined pumping. There are also many specialty impeller designs developed for specific process needs.

In this section we describe turbine impellers used in transitional and turbulent flow applications. High viscosity applications and appropriate impeller types are discussed in Section 6-6. Further discussions of impellers may be found in Chapter 21 and in Dickey et al. (2001). A number of video clips illustrating the effects of impeller selection are included on the Visual Mixing CD.

There are four types of turbine impellers, which are characterized by the flow patterns and level of shear they create: axial flow, radial flow, hydrofoil, and high-shear impellers. They have the widest use in low and medium viscosity liquid applications, solids suspension, liquid–liquid emulsification, and gas dispersion. Turbine impellers can have blades varying from 2 to 12 in number. Two blades are normally unstable mechanically, while it is difficult to install more than six blades on a hub. Axial flow impellers generally have three or four blades, and radial flow impellers are designed with six blades.

6-2.2.1 Axial Flow Impellers. Axial flow impellers (Figure 6-9) are used for blending, solids suspension, solids incorporation or draw down, gas inducement, and heat transfer. The oldest axial flow impeller design is the marine propeller, which is often used as a side-entering mixer in large tanks and as a top-entering mixer in small tanks. It can be designed with a different pitch to change the combination of pumping rate and thrust. Due to its fabrication by casting, a propeller becomes too heavy when large. It is not generally used as a top-entering impeller for tank sizes larger than 5 ft.

A pitched blade turbine consists of a hub with an even number of blades bolted and tack-welded on it. It is lighter in weight than a propeller of the same diameter. The blades can be at any angle between 10 and 90° from the horizontal, but the most common blade angle is 45°. The flow discharge from a pitched blade impeller has components of both axial and radial flow velocity in low to medium viscosity liquids, and is considered to be a mixed-flow impeller. Most

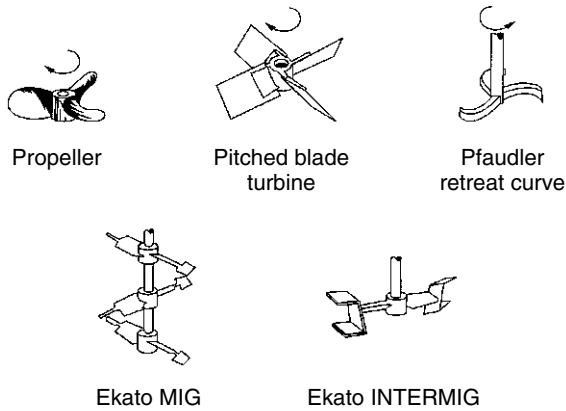


Figure 6-9 Axial flow impellers.

applications require the impeller rotation to direct the flow toward the bottom head or down-pumping. However, in some situations, such as gas dispersion and floating solids mixing, up-pumping may be more effective.

The retreat blade impeller was developed by the Pfaudler Company specifically for glass-lined reactors used for highly corrosive fluids. This was the only impeller geometry at that time which could hold a glass covering. However, current technology allows glassing of very complex impeller geometries for several impeller types, including the ability to combine two impellers on the same shaft. The retreat blade impeller is now being phased out in favor of the more effective and scalable new generation of impellers made possible by major advances in glass-lined technology. Further information on these impellers may be found in Chapter 17. In glass-lined tanks, glassed baffles (see Figure 6-7) are not installed on the wall but are supported through nozzles in the top and/or bottom head. However, one manufacturer (DeDietrich) has recently developed a three-baffle system in which the baffles are integral with the vessel wall.

The Ekato Company developed two two-bladed axial flow impellers, the Mig and the Intermig, mainly for high viscosity liquids. However, they can be effective for low to medium viscosity liquids as well. These impellers are designed at high impeller/tank diameter ratio (D/T) and have two sections of blades at opposite angles. If the inner blade pumps down, the outer blade pumps up to enhance the liquid circulation. The outer blade section of Intermig has two staggered sections designed for minimizing local form drag losses, which results in more distinct axial flow and a lower power number. Three Mig impellers are recommended for a liquid height/tank diameter ratio (H/T) of 1.0, while two Intermig impellers are adequate for the same configuration. Both impellers are sized at $D/T = 0.7$ for turbulent conditions and require wall baffles. For laminar conditions, $D/T > 0.7$ is used without wall baffles. These impellers have been found to be excellent for crystallization operations because they combine low shear with good circulation.

6-2.2.2 Radial Flow Impellers. Like axial flow turbine impellers, radial flow impellers (Figure 6-10) are commonly used for low to medium viscosity fluids. Although they can be used for any type of single- and multiple-phase mixing duty, they are most effective for gas–liquid and liquid–liquid dispersion. Compared to axial flow impellers, they provide higher shear and turbulence levels with lower pumping. Radial flow impellers discharge fluid radially outward to the vessel wall. With suitable baffles these flows are converted to strong top-to-bottom flows both above and below the impeller.

Radial flow impellers may either have a disk (Rushton turbine) or be open (FBT) and may have either flat or curved blades (backswept turbine). Impellers without the disk do not normally pump in a true radial direction since there is pressure difference between each side of the impeller. This is also true when the impellers are positioned in the tank at different off-bottom clearances. They can pump upward or downward while discharging radially. Radial discharge flow patterns can cause stratification or compartmentalization in the mixing tank. Disk-type radial impellers provide more uniform radial flow pattern and draw more power than open impellers. The disk is a baffle on the impeller, which prevents gas from rising along the mixer shaft. In addition, it allows the addition of a large number of impeller blades. Such blade addition cannot be done easily on a hub. A disk can also be used with a pitched blade turbine for use in gas–liquid mixing.

The Rushton turbine is constructed with six vertical blades on the disk. Standard relative dimensions consist of blade length of $D/4$, blade width of $D/5$, and the disk diameters of $0.66D$ and $0.75D$. The backswept turbine has six curved blades with a power number 20% lower than the Rushton turbine. The backswept nature of the blades prevents material buildup on the blades. It is also less susceptible to erosion. Typical applications include general waste and fiber processing in pulp and paper industries.

The recently developed hollow-blade impellers (e.g., Scaba SRGT, Chemineer CD6, and the Smith impeller) provide better gas dispersion and higher gas-holding

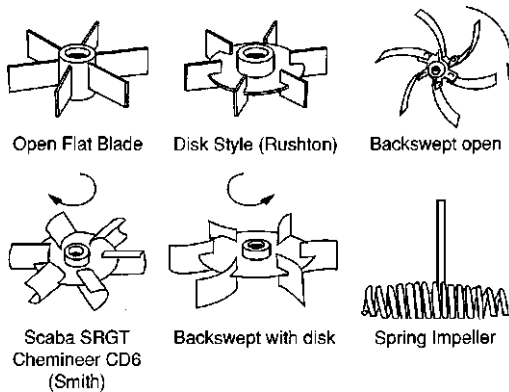


Figure 6-10 Radial flow impellers.

capacity than the Rushton turbine. The impeller blades are semicircular or parabolic in cross-section. This general shape allows for much higher power levels to be obtained in the process than that obtained by the Rushton turbine during gas dispersion. Gas dispersion is discussed in Chapters 11 and 18.

The coil or spring impeller was developed for systems where solids frequently settle to the tank bottom. When buried in stiff solids, a spring impeller is able to dig itself out of the solids without breaking an impeller blade.

6-2.2.3 Hydrofoil Impellers. Hydrofoil impellers (Figure 6-11) were developed for applications where axial flow is important and low shear is desired. They have three or four tapering twisted blades, which are cambered and sometimes manufactured with rounded leading edges. The blade angle at the tip is shallower than at the hub, which causes a nearly constant pitch across the blade length. This produces a more uniform velocity across the entire discharge area. This blade shape results in a lower power number and higher flow per unit power than with a pitched blade turbine. The flow is more streamlined in the direction of pumping, and the vortex systems of the impeller are not nearly as strong as those of the pitched blade turbine.

Lightnin A310, Chemineer HE3, and EMI Rotofoil are characterized by a low solidity ratio, defined by a projected area of impeller blades divided by the impeller horizontal cross-sectional area. They are very efficient impellers for liquid blending and solids suspension.

Hydrofoil impellers with a high solidity ratio include the Lightnin A315 and Prochem Maxflo. This feature makes them effective for gas dispersion in viscous systems in addition to liquid blending and solids suspension. The Maxflo impeller is constructed with a larger drum-type hub with three or five trapezoidal and cambered blades. The two-bladed Ekato Interprop is designed with a high angle of attack of the blade and with an additional leading blade wing. This configuration provides an improved lift/resistance ratio and more intense axial impulse compared to other hydrofoils. Interprop is, therefore, used effectively for dispersion applications in addition to blending and solids suspension.

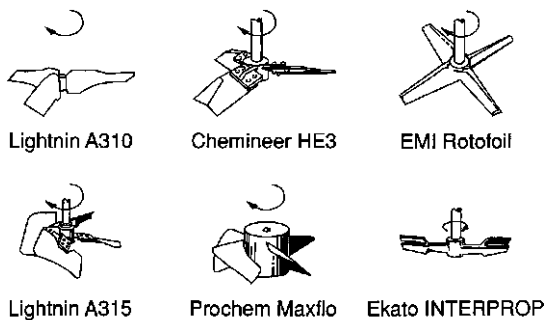


Figure 6-11 Hydrofoil impellers.

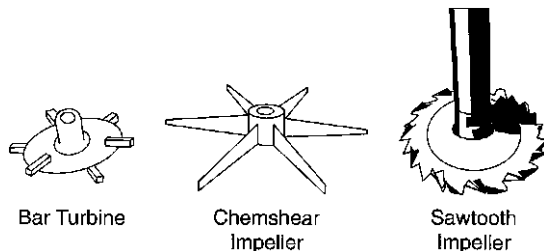


Figure 6-12 High-shear impellers.

6-2.2.4 High-Shear Impellers. High-shear impellers (Figure 6-12) are operated at high speeds and are used for the addition of a second phase (e.g., gas, liquid, solid, powder) in grinding, dispersing pigments, and making emulsions. These dispersing impellers are low pumping and therefore are often used along with axial flow impellers for providing both high-shear and homogeneous distribution. At the lower end of the high-shear range is the bar turbine, which has square cross-section bars welded to a disk. The Chemshear impeller has tapered blades and provides intermediate shear levels. A very high-shear producing sawtooth impeller consists of a disk with serrations around its circumference. It provides reasonably high intensity of turbulence in the vicinity of the impeller.

6-2.3 Impeller Characteristics: Pumping and Power

Power numbers, pumping numbers, shear levels, and flow patterns characterize the various impellers described above. All the power applied to the mixing system produces circulating capacity, Q , and velocity head, H , given by

$$Q \propto ND^3 \quad (6-1)$$

$$H \propto N^2D^2 \quad (6-2)$$

Q represents internal circulation and H provides the shear in mixing. In a sense, the velocity head, H , provides the kinetic energy that generates shear through the jet or pulsating motion of the fluid. Both expressions have not included the effects of the number of blades and blade width. Head results in shear and is dissipated by turbulence. Equation (6-1) can be rewritten as

$$Q = N_Q ND^3 \quad (6-3)$$

where N_Q is the pumping number, which depends on the impeller type, the D/T ratio, and impeller Reynolds number, defined as

$$Re = \frac{\rho ND^2}{\mu} \quad (6-4)$$

6-2.3.1 Pumping and Pumping Number. Pumping is the amount of material discharged by the rotating impeller. The values of N_Q under turbulent conditions are known for the commonly used impellers and are given in Table 6-3. As can be seen, the values of pumping number for most commonly used impellers vary in the range 0.4 to 0.8. As a result, all standard impellers will pump at about the same rate for a given diameter and mixer speed.

Figure 6-13 shows the relationship of N_Q with Re and D/T for a 45° pitched blade turbine (PBT). As evidenced in this figure, N_Q increases as Re increases up to Re of 10 000 and becomes constant at higher Re . Also, smaller diameter impellers have higher pumping numbers. Figure 6-13 also shows that these impellers should not be used below a Reynolds number of 1000 if high pumping efficiency is desired. Similar plots of N_Q are available for a variety of impellers from the respective vendors.

Table 6-3 Pumping Number, N_Q , under Turbulent Conditions for Various Impellers

Impeller Type	N_Q
Propeller	0.4–0.6
Pitched blade turbine	0.79
Hydrofoil impellers	0.55–0.73
Retreat curve blade	0.3
Flat-blade turbine	0.7
Disk flat-blade turbine (Rushton)	0.72
Hollow-blade turbine (Smith)	0.76

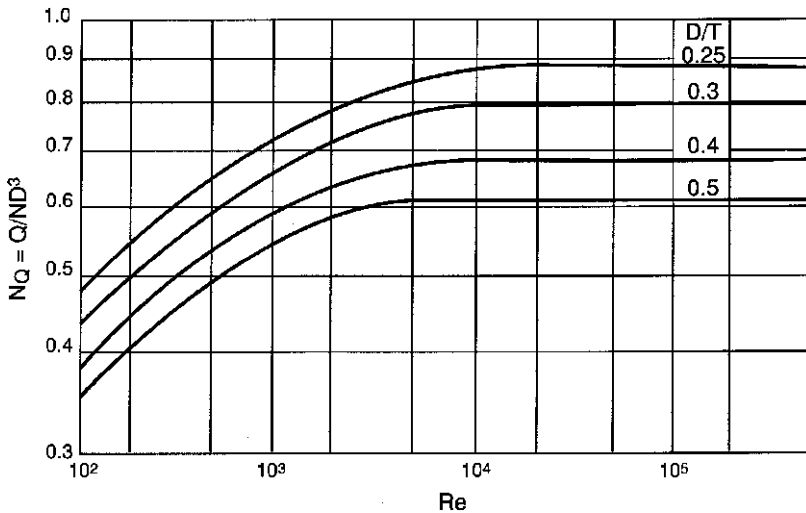


Figure 6-13 Pumping number versus impeller Reynolds number for pitched blade turbine.

Pumping of an impeller changes with the changes in impeller geometry and batch size. For example, pumping is dependent on number of blades and the blade width. Limited data are available in the literature and from vendors on these effects. Pumping also changes with varying liquid level. Unfortunately, quantification of this effect is not available.

It is important to note that some impellers and mixer configurations do not pump well. For example, the retreat curve blade impeller in an unbaffled vessel creates solid body rotation and poor pumping. Pumping with close-clearance impellers such as anchors and helical ribbon can be very high or, sometimes, very poor, depending on conditions and the materials being pumped. Turbulent impellers in laminar applications only pump locally. Often, the rest of the tank goes unmixed.

6-2.3.2 Power and Power Number. The power consumed by a mixer can be obtained by multiplying pumping, Q , and head, H , and is given by

$$P = \frac{N_p \rho N^3 D^5}{g_c} \quad (6-5)$$

where N_p is the power number and depends on impeller type and impeller Reynolds number.

Using another viewpoint, power, generated by an individual section of an impeller, is equal to the drag, F , multiplied by the impeller velocity, V , for that section or

$$P = FV \quad (6-6)$$

This is then summed over the entire impeller to obtain the total power. Form and skin drag in the turbulent regime are represented by

$$F = 0.5C_d \rho V^2 A_p \quad (6-7)$$

where C_d is drag coefficient, ρ the density of fluid around the impeller, and A_p the projected area of the impeller blade.

Substituting eq. (6-7) into (6-6) yields

$$P = 0.5C_d \rho V^3 A_p \quad (6-8)$$

Since all velocities in a mixing tank are proportional to the tip speed ($= \pi ND$) and the impeller projected area is proportional to D^2 , the power can be represented by

$$P \propto C_d \rho N^3 D^5 \quad (6-9)$$

Comparing eqs. (6-5) and (6-9), the power number N_p can be considered similar to a drag coefficient. Just as the drag coefficient under turbulent flow is a function

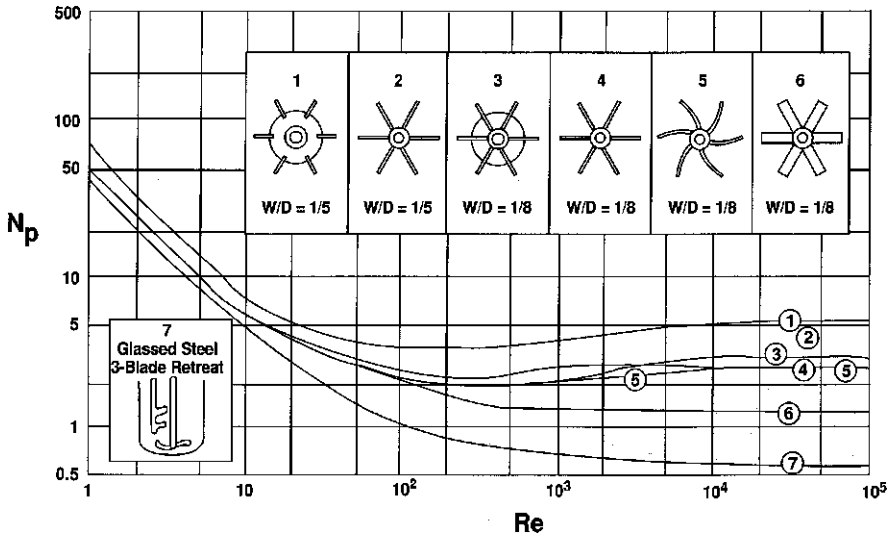


Figure 6-14 Power number versus impeller Reynolds number for seven different impellers. (Modified from Rushton et al., 1950.)

of geometry and independent of Reynolds number, N_p also is constant at high Re for a given impeller geometry.

The power number, N_p , also is a function of impeller blade width, number of blades, blade angle, D/T , baffle configuration and impeller elevation. Figure 6-14 shows the relationship between N_p and Re for seven impellers. It is important to recognize that at $Re < 100$, the conditions become laminar flow; and mixing quality, obtained using these impellers, becomes extremely poor. Under such conditions, impellers designed for laminar flow conditions are recommended.

While Figure 6-14 provides the power number data in a wide range of Re , the information should not be used below an impeller Reynolds number of 1000. The flow regimes are (1) laminar flow below a Reynolds number of 10, (2) transition between Reynolds numbers of 10 and 10^4 , and (3) turbulent above a Reynolds number of 10^4 . The functionality between N_p and Re can be described as follows:

- $N_p \propto Re^{-1}$ in the laminar regime and power depends greatly on viscosity.
- $N_p = \text{constant}$ in turbulent regime ($Re > 10\,000$) and is independent of liquid viscosity.
- N_p changes slightly in the transitional regime ($100 < Re < 10\,000$).
- N_p for turbine impellers varies with blade width as follows:
For a six-bladed Rushton

$$N_p \propto (W/D)^{1.45} \tag{6-10}$$

For a four-bladed 45° pitched blade

$$N_p \propto (W/D)^{0.65} \tag{6-11}$$

- The functionality with number of blades is given by:
For three to six blades

$$N_p \propto (n/D)^{0.8} \tag{6-12}$$

For six to twelve blades

$$N_p \propto (n/D)^{0.7} \tag{6-13}$$

- For turbines with four to eight curved blades, eq. (6-12) is valid.
- For pitched blade turbines, changing the blade angle θ changes the power number by

$$N_p \propto (\sin\theta)^{2.6} \tag{6-14}$$

The scale or size of a turbine impeller has a very small effect on its power number in the commonly used range $D/T = 0.33$ to 0.5 , when standard baffles are used.

The number of baffles (N_b) and their width (B) have a significant effect on N_p . As the parameter $N_b B$ increases, N_p increases (Figure 6-15) up to the power number of the conventional configuration, with four baffles having width equal to $T/10$. At higher $N_b B$ values, the power number is constant at a level which depends on D/T .

The effect of impeller elevation C on the power number is small for turbine impellers, especially the radial flow impellers. Figure 6-16 shows this effect for pitched blade (PBT), flat-blade (FBT), and disk flat-blade (DFBT) turbines with two different width ratios.

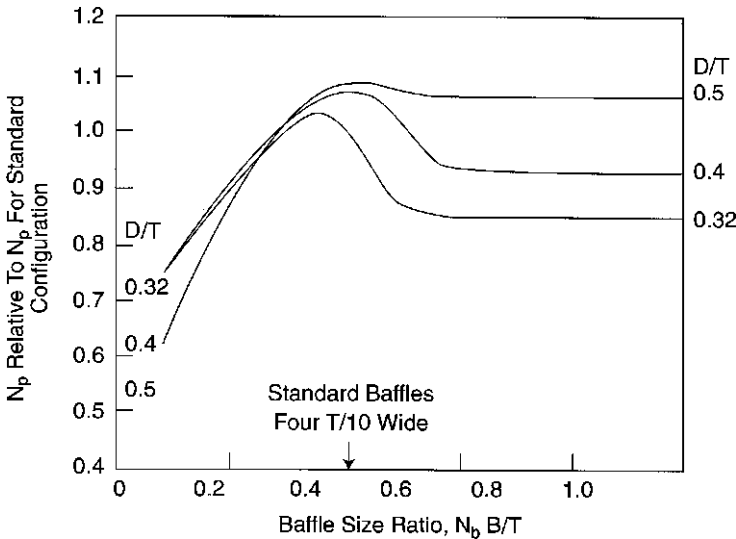


Figure 6-15 Effect of baffling and D/T on power number.

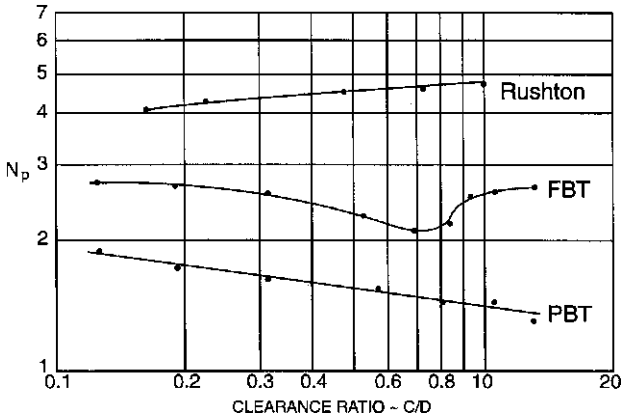


Figure 6-16 Effect of turbine clearance on power number for PBT, FBT, and DFBT with $N_b B/T = 0.33$.

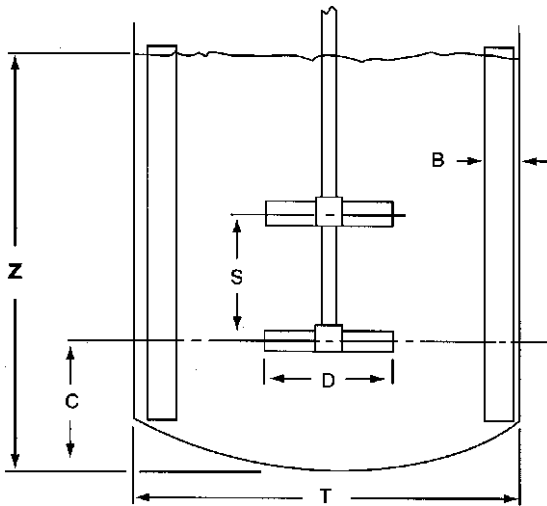


Figure 6-17 Two impellers on a shaft of top-entering mixer.

For PBTs the power number correlates with C as

$$N_p \propto (C/D)^{-0.25} \tag{6-15}$$

When multiple impellers are used on the same shaft (Figure 6-17), the combined power number may or may not be additive of individual power numbers. The power number for such a system depends on impeller type and spacing between the impellers (S/D) as shown in Figure 6-18.

Typical spacing between impellers is one impeller diameter. If impellers are placed closer than this, there is considerable interaction between them. In the

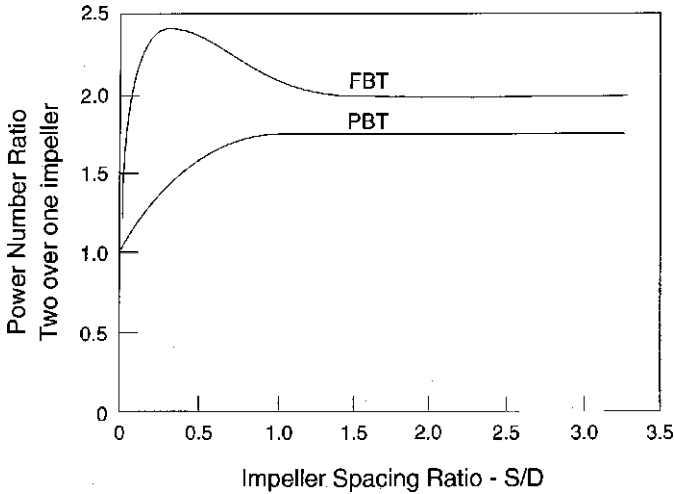


Figure 6-18 Effect of dual turbine spacing on power number for FBT and PBT.

case of an axial flow impeller such as the pitched blade turbine, the combined power is significantly less than twice the single-impeller power. With a flat-blade turbine, however, the total power may exceed twice the single-impeller power, depending on the impeller spacing. If the impellers are too close to each other, the total power is reduced.

The power number of side-entering propellers depends on the impeller Reynolds number and the pitch. The propeller pitch is defined as the distance traversed by the propeller in one revolution divided by the diameter. For a square pitch (pitch = 1.0), this distance is equal to the diameter. As shown in Figure 6-19, N_p is higher for higher-pitch propellers at all values of Re .

It is important to recognize that at $Re < 100$, the flow conditions would approach laminar flow and mixing quality with these propellers would be poor. The power number functionality with propeller pitch between 1.0 and 2.0 at $Re > 1000$ can be approximated by

$$N_p \propto (p/D)^{1.5} \quad (6-16)$$

The power numbers of several other commonly used impellers under turbulent conditions are given in Table 6-4.

6-3 FLOW CHARACTERISTICS

Flow characteristics for an impeller can be divided into:

- Flow patterns
- Pumping
- Shear

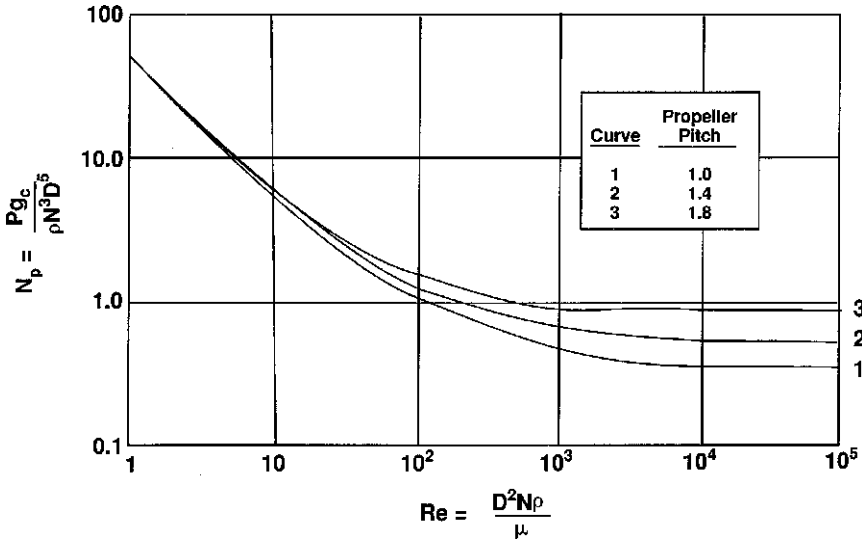


Figure 6-19 Power number of side-entering propellers versus Reynolds number.

Table 6-4 Power Numbers of Various Impellers under Turbulent Conditions with Four Standard Baffles

Impeller Type	N _p
Concave- or hollow-blade turbine	4.1
Ekato MIG—3 impellers, D/T = 0.7	0.55
Ekato Intermig—2 impellers, D/T = 0.7	0.61
High-shear disk at Re = 10 000	0.2
	(lower for lower Re)
Lightnin A310	0.3
Chemineer HE3	0.3
The following are all for D = T/3, C = T/3, and blade width W = D/5:	
45°PBT; 4 blades	1.27
45°PBT; 6 blades	1.64
Marine propeller (1.0 pitch)	0.34
Marine propeller (1.5 pitch)	0.62
Smith or concave- or hollow-blade with 6 blades	4.4

All impellers generate some sort of flow pattern. These flow patterns, coupled with the flow regime, determine relative levels of pumping and shear. All impellers can therefore be categorized by variations in their pumping and shear capabilities. For example, axial flow hydrofoils are mostly pumping and low-shear impellers. Radial flow impellers, on the other hand, provide high shear but low pumping.

6-3.1 Flow Patterns

The mixing process result is highly influenced by the impeller flow patterns. There are mainly two types of flow patterns with top-entering mixers, axial and radial, depending on the impeller type (Figure 6-20). Axial flow impellers, including propellers, pitched blade turbines, and hydrofoils, produce a flow pattern throughout the entire tank volume as a single stage, as shown in Figure 6-20*b* and *c*. The pitched blade turbine (PBT) has a good balance of pumping and shear capabilities and therefore is considered to be a general-purpose impeller. The hydrofoils produce about the same pumping but at lower shear and turbulence levels than a PBT. The discharge from hydrofoils is more streamlined compared to a PBT, which gives a small reverse loop underneath.

Radial flow impellers, on the other hand, produce two circulating loops, one below and one above the impeller (Figure 6-20*a*). Mixing occurs between the two loops but less intensely than within each loop. This is an example of compartmentalization mentioned earlier. A true axial flow is usually created with hydrofoil impellers, which provide a confined flow similar to that created in a draft tube. These differences in flow patterns can cause variations in distribution of shear rate and energy dissipation rate within the mixing tank. Depending on the process requirements, a suitable impeller can be chosen based on the flow patterns and resulting shear rates. For example, liquid blending can be achieved

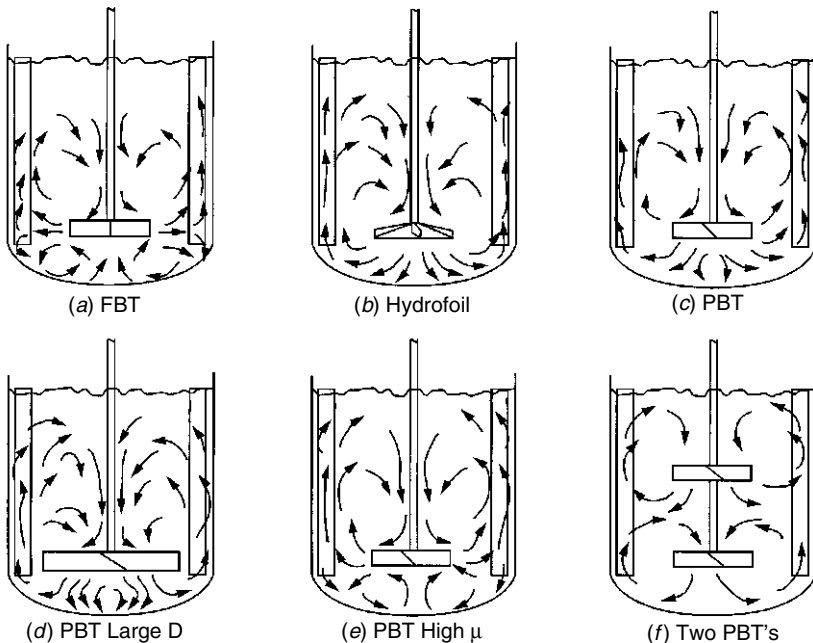


Figure 6-20 Flow patterns with different impellers, impeller diameter, and liquid viscosity.

efficiently through a single circulation loop from axial flow impellers, whereas dispersion of gas bubbles is better obtained with dual circulation loops using radial flow disk impellers.

The flow patterns with a given impeller are altered by parameters such as impeller diameter, liquid viscosity, and use of multiple impellers. For example, the flow pattern with a PBT becomes closer to radial as the impeller diameter is increased (Figure 6-20*d*) or liquid viscosity is increased (Figure 6-20*e*). Multiple impellers are used when liquid depth/tank diameter ratio is higher than 1.0. In that case, more circulation loops are formed (e.g., two loops with PBT; Figure 6-20*f*). Radial flow impellers give two circulation loops with each impeller.

For suspension of sinking solids, it is important to provide liquid velocities directed to the tank floor for an effective sweeping action. Hydrofoils perform well in this duty. However, if the solids have any tendency to be sticky and cling to the blades, the effectiveness of a hydrofoil can be reduced. This can reduce its versatility as a multipurpose impeller.

In addition to suspending solids off the tank bottom, a process may require homogeneous suspension throughout the bulk. An additional axial flow impeller, perhaps an up-pumping one, may be needed at a higher level for this purpose. Radial flow impellers can be designed to suspend solids, especially if placed on the bottom of the tank, but are less efficient and provide relatively poor solids homogeneity in the bulk.

When using axial flow impellers, the mixer rotation can be reversed to create up-pumping action. This pumping mode can be effective for some systems, such as entrainment of floating solids and gas dispersion. The up-pumping flow provides an effective mechanism for incorporating lighter solids on the liquid surface near the wall. This avoids the need for creating a vortex, which can cause air entrainment and mechanical vibrations (see Chapter 10). For gas dispersion, the up-pumping impeller is generally used at the bottom along with a down-pumping impeller at the top. Such a configuration can provide good gas-holding capacity and prevent mechanical vibrations caused by opposite flows resulting from a down-pumping impeller at the bottom. Up-pumping applications are relatively new and require careful testing and study before use (see Chapter 11).

For effective blending of liquids in large tanks using side-entering propeller mixers, it is important to create the flow patterns shown in Figure 6-21. This is achieved by positioning the horizontal mixer 10 degrees to the left of tank centerline, assuming that the propeller rotates clockwise looking from the motor side. If the mixer is positioned along the tank centerline, the jet flow can cause vortexing on the surface. This vortexing can reduce blending efficiency and possibly entrain air into the liquid product.

Variations in flow patterns for axial flow impellers can be generated to advantage by changing the impeller position or by baffling. For example, axial flow impellers provide radial flows when placed near the tank bottom. For submergence of floating solids, the tank is often unbaffled in the top half to create a controlled vortex useful for pulling down solids. The same method can also be used for surface inducement of gas from vapor space (Oldshue, 1983) and

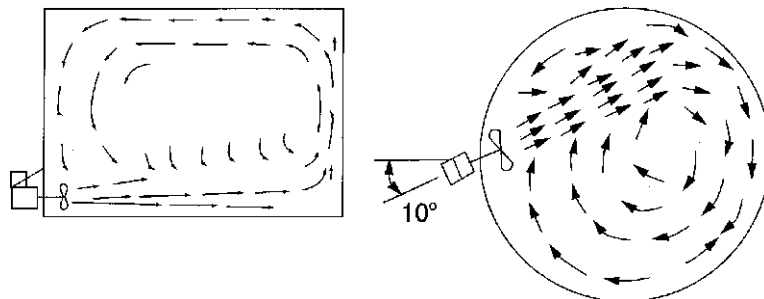


Figure 6-21 Flow patterns with side-entering propeller mixers.

has been found to be very effective in hydrogenation applications. Care must be taken, however, to avoid gas overloading that could cause mechanical vibrations and damage to seals and bearings.

Flow patterns of high-shear impellers, such as the bar turbine, Chemshear, and sawtooth impeller, are similar to those of radial flow impellers. The major difference is in lower pumping at higher shear. Backswept turbine and spring impeller also have similar radial flow patterns. It is important to understand the flow patterns around the impeller blades, where dispersion and attrition processes occur. Changing the blade geometry changes these flow patterns and alters the shear.

High-speed flows and vortices occur behind the impeller blades and remain coherent as the flow moves into the bulk. The velocities in these flows can be higher than the impeller tip velocity. Vortices are low-pressure regions that can coalesce lower-density materials and sometimes form gas pockets and cavities. Strong vortices are important for dispersion processes, while high velocity flows are desired for liquid blending and solids suspension.

While velocities and shear are high near the impeller, velocities and shear are generally low away from the impeller, particularly in corner areas and at the liquid surface. Processes such as coalescence, agglomeration, and flocculation occur in these regions where energy levels are low. For maximizing mixing efficiency, it is important to add materials away from these regions. See Chapters 13 and 17 for discussions of the impact of feed position on fast reactions.

6-3.2 Shear

Whenever there is relative motion of liquid layers, shearing forces exist that are related to the flow velocities. These forces, represented by shear stress, carry out the mixing process and are responsible for producing fluid intermixing, dispersing gas bubbles, and stretching/breaking liquid drops. The shear stress is a complex function of shear rate defined by the velocity gradients, impeller blade pressure drop, turbulence level, and viscosity. These velocity gradients represent velocity differences between adjacent portions of materials, which are therefore sheared and dispersed. By measuring time-averaged velocities near the impeller blade

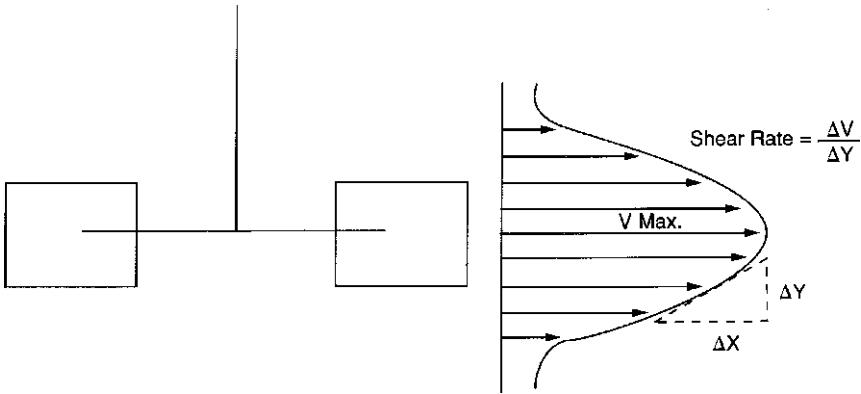


Figure 6-22 Vertical velocity profile near impeller blade.

(Figure 6-22), macroflow velocity gradient and shear rate can be obtained by taking the slope.

Shear rate, with reciprocal time as the unit, can be viewed as a time constant. If a process has a shear rate of 1000 s^{-1} , the events in the flow occur on the order of 1 ms. Such high shear rates are generated in the immediate vicinity of the impeller. However, the volume of this region is relatively small and, therefore, a very small amount of the material experiences these shear rates. The conditions in the vortices are similar, with high shear rate but small volume. The overall mixing process is defined by the combination of shear rate and the volume. Detailed information on the distribution of shear rates and respective volumes is difficult to obtain experimentally. Computational fluid dynamics can be used to extract such information for given mixing conditions.

The local shear rate in the flow for a disk turbine in Newtonian and shear thinning fluids is proportional to mixer speed, as indicated by data of Metzner and Taylor (1960) shown in Figure 6-23:

$$\gamma = KN \quad (6-17)$$

where the proportionality constant K decreases rapidly with distance from the impeller blade tip. Equation (6-17) is often referred to as the *Metzner–Otto relationship*. The validity of eq. (6-17) has been demonstrated for laminar flow, transitional flows, and a portion of the turbulent regime. The values of proportionality factor for various impellers are given in Table 6-5.

The Metzner–Otto relationship, eq. (6-17), does not apply for other non-Newtonian fluids, such as shear thickening fluids, Bingham plastics, and false body fluids. In these fluids, shear rates are highly localized around the impeller blade, with the rest of the tank stagnant. The relationship does not apply in highly turbulent flow as well.

As discussed earlier, shear rates are different in different parts of a mixing tank. Therefore, there are several types of shear rate:

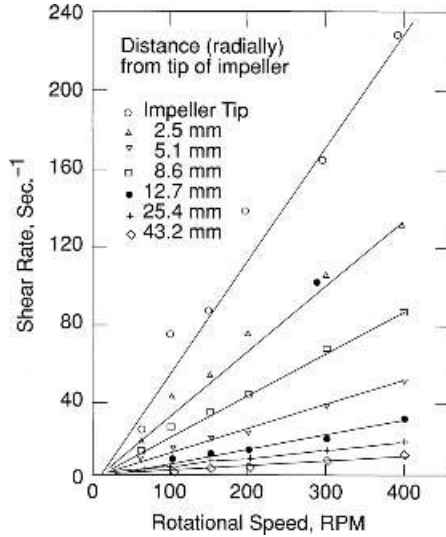


Figure 6-23 Shear rate distributions at different distances from the impeller in Karo Syrup. (Data from Metzner and Taylor, 1960.)

Table 6-5 Metzner–Otto Constant for Shear Rate versus Mixer Speed

Impeller	Propeller	Rushton	Helical Ribbon	Anchor
K	10	12	30	25

1. Maximum shear rate on the impeller blade is:

$$\gamma \sim 2000 N \tag{6-18}$$

2. Maximum shear rate in the flow has two interpretations:

$$\gamma \sim 150 N \tag{6-19a}$$

$$\gamma \propto \text{Tip Speed}(= \pi ND) \tag{6-19b}$$

with a dimensional proportionality constant. It occurs near the blade tip in high-speed jets and vortices.

3. Average shear rate in the impeller region is:

$$\gamma \sim KN \tag{6-20}$$

where the proportionality constant varies between 5 and 40 for most impellers as listed in Table 6-5.

4. Average shear rate in the entire tank: about one order of magnitude less than definition 3.

5. *Minimum shear rate*: about 25% of definition 4 and is near the liquid surface.

Understanding the magnitude and location of shear in an agitated tank has significant implications for design. For example, if the power of the feed jet is substantial, feed nozzles should be located in low-shear regions. The feed jet would do the mixing in such regions and prevent dead zones. If the feed jet has relatively little power, feeding into a dead zone is probably not advantageous to processing. Very little material actually experiences the very high shear rates on the blade in an agitated tank. Some material experiences the maximum shear rates. Maximum shear in the flow may need to be limited for shear-sensitive materials: for example, crystals (Chapter 17) and biological materials (Chapter 18).

At high Reynolds numbers, the concepts of shear, mean shear, and the impeller rotational speed, N , become unimportant relative to the impeller tip velocity, ND . Viscosity is no longer the mechanism by which momentum is transferred.

Dispersion processes are correlated with Weber number to -0.6 power and sometimes impeller tip speed. Weber number is typically defined as $\rho N^2 D^3 / \sigma$, where σ is the surface or interfacial tension.

When scaling-up agitated tanks, mixer speed generally decreases and tip speed increases; resulting in lower average shear and higher maximum shear rate at the blade tip. If scale-up is based on constant power per unit volume (P/V), the shear rate away from the impeller becomes lower in the larger vessel. This results in a wider distribution of shear rates on scale-up. The change in shear rate distributions on scale-up affects the mixer performance significantly. For example, feed nozzle location near the impeller blade tip for single-phase systems is more important in large vessels than in laboratory scale vessels. For liquid–liquid mixing, the dispersed phase drop size distribution can be wider in the large agitated tank. For crystallization, the average particle size can be larger and size distribution wider in the large tank.

6-3.3 Impeller Clearance and Spacing

Impeller clearance from the tank bottom and impeller spacing for multiple-impeller systems can have a significant impact on the power number. In addition, these parameters influence the flow patterns and the process result. The extent of these impacts depends on the type of mixing system and mixing requirements. If an impeller is located very close to the tank bottom, down-pumping axial flow impellers provide flow patterns similar to radial flow impellers. This can result in reduced pumping and higher shear. For suspension of solids, this condition may be superior for keeping the tank bottom clear of solids but at a cost of reduced bulk homogeneity.

In tall agitated tanks, multiple impellers are often used to improve circulation and narrow the distribution of shear and energy dissipation. Generally, these impellers are spaced away from each other by a distance equal to one impeller diameter. However, to avoid splashing and the formation of a vortex, the top

Table 6-6 Recommended Impeller Clearance and Spacing

Mixing System	Maximum Liquid Height, Z/T	Number of Impellers	Impeller Elevation from Tank Bottom	
			Bottom	Top
Liquid blending	1.4	1	$Z/3$	—
	2.1	2	$T/3$	2 $Z/3$
Solids suspension	1.2	1	$Z/4$	—
	1.8	2	$T/4$	2 $Z/3$
Gas dispersion	1.0	1	$T/6$	—
	1.8	2	$T/6$	2 $Z/3$

impeller should not be located too close to the liquid surface. A deep vortex can cause air or vapor entrainment and dispersion. If impeller spacing of less than D is used, higher shear is generated between the impellers. General guidelines for impeller clearance and impeller spacing for different mixing processes are given in Table 6-6.

The corollary of impeller clearance is impeller submergence, also represented by the height of liquid above the impeller, or the top impeller in a multiple-impeller system. Adequate submergence is necessary to avoid excessive vortexing and entrainment of headspace gas. The minimum submergence requirement depends on the impeller type, pumping direction, and baffle width. For example, a submergence greater than $D/2$ is sufficient for down-pumping axial flow impellers and conventional baffles (width = $T/12$), while a minimum of D is required for narrow baffles (width = $T/50$). When a deep vortex is formed with low impeller submergence, excessive vibrations can occur along with incorporation of vapor bubbles and loss of mixing. Such conditions cause the mixing performance in an agitated tank to deteriorate. Alternative gas-liquid contacting methods are discussed in Chapter 11.

6-3.4 Multistage Agitated Tanks

When near-plug flow conditions along with high intensity mixing are desired, multistage mixing tanks provide effective and economical designs. The alternatives, such as a series of continuously stirred tanks, can be highly cumbersome, requiring high maintenance. Compartmentalized horizontal cylindrical tanks require the use of several mixers each with a motor/gearbox/shaft/impeller set. Plug flow can also be achieved with in-line mixers but at a cost of high pressure drop at short residence times. A multistage mixing tank (Figure 6-24), consisting of a vertical column divided by horizontal donut baffles and multiple mixers, can provide staged mixing for a variety of fluids and can be sized for the desired residence time. These mixing tanks are commonly used for blending with chemical reaction, gas absorption, extraction, dissolution, crystallization, caustic treatment, water wash, polymerization, and alkylation.

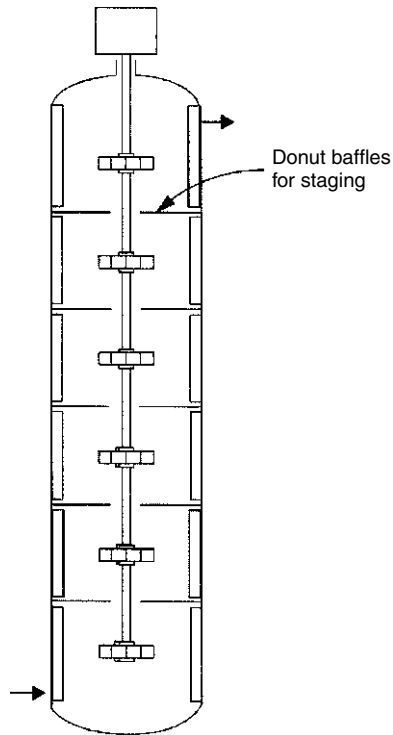


Figure 6-24 Multistage mixing tank.

Plug flow is important for continuous reacting and nonreacting processes to achieve high yield, selectivity, and mass transfer rates. As shown in Figure 6-25, the required volume of a CSTR can be two orders of magnitude higher than the volume of a plug flow reactor, depending on reaction order and conversion level.

Key issues in designing multistage mixing tanks include tank volume, height/diameter ratio, mixer design, interstage baffle opening size, and inlet–outlet locations. The tank volume is based on the desired mean residence time. The aspect ratio is determined on the basis of number of stages. Although more stages approach plug flow, generally four to six stages are satisfactory. The mixer is designed on the basis of process mixing requirements such as blend time, or quality of solids suspension, liquid–liquid emulsification, and gas dispersion. The mixer design includes type and number of impellers, diameter, mixer speed, and driver power. The interstage baffle opening must be sized based on acceptable level of exchange flows between stages. A larger opening increases exchange flow and backmixing, and as a result leads to lower stage efficiency. Draft tubes are sometimes used at these openings to reduce backmixing.

The inlet and outlet should be located at opposite ends of the mixing tank for best plug flow conditions. Several models are available in the literature for predicting backmixing and can be used to evaluate reactor performance. The

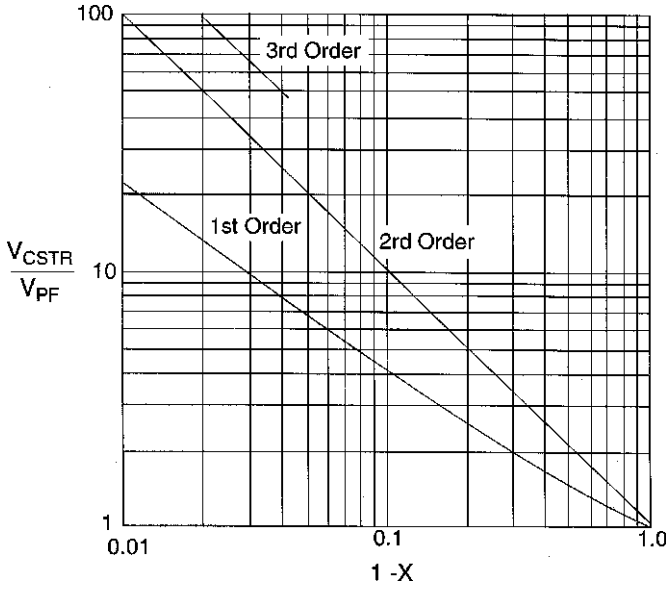


Figure 6-25 Ratio of volumes of CSTR/plug flow for chemical reactions.

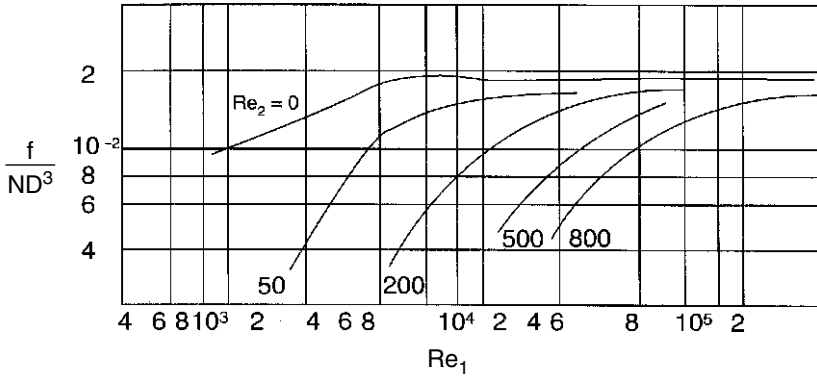


Figure 6-26 Backflow rate in a multistage mixing tank.

interstage back flow rate, f , is a function of impeller Reynolds number $Re_1 = ND^2/\nu$ and the flow Reynolds number $Re_2 = q/\nu D$, as shown in Figure 6-26 for an interstage opening of 33%. As evidenced by these data, backflow rate decreases as flow Reynolds number is increased.

The effect of forward flow velocity on backflow velocity was demonstrated by Xu et al. (1993). Their data, shown in Figure 6-27, indicate that backmixing can be reduced significantly by increasing the forward flow rate. The backflow velocity can be reduced significantly at high forward flow velocity or the reactor

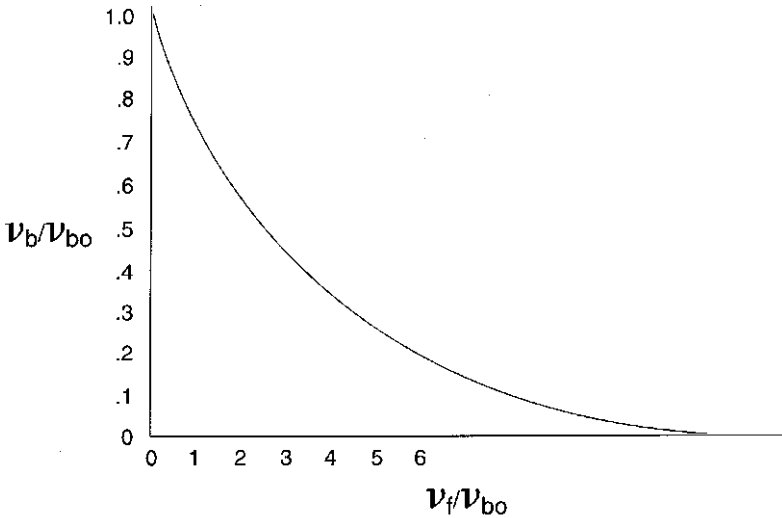


Figure 6-27 Backflow velocity as a function of forward flow velocity in a multistage mixing tank where v_b is the backflow velocity, v_{bo} the backflow velocity at zero throughput, and v_f the forward flow velocity.

throughput rate. It was also found that backflow velocity is proportional to a/A for a small opening of $a/A < 0.25$. If an opening at the wall is made available, backflow can increase considerably compared to an equal-sized opening in the center.

In multiphase reacting and nonreacting systems such as liquid–liquid and gas–liquid, very small openings of 1 to 2% of cross-sectional area may be required for high mass transfer. Small openings also minimize bypassing of the dispersed phase.

6-3.5 Feed Pipe Backmixing

For fast competitive chemical reactions, improper feed blending can cause the formation of undesired by-products. This occurs due to the high local concentrations of a feed component and the nature of the kinetics. To avoid such a problem, the feed nozzle should be located near the impeller, either in the flow of material directly to the impeller or near the exit flow of the impeller. If the feed nozzle velocity is too low or designed improperly, the tank contents may penetrate into the feed pipe and react. If the feed velocity is too high, the portions of the feed jet can pass through the impeller volume. Both situations can lead to poor reaction yield and selectivity. Backmixing in the feed pipe under poor mixing and high concentration of the feed component permits some undesirable reactions to occur, which result in poor selectivity. Similar results can occur with an excessively high velocity feed jet. For optimum design of the feed nozzle, the criteria listed in Table 6-7 are recommended based on the ratio of feed pipe velocity to impeller tip speed (v_f/v_t) for two impeller types (see also Chapter 13).

Table 6-7 Recommended v_f/v_t Values for Two Impeller Geometries for Turbulent Flow in Feed Pipe

Impeller Type	Feed Location	G/D^a	Recommended v_f/v_t
Rushton turbine	Radial	0.1	1.9
	Above impeller	0.55	0.25
Chemineer HE3	Radial	0.1	0.1
	Above impeller	0.55	0.15

^a G = Vertical distance between feed nozzle and impeller tip, $D/T = 0.53$

6-3.6 Bottom Drainage Port

Like any storage tanks, agitated tanks must be emptied frequently, especially in batch systems. Therefore, a bottom drain must be installed to minimize or eliminate any heel. These drain ports, even though closed during the mixer operation, can get plugged when sediments or solids are present in the liquid. These inventories can lead to product contamination and hinder mechanical operation of the drain valve. Pneumatically activated valves with stems designed to be flush with the inside wall can be used to avoid such problems. Small “kicker” blades ($D/T < 0.2$) positioned at a low level ($C/Z < 0.1$) can be very effective and consume little power because of the small diameter. The lower turbine of the newer glass-lined impeller combinations or as a single impeller in smaller vessels discussed in Section 6-2.2.2 can be positioned within a few inches of the bottom and can also be effective in solids discharge.

6-4 SCALE-UP

The main objective of scale-up is to design a large scale mixing system that will achieve the same mixing quality as in a laboratory tank. Since the distributions of shear rate and energy dissipation widen as the volume is increased, the mixer design must be adjusted to obtain the same process result. Therefore, it is important to understand the impact of these differences on the process. The scale-up criteria depend strongly on the process type and requirements. While the details are discussed in other chapters (liquid blending, Chapter 9; solids suspension, Chapter 10; gas dispersion, Chapter 11; immiscible liquid mixing, Chapter 12; and chemical reactions, Chapter 13), a few commonly used scale-up methods are discussed here. Other references on scale-up include Dickey et al. (2001) and Tattersson (1994).

Some scale-up methods emphasize geometric similarity. This refers to holding constant the impeller geometry, the impeller dimensional ratios (such as D/T , W/D , C/T), the liquid height/tank diameter ratio, and baffling. There are many situations when complete geometric similarity is not feasible: for example, when the aspect ratio of commercial scale tanks needs to be larger than the laboratory tank.

There are two commonly used scale-up criteria based on holding power per unit volume (P/V) or torque per unit volume (T_Q/V) constant on scale-up.

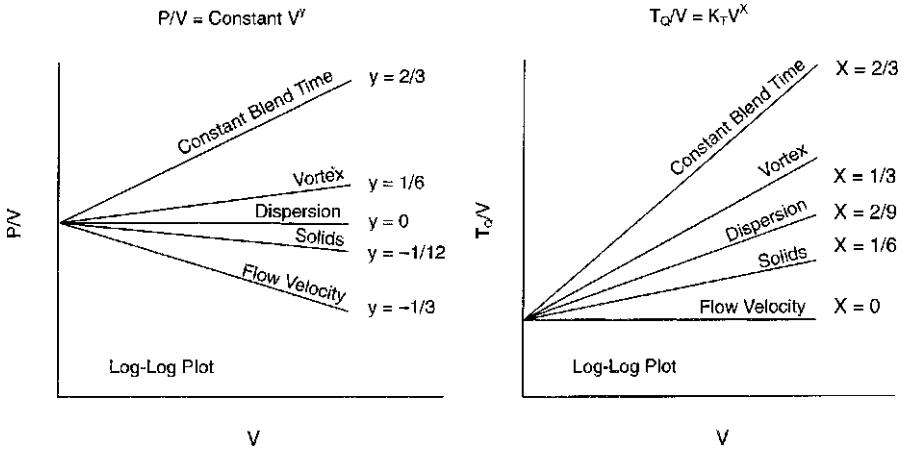


Figure 6-28 Scale-up methods for different process types and requirements.

Figure 6-28 shows changes in these parameters as the vessel volume is increased for several processes. The exponents x and y in Figure 6-28 should be determined experimentally or verified even for the processes listed in these plots. Some mixing equipment vendors prefer to use the T_Q/V criterion because it has a direct impact on the overall size and cost of the mixer, including the gearbox.

When choosing a scale-up method, one must consider changes in other flow and power parameters and their impact on the process result. Table 6-8 shows how these important parameters change on scale-up to 10 times the diameter and 1000 times the volume of laboratory mixing tank. Scale-up methods based on constant blend time require the mixer speed in the commercial vessel to be the same as in the laboratory vessel. This, however, results in a very large increase in the motor power. Such a demanding criterion is necessary for very fast to instantaneous reactions where the reaction lifetime may be a few seconds. Commercial reactors for such systems are, therefore, relatively small in size. Using constant P/V , the mixer speed decreases by 78%, but the blend time increases by a factor of 4.6. If constant P/V is used in scaling up a reacting system, the reactors may need to be sized for longer residence time than the laboratory reactor because of the increase in blend time. It should be noted that the Reynolds number increases by a factor of 21.5, and therefore,

Table 6-8 Most Important Changes in Mixing Parameters on Scale-up by a Factor of 10 in Diameter and 1000 in Volume for Geometrically Similar Systems

Quantity	N	Q/V	Tip Speed	Re	T_Q/V	We	P/V	P
Changes	1	1	10	100	100	1000	100	10^5
in	0.1	0.1	1	10	1	10	0.1	100
parameters	0.22	0.22	2.2	21.5	4.8	48.4	1	1000

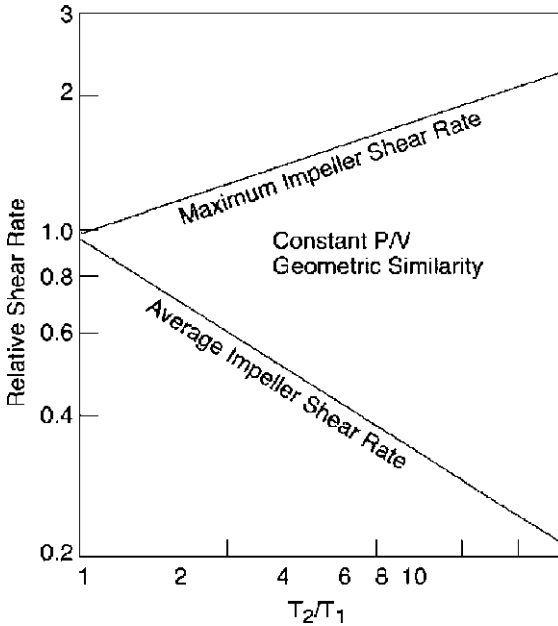


Figure 6-29 Changes in maximum and average shear rate on scale-up.

the flow regime may significantly change and affect the mixing quality. Also, the Weber (We) number increases by a factor of 48.4, which may decrease the dispersed phase drop size on scale-up of an immiscible liquid system. Constant tip speed and equal T_Q/V are some other scale-up criteria and are used only when flow velocities in the impeller region need to be the same as in the laboratory tank.

It must be recognized that rotational speed and shear rate change significantly on scale-up at constant P/V . Based on eqs. (6-19) and (6-20) average shear rate in the impeller region decreases while the maximum shear rate increases on scale-up. These changes are shown clearly in Figure 6-29.

6-5 PERFORMANCE CHARACTERISTICS AND RANGES OF APPLICATION

The performance of stirred vessels is characterized on the basis of the process result for the mixing operation. Detailed mixing mechanisms and design criteria are discussed in respective chapters for these mixing operations. In this section we cover only the general principles and mixer selection for different ranges of fluid properties.

6-5.1 Liquid Blending

Mutually soluble liquids are blended to provide a desired degree of uniformity in an acceptable mixing time. An efficient mixer design is important for good product quality at a high production rate. The critical issues that need to be addressed include number of liquids and their volumes, tank configuration, batch mixing times or residence time distribution in a continuous system, and physical properties.

Mixing system designs fall into two main categories based on liquid viscosity. Low to medium viscosity liquids up to 10 000 cP can be blended effectively by internal pumping action from turbine impellers. For higher viscosity liquids, discharge stream velocity from a turbine dissipates rapidly, resulting in poor homogeneity and very long blend times. Such systems require the use of close-clearance impellers, such as helical ribbons.

Mixing of low to medium viscosity liquids occurs at two levels: macromixing and micromixing. Macromixing is established by the mean convective flow divided in different circulation loops between which the material is exchanged. Micromixing occurs because of turbulent diffusion between small cells in the fluid causing intermingling of molecules.

The selection of mixer type for blending depends on the tank size and configuration. For large blending tanks, typically larger than 30 ft in diameter, side-entering propeller (SEP) mixers are recommended. Small tanks can be equipped with top-entering mixers with one or more impellers on the shaft. SEP mixers are useful for homogenizing two or more liquids in terms of temperature and physical properties. Such product tanks generally take hours to achieve the desired homogeneity in the range 80 to 95%. Typical applications include crude oil and chemical products blending processes. The design of SEP mixers involves sizing the propeller and drive on the basis of required pumping rate using eq. (6-3). Desired blend time and number of turnovers dictate the pumping rate. The number of turnovers to achieve 95% homogeneity is a function of liquid viscosity. General guidelines for the required number of turnovers are given in Table 6-9. For low viscosity liquids, eq. (6-3) sometimes can lead to an undersized SEP mixer. It is recommended that these mixers be sized at a minimum P/V of 0.25 hp per kilobarrel (kbbbl; 1 barrel = 42 gal = 0.159 m³) required for creating a full tank recirculation.

Top-entering mixers can perform a wide range of mixing duties, from gentle blending for product homogeneity to concentration homogenization in reacting

Table 6-9 Number of Tank Turnovers for 95% Homogeneity

Liquid viscosity (cP)	<100	100–1000	1000–5000	>5000
Number of turnovers for 95% homogeneity	3	10	50	>100

^aSee also Chapter 9.

systems. Mixing times can be minutes to a few seconds, and often a high degree of homogeneity, better than 99.9%, is required. Since pumping liquid causes homogenization, axial flow impellers especially hydrofoil type, are more efficient than radial flow impellers. The impeller sizing and mixer speed requirements are determined from the tank turnover method or blend time estimation. These design methods are discussed in Chapter 9 for stirred vessels.

6-5.2 Solids Suspension

Stirred tanks are commonly used for suspending both types of solids, sinking and floating. Suspending solid particles in a turbulent liquid can be considered as balancing of energy supplied by a rotating impeller and energy needed to lift and suspend solids. Industrial applications requiring adequate mixing of solids in liquids include coal slurries, catalyst-polymer systems, solids dissolution, crystallization, paper pulp, ore slurring for leaching, and so on. Axial flow impellers with high pumping efficiencies are most suitable for solids suspension. These impellers generate a flow pattern which sweeps the tank bottom and suspends the solids.

For suspension of sinking solids, the mixer must be designed for a variety of mixing conditions. At the minimum, good motion of solids on the tank bottom is needed, although this condition is rarely sufficient. For most applications, off-bottom suspension is necessary. For enhanced solid-liquid contacting and mass transfer, complete uniformity of particles may be sought. The design guidelines for these different degrees of mixing are discussed in Chapter 10. An effective mixing system consists of a tank with dished or ellipsoidal bottom head, a down-pumping axial flow impeller, four wall baffles having width equal to $T/12$, a baffle wall clearance of about 1.5% T , and an impeller bottom clearance equal to $T/4$. A variety of other mixing objectives may also affect the design of the mixer.

For entrainment of floating solids, a mixer must be designed to provide downward pulling drag force to offset the upward buoyancy force. There are three types of floating solids encountered in the industry: solids lighter than the liquid, difficult-to-wet solids, and solids with low bulk density. Two mechanisms are used for mixing these solids; one uses a central controlled vortex on the surface, and the other uses a recirculation loop to entrain floating solids near the wall at the liquid surface. The vortex is formed using a down-pumping axial flow impeller and narrow baffles (width = $T/50$) at the wall. An effective circulation loop can be generated with an up-pumping axial flow impeller and standard baffles having width = $T/12$. In this case, the solids with upward circulation loop move to the wall on a liquid surface where they are incorporated.

A variety of mixing issues need to be addressed when mixing floating solids. The mixing requirements vary from just dispersion to complete slurry homogeneity, solids wetting, shearing, and breakup of agglomerates. In continuous processes it is important to achieve an entrainment rate exceeding the solids feed rate. If the solids are sticky, such as polymers, they can agglomerate and accumulate on the impellers, baffles, and supports. When mixing with narrow baffles, vortex formation can also result in vapor entrainment and mechanical vibrations.

Testing in the lab or pilot plant will help define the appropriate design and scale-up requirements. The reader is referred to Chapter 10 on solid–liquid mixing and Chapter 13 on reacting solids.

6-5.3 Immiscible Liquid–Liquid Mixing

Intermixing of mutually insoluble liquids can be achieved in stirred tanks with turbine impellers for the purpose of creating large enhancements in interfacial area. This significantly boosts the rate of mass transfer and reaction. These operations are frequently encountered in industries such as chemical, petroleum, pharmaceutical, cosmetics, food, and mining. Several reacting and nonreacting systems include extraction, alkylation, suspension polymerization, emulsification, and phase transfer catalysis. Energy spent in maximizing the liquid–liquid interfacial area is generally cheaper than the improved process result. However, optimization of mixing energy is necessary because too much energy can create undesirable process results. It can create highly stable emulsions and generate excessive heat, which may have adverse impact on product quality. In addition, it can cause foaming and vapor entrainment from the headspace through the vortex, which can seriously affect liquid–liquid dispersion.

To design an optimum mixer, it is important to define the process needs (e.g., homogenization of phases, fine dispersions for fast reactions, dispersion with narrow drop sizes, minimize diffusional resistance in the continuous phase, induce convection within the drops, generate very fine stable emulsions, etc.). Turbine impellers provide the desired mixing conditions for contacting of immiscible liquids. Even with high viscosity liquids, the shear needed for emulsification must be supplied with turbines and not with close-clearance impellers. Typically, low shear hydrofoils can be used for coarse dispersions. Axial and radial flow impellers are effective for fine emulsions. High-shear impellers are necessary for preparing stable emulsions.

Several correlations have been published in the literature for predicting average drop size and drop size distribution based on mixer design parameters and liquid physical properties. These correlations, discussed in Chapter 12, are based on balancing the rates of drop breakup and coalescence. Dispersed drops break up due to shearing action near the impeller as they are circulated, and then coalesce when they reach low shear zones away from the impeller. The time required to reach an equilibrium drop size distribution depends on system properties and can sometime be longer than the process time.

The criterion of maintaining equal power per unit volume has commonly been used for duplicating dispersion qualities on scale-up and scale-down. However, this criterion would be conservative if only gentle homogeneity of the two phases is desired. Other scale-up criteria may be needed for different processes and should be developed through pilot plant testing.

The mixing conditions in a stirred tank can be modified to cause a phenomenon called *phase inversion*. This involves interchange of dispersed and continuous phases. The phase, which will become dispersed, depends on the position of the

impeller, liquid volumes and their physical properties, the feeding conditions, and the dynamic characteristics of the mixing process. There is always a range of volume fractions throughout which either component would remain dispersed, and this is called the *range of ambivalence*. The limits of this range are influenced by the size and shape of the vessel, mixer speed, physical properties of the liquids, and presence of contaminants. Depending on specific process requirements, phase inversion may be desired for product quality or avoided to maintain high mass transfer and reaction.

6-5.4 Gas–Liquid Dispersion

Mechanically agitated gas–liquid contactors are widely used in industrial processes for absorption, stripping, oxidation, hydrogenation, chlorination, carbonylation, fermentation, and so on. They are also used for carrying out biochemical processes such as aerobic fermentation, manufacture of protein, and wastewater treatment. The fractional hold-up of gas (ϕ) in these contactors is a basic measure of their efficiency. The hold-up in conjunction with Sauter mean bubble diameter (d_{32}) determines the interfacial area (i.e., $a = 6\phi/d_{32}$) and hence the mass transfer rate. Knowledge of ϕ also gives the residence time of each phase.

Disk turbine impellers are the most suitable type for gas–liquid dispersion. The disk is useful in forcing the sparged gas bubbles to move through high shear zones near the impeller blade tip. Recently, many concave-blade impellers (e.g., SRGT, CD-6, in Figure 6-10) have been developed to obtain even higher gas holding capability. This impeller characteristic reflects the maximum rate of gas sparging before the mixer approaches the flooding regime. The flooding regime represents excessive bypassing of gas bubbles along the shaft and large reduction in power consumption. A mixer under flooding conditions loses its capability of providing adequate gas hold-up and liquid pumping, and thus gives poor process result.

Although all turbine impellers can be used to disperse gas, axial flow impellers are inferior to radial flow impellers. In addition, down-pumping axial flow impellers can create an unstable hydrodynamic regime due to opposite and out-of-phase frequencies of liquid pumping and bubble rise. This can cause severe torque fluctuations and mechanical vibrations. Large vessels such as fermenters can use high solidity-ratio hydrofoils to achieve high circulation throughout the vessel, which is especially critical in high viscosity biological operations to prevent local oxygen starvation (see Chapters 11 and 18).

When the gas used in the process is hazardous and/or expensive, it is desirable to recycle it from the vapor space in the stirred tank. This can be achieved by using gas-inducing mixing systems. Typical applications include hydrogenation, chlorination, carbonylation, and phosgenation processes. There are three types of gas-inducing mixing systems: a hollow shaft/impeller, axial flow impellers with narrow baffles, and Praxair AGR system (Figure 6-30).

A hollow shaft/impeller system uses the acceleration of the liquid over the blades to reduce the pressure locally at an orifice and induce the gas flow through

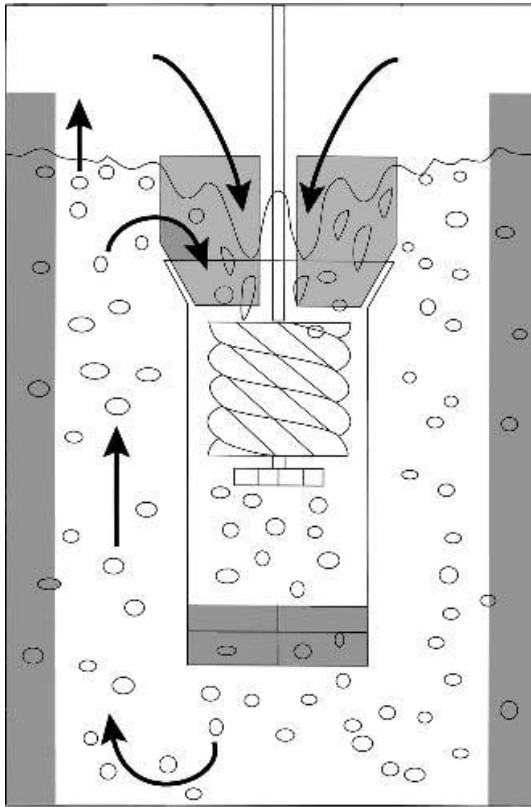


Figure 6-30 Advanced gas reactor by Praxair.

a hollow shaft. An axial flow impeller with narrow baffles creates a surface vortex through which vapors are entrained and dispersed away. The AGR system uses a combination of high-speed helical screw impeller and draft tube to entrain vapors with a flat-blade impeller rotating just below the draft tube.

6-6 LAMINAR MIXING IN MECHANICALLY STIRRED VESSELS

A laminar mixing regime occurs when the impeller Reynolds number drops below 10, due primarily to high fluid viscosity rather than low impeller rotational speed. If turbine impellers are used with highly viscous liquids, flow velocities rapidly decay to low values away from the impeller. This results in formation of a cavern around the impeller. Mixing can be good inside the cavern and poor outside. Flow patterns flatten out and axial flow impellers produce radial flow. These flow changes significantly diminish the blending quality. Turbine impellers are therefore not recommended for use in the laminar regime. For such conditions, close-clearance impellers such as anchors and helical ribbons are commonly used.

There are a variety of viscous materials that are mixed in the laminar regime, including polymer solutions, pastes, gums, and semisolids. As the viscosity of the material increases, the material undergoes different fluid motions, including (1) slipping over itself, (2) fracturing, (3) stretching and relaxing back, (4) agglomerating, and (5) clinging to walls or impeller blades. As a result, mixing is poor. If an additional phase is present, mixing in processes such as reactions, adsorption, melting, dissolution, polymerization, dispersion, and contacting can become very difficult (see also Chapter 16).

The mechanism of laminar mixing involves reorientation and redistribution of the viscous material. This is achieved by cutting, dicing, chopping, and so on, and then restacking the sectioned material. The stacked material is then sheared or normally elongated and then redistributed by folding for further reorientation. As the number of reorientations and redistributions increases, the interfacial area increases. This large interfacial area eventually allows diffusion to homogenize the material.

Power for laminar mixing can be derived based on Stokes' drag and written as

$$P \propto \frac{\mu N^2 D^3}{g_c} \quad (6-21)$$

This correlation does not include the effects of blade number and blade width as expected from Stokes' drag. Using the definition of Reynolds number in eq. (6-4) and turbulent power number N_p in eq. (6-5), this power expression can be rearranged to

$$N_p Re = B \quad (6-22)$$

where B is a constant dependent on the mixer geometry. Typically, B has an average value of 300 and can range between 10 and 40 000 for a variety of impellers. A number of relationships are available for calculating power input under laminar flow conditions in Tatterson (1991).

The power draw can be very high in laminar mixing compared to turbulent mixing. In addition, these mixers are operated at low speeds and the torque on the shaft can be extremely high. The mixer drives designed for high torque require high investment costs. Since most of the power consumed by the mixer is dissipated into heat, removal of heat may be required to avoid possible adverse effects on the process and product quality.

Pumping numbers for the helical ribbon and screw impellers are available in the literature. They range from 0.04 to 0.5 and are highly dependent on the geometry. The anchor impeller only pumps along its radial arms, and pumping numbers are not readily available for this impeller.

Quite often, the fluid viscosity may change during processing and the mixing system design may be based on average process viscosity. This can lead to a very large increase in power inputs unless the mixer speed is dropped as viscosity increases. Use of a variable speed mixer becomes necessary for such systems. Since power going to the mixing is proportional to viscosity, the fluid viscosity can be estimated through power measurements.

A number of mixing system designs are used for mixing of viscous fluids in laminar regime. They include (1) close-clearance impellers, (2) planetary impellers that move throughout the tank, and (3) fixed impellers in tanks that move to expose the material to the impeller. All of these systems generate the necessary three dimensional flows required for mixing.

6-6.1 Close-Clearance Impellers

These impellers are designed to physically turnover the fluids because viscous fluids are difficult to pump. These impellers are typically large in size, nearly the same size as the tank diameter, and provide gentle macroscale blending of liquids at low shear. The most common designs are the anchor and the helical ribbon, shown in Figure 6-31.

Anchors are used for liquid viscosities between 5000 and 50 000 cP because at low viscosities there is not enough viscous drag at the wall to provide pumping. Above 50 000 cP, especially with non-Newtonian fluids, the pumping capacity of the anchor declines and the impeller slips in the liquid. When heat transfer through a jacket is desired along with good mixing, the anchor blades are designed with wipers for scraping the wall. A typical wall scraper design is shown in Figure 6-32. Mixing with an anchor can be complemented by adding inside turbines and/or using a draft tube.

Helical ribbon impellers provide top-to-bottom physical movement of the liquid. In addition to one outer helix, they can be designed with an inner helix pumping in the opposite direction. This is particularly needed for direct-action mixing for high viscosity materials. These impellers can also have two outer helices. The most commonly used pitch for the helices is 0.5. A higher pitch

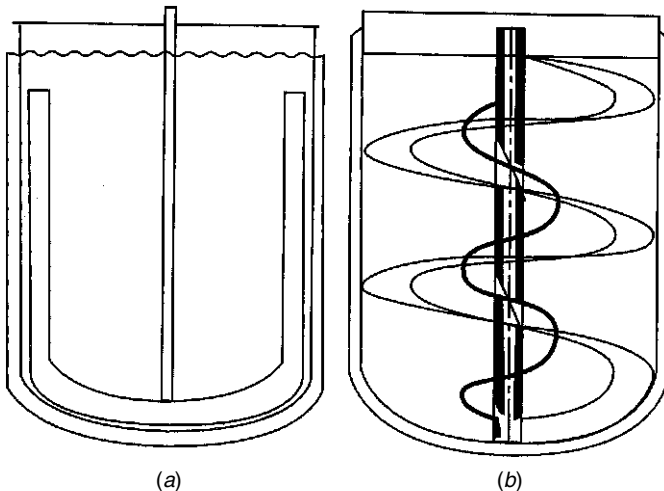


Figure 6-31 Close-clearance impellers: (a) anchor; (b) helical ribbon. The differences in flow are illustrated on the Visual Mixing CD affixed to the back cover of the book.

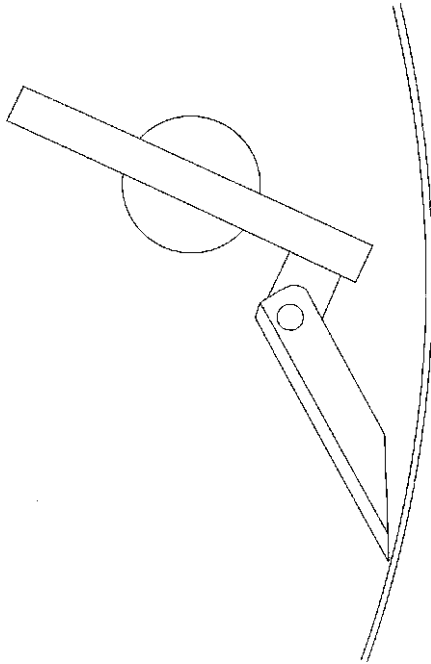


Figure 6-32 Wiper attachment for anchor impeller blade.

reduces top-to-bottom mixing, while a lower pitch causes excess friction and energy consumption. For enhancing heat transfer through a jacket, wipers and scrapers can be attached to the blades. Helical ribbons are also designed at $D/T = 0.7$ with a draft tube to provide top-to-bottom recirculation.

The power number of anchor agitators depends on the wall clearance, in addition to the impeller Reynolds number. This relationship is shown in Figure 6-33 for two anchor geometries: flat and round blade anchors, at two values of wall clearance.

The effect of wall clearance can also be expressed mathematically for different flow regimes. For laminar flow conditions, $Re < 30$:

$$N_p \propto (e/T)^{-0.5} \quad (6-23)$$

For transitional conditions, $30 < Re < 1000$:

$$N_p \propto (e/T)^{-0.25} \quad (6-24)$$

The height of anchor arm (h) also changes the power number as

$$N_p \propto [0.89(h/D) + 0.11] \quad (6-25)$$

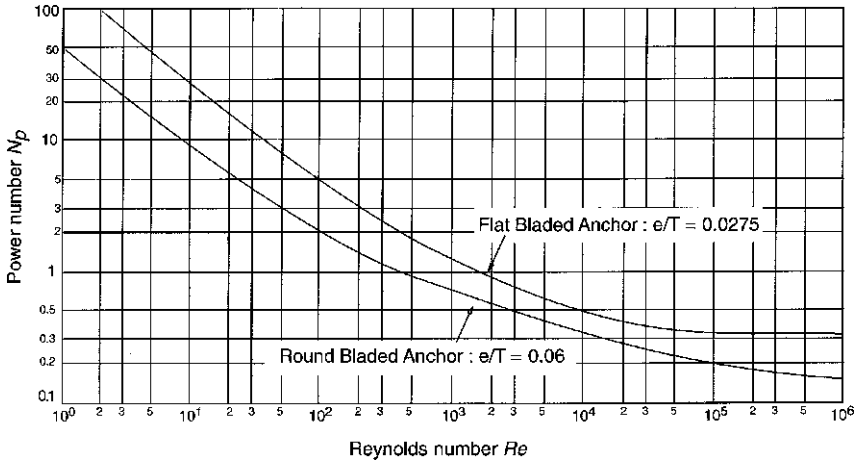


Figure 6-33 Power number curves for anchor agitators at two wall clearances.

The power number for helical ribbon mixers depends on Reynolds number; blade/wall clearance, e ; height, h ; pitch of the helix, p (height of one turn around the helix); blade width, w ; and number of helical flights, n . The relationship is described as

$$N_p = \frac{150 h}{Re D} \sqrt{\frac{n}{\frac{p}{D} \left(\frac{e}{w}\right)^{0.67}}} \tag{6-26}$$

Anchor and helical ribbon impellers can also be used in turbulent applications where high shear is not necessary. This is an advantage for processes in which the fluid viscosity changes significantly and both laminar and turbulent conditions occur at different stages. Although laminar impellers do mix well in turbulent applications, they are not generally recommended, due to their high investment costs.

Direct-action impellers are needed for extremely high viscosity liquids and plastic masses. Such materials include bread dough, battery paste, saltwater taffy, carbon black mixed in rubber, and so on. Suitable mixers for such systems include the co-kneader, extruders, and the Banbury mixer. These are described in Chapter 16.

For specifically difficult applications, special combinations of anchors/helices and anchor/turbines can be used. For example, a helical ribbon impeller can be supported on an anchor for providing both top-to-bottom material movement and folding action. For dispersing powder into a viscous liquid, a high-speed dispersing disk is used in combination with the helix. Intermeshing cone helical ribbon impellers also exist for self-cleaning action and for viscous plastic masses, which may accumulate on the impeller blades.

The time it takes to achieve the desired mixing quality in laminar mixing depends on the mixer geometry and mixer speed. For most processes it takes

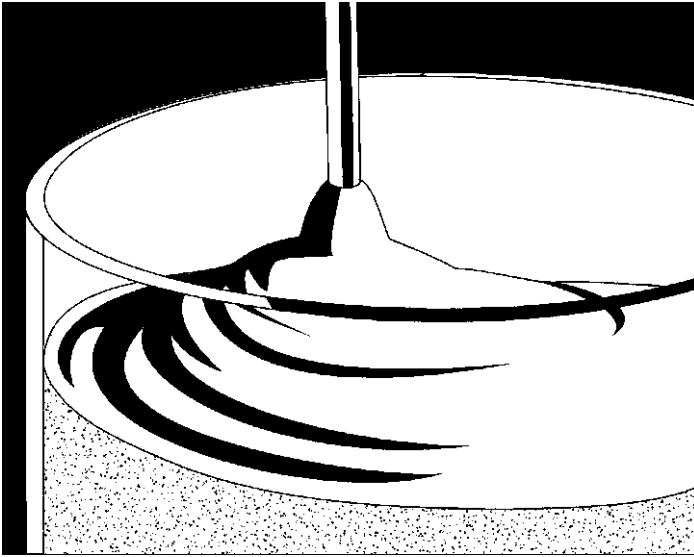


Figure 6-34 Weissenberg effect with mixing of viscoelastic liquid.

between 15 and 300 revolutions with well-designed geometries. This mixing time and mixer speed should be determined through pilot plant testing. The data for scale-up should be obtained for conditions that ensure the elimination of dead zones. It is also important to study the effect of location and rate of material addition.

For viscoelastic liquids, both turbine and close-clearance impellers are used, depending on the liquid viscosity ranges. Due to viscoelasticity, normal stresses are created in addition to the usual tangential stresses during impeller rotation. These stresses give rise to the Weissenberg effect, which causes the fluid to climb up a rotating shaft (Figure 6-34). As a result, mixing quality deteriorates and blend times become longer, and the impeller power number increases in the laminar regime. This reduced mixer performance is more pronounced in the laboratory scale than in the commercial scale.

NOMENCLATURE

a	area of opening, interfacial area
A	tank or column cross-sectional area
A_p	projected area
B	baffle width, constant, function of geometry
C	clearance
C_d	drag coefficient
d_{32}	Sauter mean diameter
D	impeller diameter

e	blade/wall clearance
f	interstage back flow rate
F	force, drag force
g_c	gravitation constant
G	distance between feed nozzle and impeller tip
h	blade height
H	velocity head
K	constant
n	number of blades, number of flights
N	impeller rotational speed
N_b	number of baffles
N_p	power number
N_Q	impeller pumping number
p	blade pitch, height of one turn around the helix
P	power
q	forward flow rate
Q	impeller pumping capacity
Re	impeller Reynolds number
S	impeller separation or spacing
T	tank diameter
T_Q	torque
v_b	backflow velocity
v_{bo}	backflow velocity at zero throughput
v_f	forward flow velocity, feed pipe velocity
v_t	impeller tip velocity
V	velocity, volume
W_w	blade width
Z	liquid height

Greek Symbols

γ	shear rate
θ	blade angle
μ	viscosity
ν	kinematic viscosity
ρ	density
σ	surface or interfacial tension
ϕ	hold-up fraction

REFERENCES

- Dickey, D. S., et al. (2001). *Mixing Equipment (Impeller Type): AIChE Equipment Testing Procedure*, 3rd ed., AIChE, New York.
- Dimoplou, W. (1974). How to determine the geometry of pressure vessel heads, *Hydrocarbon Process*, Aug., 71–74.

- Jo, M. C., W. R. Penney, and J. B. Fasano (1994). Backmixing into reactor feedpipes caused by turbulence in an agitated vessel, *Industrial Mixing Technology*, G. B. Tatterson, R. V. Calabrese, and W. R. Penney, eds., *AIChE Symp. Ser.: Chemical and Biological Applications*, **90**, #299, p. 41.
- Metzner, A. B., and J. S. Taylor (1960). Flow patterns in agitated tanks, *AIChEJ.*, **6**, 109.
- Oldshue, J. Y. (1983). *Fluid Mixing Technology*, McGraw-Hill, New York.
- Rautzen, R. R., R. R. Corpstein, and D. S. Dickey (1976). How to use scale-up methods for turbine agitators, *Chem. Eng.*, Oct. 25, 119.
- Rushton, J. H., E. W. Costich, and H. J. Everett (1950). Power characteristics of mixing impellers, *Chem. Eng. Prog.*, **46**(8), 395–476.
- Tatterson, G. B. (1991). *Fluid Mixing and Gas Dispersion in Agitated Tanks*, McGraw-Hill, New York.
- Tatterson, G. B. (1994). *Scaleup and Design of Industrial Mixing Processes*, McGraw-Hill, New York.
- Xu, B. C., W. R. Penney, and J. B. Fasano (1993). Private communication, Mixing XIV, Santa Barbara, CA, June 20–25.